THERMALLY METASTABLE FULLERENES IN FLAMES

BY

TAPESH KUMAR YADAV

Submitted to the Department of Chemical Engineering
in partial fulfillment of the requirements for
the degree of

DOCTOR OF PHILOSOPHY

at the

MASSACHUSETTS INSTITUTE OF TECHNOLOGY

May 1994

© 1994 Massachusetts Institute of Technology
All rights reserved

Signature of Author _____
Department of Chemical Engineering
March 10, 1994

Certified by _____
Jack B. Howard
Thesis Supervisor

Accepted by _____
Robert E. Cohen
Department Committee for Graduate Students

Science
MASSACHUSETTS INS
JUN 06 1994

Thermally Metastable Fullerenes in Flames

by

Tapesh Yadav

Submitted to the Department of Chemical Engineering on March 10, 1994 in partial fulfillment of the requirements for the Degree of Philosophy in Chemical Engineering.

ABSTRACT

Fullerenes are closed caged molecules of pure carbon. These carbon molecules are produced in abundant quantities by certain sooting processes. In particular, fullerenes are observed in large quantities in the soot produced by low pressure (100 Torr), inert environment, vaporization of pure carbon and in the soot produced by low pressure (40 Torr) laminar combustion of premixed benzene/oxygen/inert vapors. Along with the observation of large quantities of fullerenes, many more observations can be made from the soot of the two processes. One particularly significant observation is the presence of many thermally metastable fullerenes in the soot produced by flames. This thesis focuses on an experimental and modeling study of one of the many thermally metastable fullerenes. Specifically, this thesis establishes the true identity of one of the thermally metastable fullerene produced in flames; the thesis investigates where in the flame the thermally metastable fullerene forms; the thesis reports thermochemical properties obtained from structural modeling of the thermally metastable fullerene; and finally, the thesis reports computational chemistry based modeling of the thermochemical kinetics of the formation of the thermally metastable fullerene.

The study began by experimentally investigating low pressure, premixed, laminar, flat benzene/oxygen/ inert flames. Process conditions explored ranged from pressures of 20 Torr to 100 Torr, C/O ratios from 0.91 to 1.08, inerts such as helium, argon and nitrogen, inert dilutions from 0% to 50%, and input gas velocities from 29 cm/sec to 52 cm/sec (300 K). Flame conditions that produced large quantities of the thermally metastable fullerene were identified and used to produce sufficient quantities needed to analytically establish the identity of the thermally metastable fullerene. The thermally metastable fullerene so produced was purified from other fullerenes by developing and using a three step preparative chromatography. The identity of the thermally metastable fullerene was established with the help of analytical high performance liquid chromatography, UV-Visible spectroscopy, electron impact mass spectrometry, ion-spray mass spectrometry, fourier transformed infra-red spectroscopy, proton nuclear magnetic resonance spectroscopy, proton coupled and proton decoupled ^{13}C nuclear magnetic resonance spectroscopy and chemical tests. The query: where in the flame does the thermally metastable fullerene form, was examined by performing a profile analysis of the flame process. The thermochemical properties of the thermally metastable fullerene was obtained by molecular mechanics modeling and semi-empirical quantum modeling. The thermochemical kinetics of the formation of the thermally metastable fullerene was predicted using transition state theory and by identifying and modeling the transition state for the chemical transformation using a semi-empirical quantum model.

The results establish that the thermally metastable fullerene observed in the flame is $C_{60}C_5H_6$, a Diels-Alder adduct of C_{60}. The profile study suggests that the adduct is not formed in the flame, but is generated by post flame chemistry. The computational chemistry results qualitatively predict the experimental observations. The method followed by the thesis is fairly universal in nature and can be used in the study of other metastable fullerenes in particular and chemical species in general.

Thesis Supervisor: Dr. Jack B. Howard, Professor of Chemical Engineering

Acknowledgments

I thank:

- Professor Jack B. Howard for his guidance, his critiques, his suggestions and the freedom he offered me during the course of this thesis. Working with him has been one of the most productive experiences in my life.

- Dr. Arthur L. Lafleur for his timely guidance and his insightful comments during the analytical work of this thesis.

- Professor Janos M. Beér and Professor Adel F. Sarofim for their comments and their encouragement during the course of this thesis.

- Dr. Vincent Rotello for his assistance in NMR and mass spectrometry work and for general discussions.

- Dr. Joseph Anacleto and Dr. Robert Boyd of National Research Council, Canada and Dr. Stephen McElvany and Dr. Mark Ross of Naval Research Laboratories, Washington D.C. for the assistance with the specialized mass spectrometry required during this thesis.

- The MIT's UROP team for their assistance and for their excitement in fullerenes research. In particular, the following deserve special thanks: Lorin Theiss, Mika Nyström, Laura Giovane, Elaine Johnson, Anna Chwang, Diana Goldenson, Albert Dietz and Michael Chung.

- The MIT's combustion team for the extensive discussions about fullerenes and future. Working with them has been a wonderful experience. In particular, Kathy Brownell and Dr. Joseph Marr deserve a special mention.

- Professor Klavs Jensen and Professor Daniel Blankschtein for the productive discussions on chemical engineering fundamentals; particularly, during my work as a teaching assistant to them in Chemical Reactor Engineering (10.65) and Chemical Engineering Thermodynamics (10.40) respectively.

- The Division of Chemical Sciences, Office of Energy Research, U.S. Department of Energy for the financial support of this research under Grant DE-FG02-84ER13282.

Table of Contents

1. Introduction 8
   Thesis Objectives 12

2. Literature Review 13
   2.0 Overview 13
   2.1 Fullerene Production 13
      2.1.1 Carbon Vaporization Processes 13
      2.1.2 The Flame Process 15
      2.1.3 Contrasting Fullerene Processes 19
      2.1.4 The Thermally Metastable Fullerenes 20
   2.2 Fullerene Structures and Computational Chemistry 21
      2.2.1 Fullerene structures 23
      2.2.2 Computational Chemistry 24
   2.3 Fullerene Reactions and Kinetics Modeling 26

3. Equipment and Experimental 28
   3.0 Overview 28
   3.1 The Synthesis 28
      3.1.1 The Fuel and Gas Feed System 29
      3.1.2 The Burner System 31
      3.1.3 The Sampling System 33
      3.1.4 The Post Run Activities 36
   3.2 The Analysis 37
      3.2.1 High Performance Liquid Chromatography 37
      3.2.2 Preparative Column Chromatography 38
      3.2.3 Ultraviolet-Visible Spectroscopy 40
      3.2.4 Mass Spectrometry 41
      3.2.5 Fourier Transformed Infra Red Spectroscopy 42
      3.2.6 Nuclear Magnetic Resonance Spectroscopy 43
      3.2.7 Chemical Tests 46
   3.3 The Computational Chemistry Software 46
      3.3.1 The Molecular Mechanics Models 48
      3.3.2 The Semi-empirical Quantum Models 49

3.3.3 Thermochemistry 49
3.4 The Experimental Strategy 53
3.4.1 Optimizing the Flame 54
3.4.2 Optimizing the Purification Method 55

4. Experimental Results and Discussion 57
4.0 Overview 57
4.1 The Flame 57
4.1.1 Correlating C_{60}+C_{70} Yield with Yield of the Thermally Metastable Fullerene 57
4.1.2 Developing the Flame Process for Increased C_{60}+C_{70} Yield 58
4.2 The Purification 64
4.2.1 The Jordi-Gel Column 65
4.2.2 The C-18 Column 66
4.2.3 The Hypersil Column 67
4.3 Characterization 68
4.4 The Species Profile in the Flame 81

5. Modeling Results and Discussion 85
5.0 Overview 85
5.1 Structural Studies 85
5.2 Thermochemical Kinetics Studies 93
5.2.1 Determining the structure of the transition state 95
5.2.2 Modeling the thermochemical properties of the transition state 96
5.2.3 Predicting the activation energy and the pre-exponential factor 97

6. Conclusions 103

7. Appendices 107
Appendix A 107
Appendix B 111
Appendix C 115
Appendix D 121

8. References 127

List of Figures

Figure 1.1 Carbon Polyhedrons 8
Figure 1.2 Schematic Structure of C_{70} 10

Figure 2.1 Schematic of the carbon vaporization process 15
Figure 2.2 Schematic of the flame process 16
Figure 2.3 Chromatogram of the flame soot extract 17
Figure 2.4 Mass spectrum of the flame soot extract 18
Figure 2.5 UV-Vis spectrum of the peak A and the peak B in the chromatogram of the flame soot extract 18
Figure 2.6 The schematic structures of C_{60} and C_{70} 21
Figure 2.7 Stone-Wales Transformation of icosahedral C_{60} into a C_{60} isomer with adjacent pentagons 23

Figure 3.1 The Flame Process 29
Figure 3.2 The flat flame burner system 31
Figure 3.3 Schematic of the burner 32
Figure 3.4 The sampling system 34

Figure 4.1 The relationship between fullerenes (C_{60} + C_{70}) yield and the relative abundance of the thermally metastable fullerene 58
Figure 4.2 The effect of C/O ratio on the C_{60}+C_{70} yield 59
Figure 4.3 The effect of diluent concentration on the C_{60}+C_{70} yield 60
Figure 4.4 The effect of diluent types on the C_{60}+C_{70} yield 61
Figure 4.5 The effect of burner gas velocity on the C_{60}+C_{70} yield 62
Figure 4.6 The effect of combustion chamber pressure on the C_{60}+C_{70} yield .. 63
Figure 4.7 The chromatogram obtained on a Jordi-Gel preparative column 65
Figure 4.8 The chromatogram obtained on a C-18 preparative column 66
Figure 4.9 The chromatogram obtained on a Hypersil preparative column 67
Figure 4.10 HPLC chromatogram of soot extract and the UV-Vis spectra of peaks marked A and B in chromatogram 68
Figure 4.11 HPLC/MS spectrum 70
Figure 4.12 EI mass spectrum 70
Figure 4.13 FTIR spectrum of the thermally metastable fullerene 74

Figure 4.14 The proton NMR of the thermally metastable fullerene 75
Figure 4.15 (a) ^{13}C NMR spectra of the thermally metastable fullerene with broad band decoupling (b) ^{13}C NMR spectra with broad band proton coupling 76
Figure 4.16 Reconstructed ion chromatogram from a charge transfer ionspray based HPLC/MS/MS analysis of a sample containing the thermally metastable fullerene 77
Figure 4.17 Two possible isomers of $C_{60}C_5H_6$ 79
Figure 4.18 EI Mass Spectrum of thermal fragment 81
Figure 4.19 The concentration profile of fullerene species in the flame 81

Figure 5.1 Illustrative $C_{60}C_5H_6$ isomers 86
Figure 5.2 The structure of $[C_{60}C_5H_6]^{\ddagger}$ as identified using PM3 (MOPAC) ... 95

Chapter One

Introduction

The element carbon is the atomic basis of life. Compounded with other elements, carbon forms an extraordinary array of molecules -- from simple methane to complex proteins. Even without compounding with other elements, carbon forms an extraordinary array of lattices -- from amorphous coal to crystalline diamonds. Somewhere in between these two arrays of structures -- carbon based molecules and carbon based lattices -- lies yet another form of carbon: polyhedral structures of carbon.

Four polyhedrons of carbon have piqued interest of synthetic organic chemists during the past 40 years: tetrahedrane (C_4H_4), cubane (C_8H_8), dodecahedrane ($C_{20}H_{20}$) and buckminsterfullerene (C_{60}) [1]. Figure 1.1 shows these four beautiful polyhedral shapes.

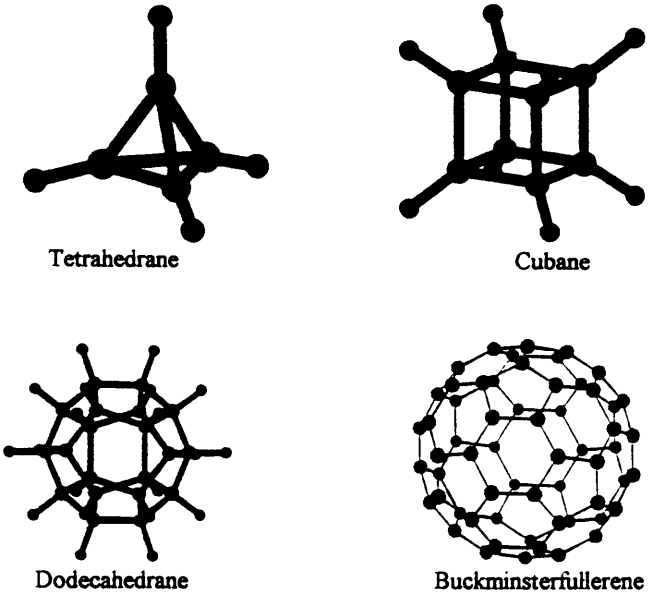

Figure 1.1 Carbon Polyhedrons

As is apparent from Figure 1.1, all these structures impose strain on the carbon (which prefers to form an angle of 109.5 degrees with its neighbors in sp^3 hybridized state). This structural strain makes cubane, tetrahedrane and dodecahedrane instable. Consequently, it is not surprising that researchers have not observed these molecules in nature [1].

Buckminsterfullerene (C_{60}) has a different story. Its existence was speculated by David Jones in 1966 [2], and it was theoretically studied by Osawa and Yoshida in 1970 [3, 4] and Bochvar and Gal'pern in 1973 [5]. Orville L. Chapman independently thought of the C_{60} structure and devoted much time to the planned, systematic synthesis of C_{60}. Despite a ten year effort, Chapman and his students failed to make C_{60} [1]. The first evidence of buckminsterfullerene's existence was serendipitiously obtained by Kroto et al. [6] in 1985 while doing experiments to answer questions relating to interstellar research.

The questions relating to interstellar research, that Smalley, Curl and Kroto were seeking to answer, have their origins in 1970s. During late 1970s the long chained cyanopolyynes (HC_nN (n= 5-11)) had been discovered in the interstellar space by radio astronomy. The subsequent quest for their source indicated that they were being blown out of red giant carbon stars [7, 8]. Kroto et al. in 1985, confirmed these stars to be likely sources by simulating the chemistry in these stars with laser focused on a pure carbon (graphite) target [6]. During these cluster studies, they observed an exceptionally large presence of a stable pure carbon species. The pure carbon species had a molecular weight of 720, which if made of pure carbon suggests the formula C_{60}. Kroto et al., without being aware of the earlier theoretical work on C_{60} [2-5], conjectured C_{60} to be closed caged and to have the truncated icosahedron polyhedral structure (soccer ball shaped) as shown in Figure 1.1. Furthermore, they gave C_{60} the name buckminsterfullerene.

The buckminsterfullerene discovery was accompanied by the discovery of a whole family of stable closed caged pure carbon molecules - and the family is now known as "fullerenes." Kroto et al. [6] while observing C_{60}, observed another member of this family in 1985. This other observed fullerene member had a molecular weight of 840

that implied a polyhedral with the molecular formula: C_{70}. The molecule C_{70} turns out to be ellipsoid (rugby ball) in shape [9]. Figure 1.2 shows a schematic of C_{70}.

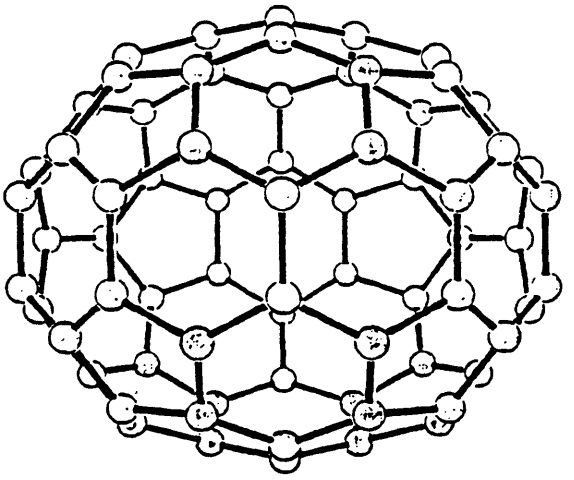

Figure 1.2 Schematic Structure of C_{70}

The laser vaporization method used to discover buckminsterfullerene produced only trace amounts of C_{60}. The trace amounts so produced were sufficient to establish the existence of C_{60} in nature. However larger quantities of C_{60} were needed to establish the symmetrical structure of C_{60}. Subsequent attempts to produce "large" quantities of C_{60} in the laser vaporization equipment failed.

Between 1985 and 1989, Homann et al. performed a series of well-designed experiments with hydrocarbon flames [10-12]. They studied a flat premixed acetylene- and benzene-oxygen flames under stationary conditions on a flat disk burner. They sampled the flame gases at different heights above the burner and analyzed the samples with an on line mass spectrometer. The charge to mass ratios they observed provided the intriguing evidence that flames produce pure carbon species with molecular weights resembling those reported for fullerenes in graphite vaporization. However, the evidence could not establish that the observed carbon species were closed and that flames can produce macroscopic quantities of neutral fullerenes, and that these fullerenes can be recovered as a product.

In 1990, Krätschmer et al. succeeded in producing large quantities of C_{60} and other fullerenes by a different process [13, 14]. Their process involved electrically striking an arc across graphite electrodes in a low pressure helium atmosphere. The arc produced a high temperature carbon vapor. The vapor then cooled by natural heat transfer processes and produced a soot rich in fullerenes. This process has come to be known as the graphite vaporization process.

The large quantities of C_{60}, produced by the graphite vaporization process, enabled the testing of proposed C_{60} structure using standard analytical methods (for example: ^{13}C NMR should show a single line for C_{60}). The standard tests confirmed the truncated icosahedral structure of C_{60} [15]. The identity of C_{60} had been established.

In 1991, Howard et al. [16] reported an alternative process for producing macroscopic quantities of soot rich in C_{60} and other fullerenes. The alternative process produced fullerenes by combusting benzene vapor with oxygen in presence of argon. The process required operating a fuel rich premixed flame at low pressures. The fuel rich flame produced soot with macroscopic quantities of fullerenes.

Along with the discovery of fullerenes in flames, Howard et al. [17] noted that flame produced fullerenes have certain features that are unique to the flame and these features are not observed in the fullerenes produced by graphite vaporization process. First Howard et al. noted that flames can produce C_{70} to C_{60} molar ratio in the range 0.26-5.7 compared to 0.02-0.18 for graphite vaporization process. Next, they noted that flames produce many metastable fullerene isomers. These isomers, they hypothesized, were apparently the first production and collection of fullerenes having adjacent five-membered rings in their structure. Finally, Howard et al. noted another contrast between fullerene synthesis in flames and in graphite vaporization process; namely, the graphite vaporization process contains only carbon, while in flames oxygen and hydrogen are present along with carbon during fullerene production.

We conjectured that understanding the features that differentiate the graphite vaporization process from the flame process may hold the key to understanding fullerene synthesis in premixed flames and perhaps ultimately to understanding the chemistry of fullerene formation in general.

Thesis Objectives

The focus of this thesis is to investigate the production of one of the many thermally metastable fullerenes in flames. In particular, the thesis seeks to establish the structure of a thermally metastable fullerene, to determine how it is formed in flames and to model the kinetics of its formation.

Chapter Two

Literature Review

2.0 Overview

Even though macroscopic amounts of fullerenes have been available only recently, the research relating to fullerenes has been intense and extensive. This can be estimated from the fact that more than 2300 papers have already been published [18] and currently a paper is published every thirteen hours [19]. As a result of these accelerating additions to fullerene research, it is almost impossible to completely review all the literature. This chapter, nevertheless, attempts to review some highlights of the fullerenes research that is relevant to this thesis. The literature review is subdivided into three sections so as to focus on the major themes of this thesis. These sections are:

2.1 Fullerene Production
2.2 Fullerene Structures and Computational Chemistry
2.3 Fullerene Reactions and Kinetics Modeling

Each of these sections is now discussed.

2.1 Fullerene Production

Since the discovery of graphite vaporization process by Krätschmer et al. in 1990 [13], numerous alternative processes have been demonstrated to produce fullerenes. These processes can be divided into two major groups, the classification being based on a fundamental difference in the mechanism of fullerene formation:

2.1.1 Carbon Vaporization Processes

These processes vaporize solid carbon by one or more sources of energy input. The carbon source for these processes varies from graphite to coal and the energy input

varies from resistive heating to inductive coupling. However, in all these processes, carbon is heated in low pressure inert environment to a temperature above the sublimation temperature of carbon. The sublimation causes the formation of atomic carbon vapor. The carbon vapor then condenses to form soot rich in fullerenes. Thus, the overall mechanistic reaction for carbon vaporization processes can be summarized as:

$$nC_{(vapor)} \xrightarrow{Inert} Fullerenes \quad + \quad Soot$$

There are numerous carbon vaporization processes. Table 2.1 summarizes some of the more researched processes indicating the source of carbon and the form of energy input in these processes.

The fullerene production technique currently in widest use is the Haufler et al. process [22]. The process is shown schematically in Figure 2.1. During this process, graphite rods are evaporated by arc-discharge in a quenching atmosphere of inert gas (typically 75-200 torr of helium). The evaporated graphite when quenched produces a light, fluffy condensate commonly called soot. The soot is collected and the fullerenes are solvent extracted from the soot. The solvent extract, when analyzed, is found to consist only of fullerenes [15].

Source of carbon	Form(s) of energy input	Reference
Graphite	Resistive heating, electrode arcing	Krätschmer et al. [13, 22]
Coal	Resistive heating, electrode arcing	[20]
Graphite	Radio frequency induction	[21]
Graphite/Coal	Plasma arc coupled with radio frequency	[23]

Table 2.1

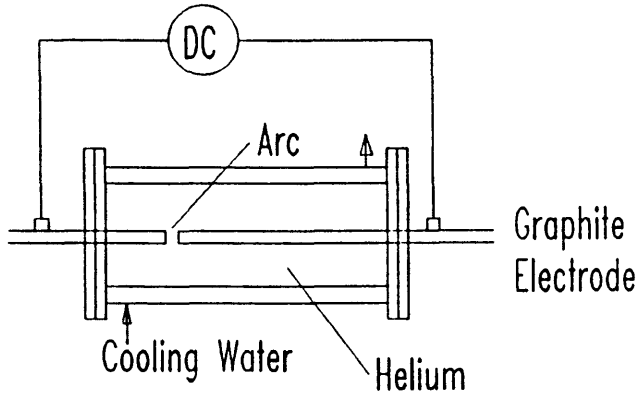

Figure 2.1 Schematic of the carbon vaporization process

All the carbon vaporization processes reportedly produce soot that contains from 4% to 14% C_{60} by soot weight, from 0.5% to 3% C_{70} by soot weight and small amount of higher fullerenes [20, 21]. The alternative fullerene production process, on the other hand, shows a different fullerene composition distribution. This process is discussed next.

2.1.2 The Flame Process

Fullerenes can also be produced from hydrocarbon/oxygen/inert flames operated over a range of conditions.

Homann et al. [10-12] in a carefully designed set of experiments studied low-pressure premixed flames of acetylene and benzene with oxygen. They used a molecular beam system to sample the premixed flame. The sample was processed through a linear time-of-flight mass spectrometer (TOF-MS) and a reflectron TOF-MS. They observed along with the ions of polycyclic aromatic hydrocarbons (PAHs), positive and negative ions whose molecular weights corresponded to C_{32} to over C_{600}. In order to check whether these ions had hydrogen, they combusted deuterated acetylene and benzene. They noted that the substitution of $^1H_1$ with $^2D_1$ did not change the molecular weights

of the observed molecular weights (C_{32} etc.). This observation implied that the ions could not be large hydrogen containing species and should be made of pure carbon or may be carbon and oxygen. These experiments, therefore, gave strong support to the conjecture that fullerenes may form in flames. However, these experiments did not establish that the ions they observed corresponded to closed cages; an open cage structure, although unlikely, could as well explain all their observations. Furthermore, these experiments did not establish that flames can produce neutral fullerenes that are stable. The existence of stable closed caged neutral fullerenes was established by the later work of Howard et al. [16, 17].

The fullerenes producing flames that have been studied most are premixed one-dimensional flames of benzene and oxygen with or without an inert (helium, argon, nitrogen) [10-12, 16, 17, 30]. Benzene combustion has been an actively researched area for many years prior to the discovery of fullerenes [24-29]. To summarize the results in an over-simplified way, the combustion causes first a breakdown of benzene into smaller species. These species then participate in a series and parallel molecular weight growth reactions forming a host of gaseous and solid products. The overall reaction can be summarized as:

$$C_6H_6 + O_2 + He \rightarrow CO + CO_2 + H_2 + H_2O + PAHs + Fullerenes + Soot + He$$

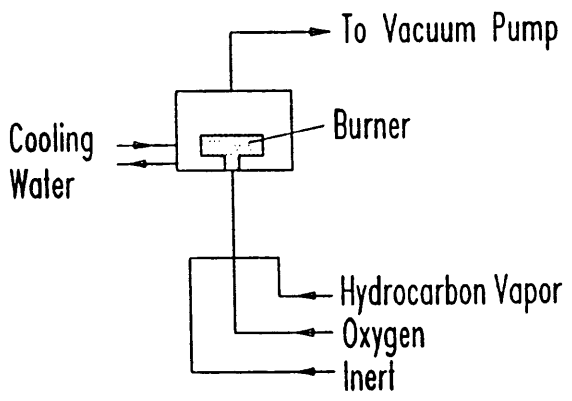

Figure 2.2 Schematic of the flame process

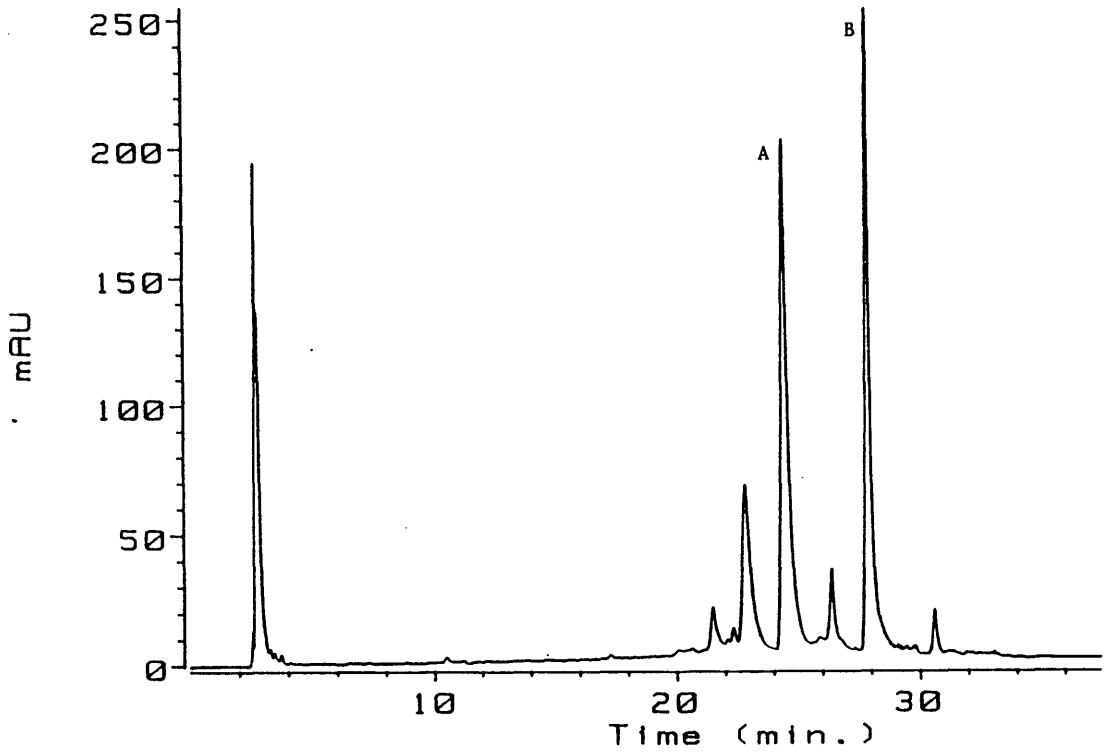

Figure 2.3 HPLC chromatogram of the flame soot extract

The flame process is shown schematically in Figure 2.2. The premixed flames are often operated under fuel rich conditions and under low pressures (typically 25-200 torr). The fuel rich conditions favor the production of soot. The soot is collected and extracted with solvent (usually benzene or toluene). The solvent extract, when analyzed, is found to consist of polycyclic aromatic hydrocarbons (PAHs), fullerenes observed in the carbon vaporization processes and fullerene like molecules not observed in the carbon vaporization processes. For instance, Figure 2.3 shows results from high performance liquid chromatography (HPLC) of the toluene extract. The identity of the two most prominent peaks "A" and "B" in the chromatogram, is established by the mass spectrum of the toluene extract (Figure 2.4) and by the ultraviolet-visible (UV-Vis) spectra of the fullerene peaks (Figure 2.5). These analytical results establish that peak "A" corresponds to C_{60} and peak "B" corresponds to C_{70} [17]. Notice that in the chromatogram (Figure 2.3) many more peaks are present other than the C_{60} and the C_{70} peaks. Many of these peaks are not observed in

the HPLC chromatogram of toluene extract from the soot produced using carbon vaporization. The fullerenes that are observed in both the flame process and the carbon vaporization process show features that are significantly different.

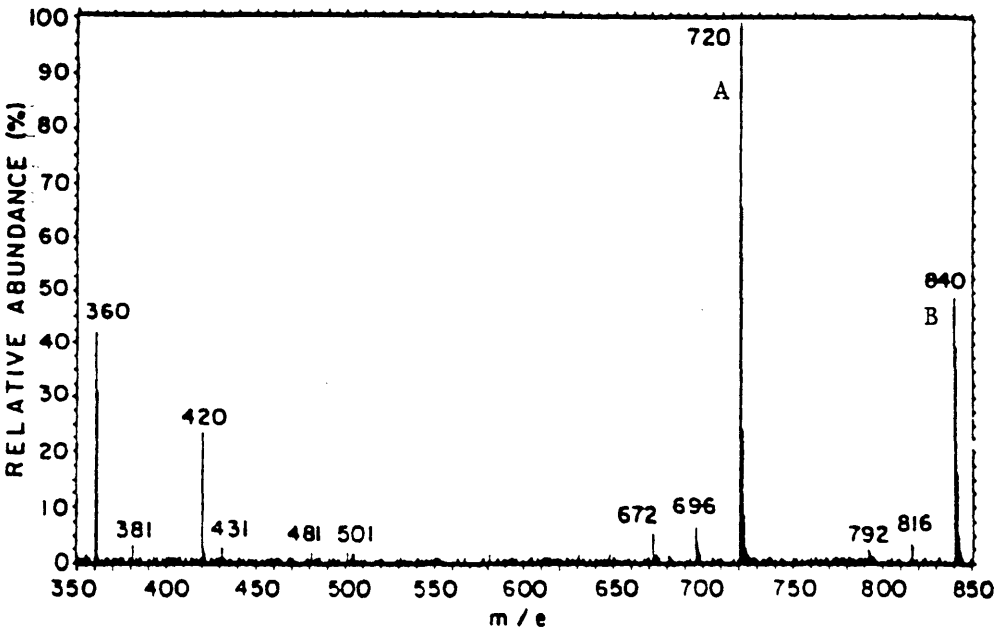

Figure 2.4 Mass spectrum of the flame soot extract

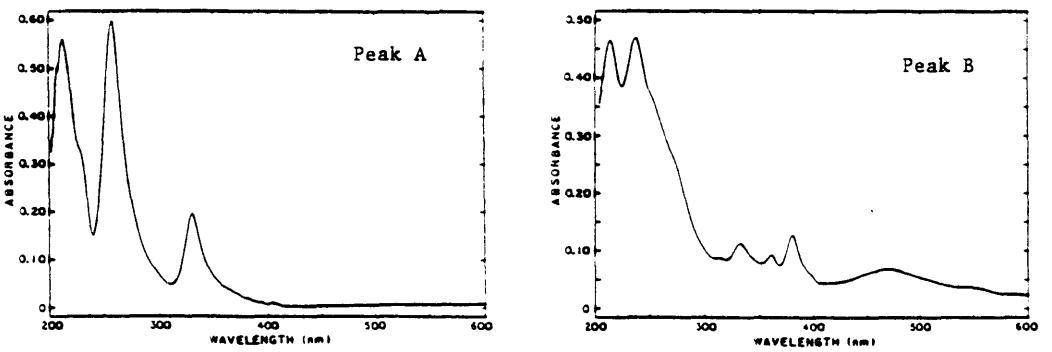

Figure 2.5 UV-Vis spectrum of the peak A and the peak B in the HPLC chromatogram for the flame soot extract

2.1.3 Contrasting Fullerene Processes

Comparison of the flame process with the carbon vaporization process reveals three striking differences: the different C_{70}/C_{60} ratios, the maximum reaction temperatures, the effect of the presence of oxygen and hydrogen in the two processes and the production of metastable fullerenes in the flame process.

The carbon vaporization processes produce a C_{70}/C_{60} molar ratio that varies between 0.02-0.18. The flame process, on the other hand, shows a much larger C_{70}/C_{60} molar ratio and the ability to set this ratio to different values over more than a 30-fold range by the adjustment of flame conditions. The ability to promote the yield of certain products apparently extends, at least to some degree, to larger fullerenes [30].

The carbon vaporization processes reach peak initial temperatures in excess of 6000 K [23, 34] so as to sublime the carbon. These temperatures are enough to completely atomize the carbon. The flame processes, on the other hand, reach peak initial temperatures of about 2300 K [30, 33]. At these flame temperatures, the feed molecules do not atomize, instead larger molecules break down into smaller species [33].

Another contrast between fullerenes synthesis in flames and in carbon vaporization systems, which contain only carbon, is the presence of oxygen and hydrogen as well as carbon in the flames. The presence of oxygen or hydrogen severely reduces fullerene yields in carbon vaporization processes [35]. Therefore, the starts up procedures for carbon vaporization processes include the reactor purging with inert (usually helium). On the other hand, in the case of flame processes, not only are oxygen and hydrogen present at the beginning of the reaction, oxygen is abundant during fullerenes formation, as is also OH radical – both of which are known to react with PAH and soot particles [31]. Thus flame chemistry that yields fullerenes is different, if not more complicated, than the carbon vaporization chemistry that yields fullerenes.

Another major contrast between the carbon vaporization process and the flame process was mentioned above -- that is, the formation of molecules that appear solely in the chromatogram of the toluene extract from flame process soot. Some of these

peaks were identified to belong to $C_{60}H_2$, $C_{60}H_4$, $C_{70}H_2$, $C_{60}CH_4$ and $C_{60}(CH_4)_2$ by Anacleto et al. [36, 37]. These derivatives are not observed in the regular carbon vaporization process. Thus flame processes produce numerous fullerene derivatives that the carbon vaporization process does not produce. Anacleto et al. [36] also discovered that some of the peaks in the chromatogram (Figure 2.3) correspond to molecules that are thermally metastable. These metastable peaks are the focus of this thesis and are discussed next.

2.1.4 The Thermally Metastable Fullerenes

Anacleto et al. [36] found that the molecules corresponding to the peak "C" in the chromatogram (Figure 2.3) were thermally metastable. Specifically, at the temperature of boiling toluene (111 ^{o}C), the researchers found that these molecules converted to a molecule that was indistinguishable from buckminsterfullerene (C_{60}). The conversion had a half life of about 1 hour. Furthermore, Anacleto et al. discovered that as the reaction proceeds, the amount of thermally metastable molecule consumed is essentially equal to the amount of the stable C_{60} fullerene produced. This fact suggested that C_{60} is the stable form to which the thermally metastable molecules revert to.

Anacleto et al. [36, 37] initially suggested that these thermally metastable molecules were apparently the isomers of buckminsterfullerene (C_{60}). Their hypothesis was consistent with all qualitative theoretical arguments. For instance from structural viewpoint, discussed below, at least 1812 isomers of C_{60} are feasible [56-58]. The isomers will necessarily have adjacent five-membered rings that will introduce extra strain in the structure. The strain will lead to the metastability as observed. Finally, the transformation of a metastable isomer to stable C_{60} will require intramolecular arrangements, and these intramolecular arrangements had already been suggested [37]. The true identity of these thermally metastable molecules (which isomer, if it is an isomer?) was, however, unknown. Furthermore, it was not clear if any alternate hypothesis (for instance: the hypothesis that the thermally metastable molecules are just fragile adducts of C_{60}) might explain all the observed facts. These questions and more are discussed in detail in the later chapters of this thesis.

While this thesis was being completed, Anacleto et al. [32] made excellent progress in studying one of these metastable molecules using mass spectrometric techniques. This thesis focussed on a thermally metastable molecule not studied by the Anacleto et al. group [32]. Unlike the Anacleto et al. group which used only mass spectrometric methods, this thesis systematically used many analytical methods to establish the true identity of the thermally metastable fullerene studied by this thesis. The thesis also meets all the other thesis objectives set out in the introduction chapter.

2.2 Fullerene Structures and Computational Chemistry

The enumeration of fullerene structures and the modeling of these fullerene structures began almost immediately after Kroto et al. [6] first proposed the truncated icosahedral structure for C_{60}.

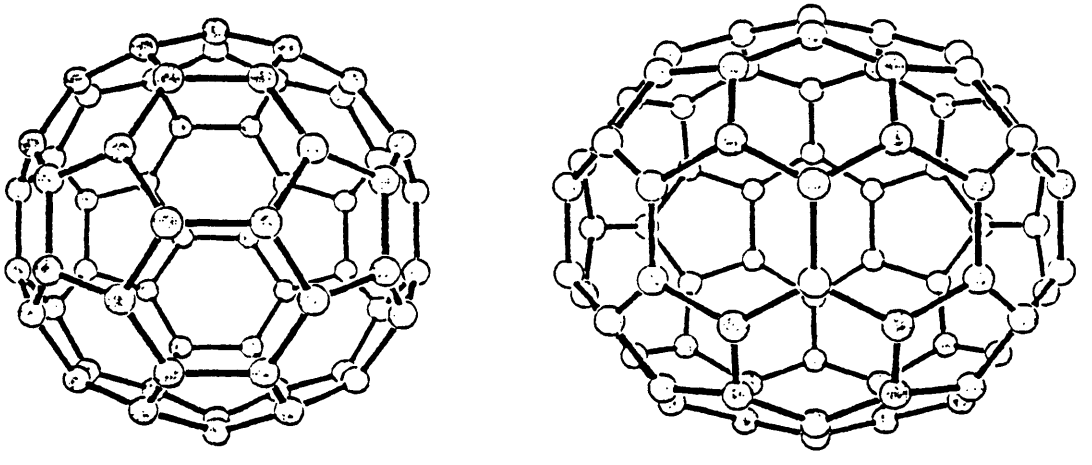

C_{60} C_{70}

Figure 2.6 The schematic structures of C_{60} and C_{70}

Kroto et al. [6] proposed that the C_{60} structure can be described as a closed caged convex polyhedron - truncated icosahedron (buckminsterfullerene). A truncated

icosahedron consists of 12 pentagonal faces arranged with 20 hexagonal faces in such a way that no two pentagons are adjacent. Furthermore, each vertex in the polyhedron is connected to three other vertices as shown in Figure 2.6. They also proposed that C_{70} is an extension of the truncated icosahedron structure in the sense that C_{70} structure can be obtained by adding a ring of five hexagonal faces at the center as shown in Figure 2.6. Because of the convex polyhedron structure, the truncated icosahedron structure proposed by Kroto et al. can be mathematically derived. Haymet [40], even before Kroto et al. [6] presented their results, independently used Euler's famous theorem:

$$vertices + faces = edges + 2$$

to show that carbon clusters (fullerenes) can have only an even number of carbons (vertices); that only 12 pentagons can exist in a fullerene made of pentagons and hexagons; and that the number of hexagons in fullerenes can be given by the exact equation:

$$Number\ of\ Hexagons = vertices/2 - 10$$

Fowler and Woolrich [42] studied C_{60} and C_{70} as three dimensional pi-systems. Using Hückel calculations they predicted stable closed shell structures for neutral C_{60} and C_{70} confirming the experimental results of Kroto et al. [6]. Fowler and Woolrich further found that neutral C_{20} and C_{80} are not closed-shell in icosahedral symmetry. Fowler [43, 44] determined magic numbers for carbon clusters and found that irrespective of point group symmetry, structures of large clusters may be generated by a leapfrog method from smaller ones. Haddon et al. [45, 46] analyzed the re-hybridization and bonding in large carbon spheroids using POAV/3D HMO theory. They concluded that bigger clusters would be more stable and that spherical graphite would be most stable (By spherical graphite, Haddon et al. [45, 46] mean a carbon structure that consists of graphitic sheets folded in the form of a sphere and thereby having no dangling bonds. Such a structure would, they suggested, be made of concentric shells such as those in onions. Six years after they published their results, Ugarte's [47] experimental discovery of bucky-onions proved them to be right). Klein et al. [48] calculated that clusters made up of 60 atoms (with no hydrogen atoms) are

likely to be highly stable. Haymet [40, 41] presented theoretical evidence for the stability of C_{60} and proposed that because of sp^2 hybridization, C_{60} should be an alkene. Furthermore, Haymet suggested that because of the high symmetry of C_{60}, ab initio molecular modeling calculations can be used to calculate more accurately the properties of the molecule. Haymet also suggested that the C_{60} structure proposed by Kroto et al. [6] is not unique. Stone and Wales [39] confirmed Haymet's proposition by showing that there are many stable C_{60} structures other than the icosahedral one proposed by Kroto et al. [6]. Stone and Wales also reported in the same paper that these alternate C_{60} structures are related to each other by transformations involving the movement of just two atoms as shown in Figure 2.7. These transformations, they determined, are thermally forbidden in the Woodward-Hoffmann sense (though photochemically allowed). Finally, Stone and Wales [39] suggested that the observed C_{60} mass peak is likely to arise from a mixture of isomers.

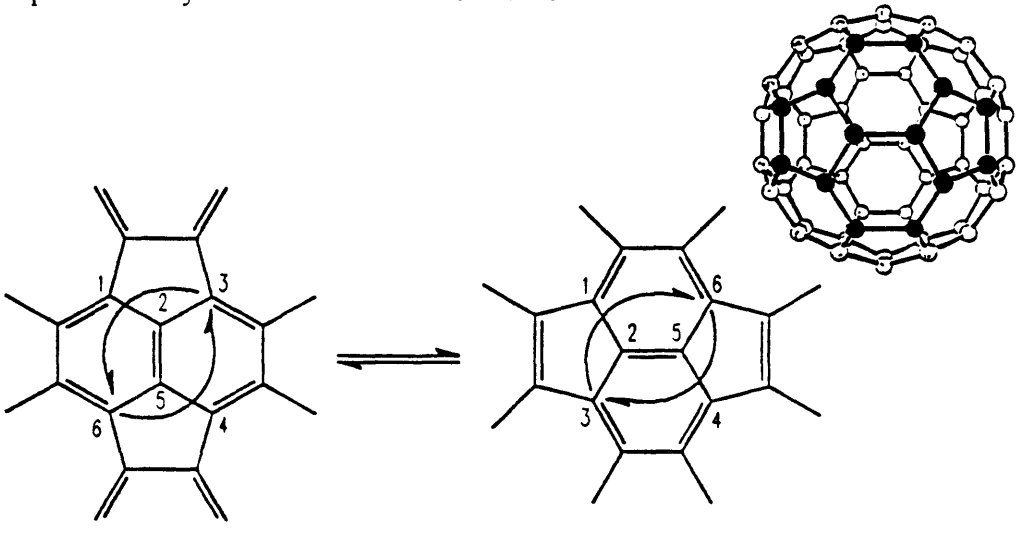

Figure 2.7 Stone-Wales Transformation of icosahedral C_{60} into a C_{60} isomer with adjacent pentagons

2.2.1 Fullerene structures

Schmalz et al. [49] studied possible carbon clusters made of 30-100 atoms. They identified six especially stable isomers of C_{60}. From Hückel HOMO-LUMO gap criterion, they found the truncated icosahedral isomer of C_{60} to have the largest HOMO-LUMO gap (0.7566) and therefore they expected it to be most stable.

However, they identified two more isomers of C_{60} that had positive HOMO-LUMO gap. Their results suggested that C_{60} isomers may exist naturally.

Bakowies and Thiel [50] reported results from extensive quantum calculations on C_{60} and many other clusters. The semi-empirical quantum calculations they used to optimize C_{60} structure include MNDO, AM1, INDO and PRRDO. They also performed ab initio SCF level calculations with STO-3G and double-ζ basis sets. They found that all theoretical methods suggest that buckminsterfullerene is more stable than other C_{60} isomers. Their results were consistent with many other reported results [39, 41, 42, 49, 51-56].

Coulombeau and Rassat [51] enumerated 71 isomers of C_{60} by repeatedly applying the Stone-Wales transformation on buckminsterfullerene C_{60}. Manopoulos et al. [57, 58] and Liu et al. [59, 60] enumerated all isomers of C_{60} and found the number of spectrally distinct isomers to equal at least 1812. These research results establish, that, at least from geometric viewpoint, C_{60} isomers are feasible.

As discussed in section 2.2, the buckminsterfullerene structure requires that each carbon bond to three neighbors. Since carbon's valency is four, one can deduce that C_{60} has thirty double bonds. The existence of double bonds in turn suggests that derivatives of C_{60} are feasible. Scuseria and Guo [61, 62], Cioslowki [63] and Dunlap et al. [64] have reported semi-empirical calculations on hydrogenated and fluorinated C_{60}. Matsuzawa et al. [65] studied C_{60} derivatives obtained by addition to double bonds radiating from a five membered ring. They found by using MNDO with PM3 parameterization, that the bond lengths near the vicinity of the adduct are longer and that the C_{60} derivatives are energetically feasible.

2.2.2 Computational Chemistry

Fullerenes have been extensively modeled with molecular mechanics and with semi-empirical quantum models. These modeling efforts have predicted a wealth of data about fullerenes. For instance, Wu et al. [66], Cyvin et al. [67], Stanton and Newton [68] and Weeks and Harter [69] have predicted the infrared spectra of C_{60}. Their

predictions were used by Krätschmer et al. [14] to discover fullerenes in laboratory produced carbon dust.

Other than predicting the spectroscopic data for fullerenes, modeling efforts have also predicted thermodynamic properties such as heat of formation [50, 53, 70-75] and the heat capacity of C_{60} [66, 68-69, 76-77]. These predictions have been experimentally evaluated and have been found to be, in most cases, satisfactory. For example, Beckhaus et al. [78] have predicted the heat of formation for C_{60} with MM3 molecular mechanics package. Their prediction of 574 kcal/mol is in excellent agreement with the reported experimental value of about 548 kcal/mol [78-81]. However, semi-empirical quantum models do not predict the heat of formation of C_{60} with the same accuracy as the MM3 package (see Table 2.2).

Source of data	Heat of formation kcal/mol	Specific heat cal/(mol K)
Experimental	548	128
MM3'92	574	134
PM3 (MOPAC)	812	105

Table 2.2 Thermochemical data for C_{60} at 298.15 K

Even though MM3 package predicts the thermochemical for C_{60} quite impressively, the package performs poorly in predicting other thermochemical properties, i.e., the entropy and the specific heat as a function of temperature. Furthermore, the MM3 package can not, yet, compute the thermochemical data for transition states. For these thermochemical data, the semi-empirical quantum models are the only practical alternative available (Table 2.2). For chemical kinetics purposes - where differential thermochemical properties between the reactants and the products is important - the semi-empirical quantum models are qualitatively reliable and effective. This is so, because the errors in predicting the absolute properties of each reactant and each product, tend to cancel when differential property for the reaction is calculated.

However, since the molecular mechanics packages such as MM3 and the semi-empirical quantum modeling packages such as MOPAC are at various stages of development, the modeling results have to be interpreted and used with prudence.

2.3 Fullerene Reactions and Kinetics Modeling

Wudl et al. [82] were amongst the first to report the chemistry of C_{60}. They reported that C_{60} readily reacts with a host of reactants including anthracene, furan and cyclopentadiene. Since the pioneering efforts of Wudl et al, numerous other fullerene reactions have been reported. Taylor and Watson have recently provided an excellent review [83].

Reactions and kinetics of sooting flames have been extensively studied because of their overwhelming commercial importance in areas such as internal combustion engines and furnaces. Over the years, numerous papers have contributed to the increased understanding of the flame reactions and to the modeling of soot formation mechanisms. McKinnon [31] has reviewed the sooting flame reactions and modeling literature. Pope et al. [33] have extended the flame chemistry to the formation of C_{60} and C_{70} in flames and discuss a kinetically plausible mechanism of fullerene synthesis from polycyclic aromatic hydrocarbons.

The presence of numerous reactive species in flames makes in-situ production of fullerene derivatives very plausible. Other than above mentioned work by Pope et al. [33] which discusses the formation of fullerenes per se, the actual chemistry of fullerene derivatives in flames, the mechanism behind the chemistry and the thermochemical modeling of the mechanisms is a new venue for research and at the time of publication of this thesis no results were known to the author of this thesis. Some modeling of non-flame fullerene chemistry, on the other hand, has been reported. Stanton [84], for example, performed semi-empirical calculations using MNDO and estimated the enthalpy changes of Stone-Wales transformation (Figure 2.7) to be 44 kcal/mol for a neutral C_{60} molecule.

Henderson et al. [85, 86] have reported semi-empirical and ab-initio modeling results for hydrogenation reactions on fullerenes. Their results suggest that semi-empirical calculations are not reliable predictors of the heats of formation of fullerenes and fullerene compounds.

For reactions between species other than fullerenes, Ventura [87] has provided an excellent overview of the state of art in modeling chemical reactions using molecular mechanics, semi-empirical quantum models and ab-initio models. Ventura's review suggests that computational chemistry has reached a state such that its use in the study chemical kinetics is possible and desirable. The results from this thesis confirm Ventura's optimism.

Chapter Three

Equipment and Experimental

3.0 Overview

The equipment and the experimental method used to accomplish the goals of this thesis are described in four sections:

3.1 The Synthesis
3.2 The Analysis
3.3 The Computational Chemistry
3.4 The Experimental Strategy

The synthesis section deals with the apparatus and the experimental method that was used to produce the thermally metastable fullerene studied by this thesis and to establish the facts about where in the flame does it form. The analysis section deals with the apparatus and the experimental method that was used to answer the questions: what is the identity of the thermally metastable molecule? and what is the nature of the thermally metastable fullerene? The computational chemistry section deals with the software and the hardware that was used to answer the questions: how does the metastable fullerene form? and why is the molecule thermally metastable? The experimental strategy describes the overall experimental strategy used by this thesis to answer the above questions in a systematic manner.

Each section is now described in detail.

3.1 The Synthesis

The synthetic apparatus used for this thesis' work was a combustion apparatus designed by McKinnon [31] for the study of polycyclic aromatic hydrocarbons and

soot in benzene/oxygen/argon flames. The combustion apparatus consists of the fuel and gas feed system, the burner system and the sampling system. These systems are described below along with the start up and the shut down procedure. Figure 3.1 schematically shows all these systems together.

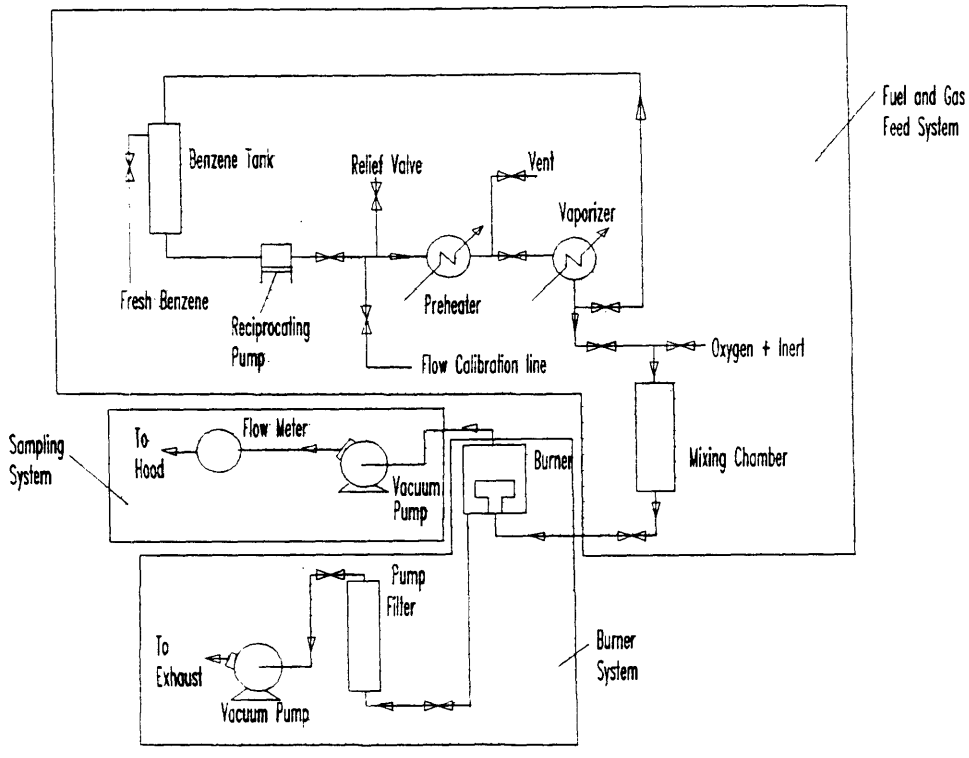

Figure 3.1 The Flame Process

3.1.1 The Fuel and Gas Feed System

The function of the fuel and gas feed system is to prepare and control the feed for combustion in the burner system (Figure 3.1). This system vaporizes the benzene,

premixes the fuel with oxygen and the desired inert in a desired ratio and then the system feeds the desired composition to the burner system at a precise flow rate.

Liquid benzene was pumped by ISCO Model LC-5000 syringe pump (for precise flow control) to a preheater with a pump head of 100 psig. The preheater's purpose was to provide for the sensible heat of benzene. The preheater was maintained at 85 °C and at 60 psig. The high temperature was achieved by electrical heating and was maintained by a temperature controller. The high pressure ensured that the benzene will not vaporize in the preheater. The preheated benzene then was flashed across a metering valve into a vaporization chamber. The vaporization chamber vaporized the preheated benzene by electrical heating and was maintained at 225 °C and held at 40 psig. In order to ensure high heat transfer rates, the chamber was filled with marbles. The vaporized benzene from the vaporization chamber was let down across a metering valve to a mixing chamber operating at slightly higher pressure than the burner system. The benzene vapor and a metered supply of oxygen and inert were mixed in the mixing chamber. The mixing chamber was also packed with marbles to enhance the mixing and was maintained at 95 °C to ensure that the benzene doesn't condense because of cold mixing chamber walls. From the mixing chamber, the premixed gases were fed directly to the burner system.

The gas (oxygen, ethylene and inerts) feed system consisted of securely fastened gas cylinders (Matheson, 1A size cylinders) with gas specific pressure regulators. The gases were supplied to the burner system at controlled rates by the use of critical orifice meters as described by McKinnon [31]. The essential principle to achieve controlled flow rate was to note that the mass flow through a critical nozzle is directly proportional to the upstream pressure. The orifice meters were calibrated for each gas in the manner suggested by McKinnon [31].

The startup procedure for the benzene vaporization system involved first letting the system heat up to the operating temperatures. Next benzene was pumped through the system in a vent mode. The vent mode required that the benzene vapor be vented from the fuel system just after the metering valve between the vaporizer and the mixing chamber. The vented benzene was recollected as liquid in a catch flask at atmospheric pressure.

All benzene handling piping material and vessels used were made of stainless steel or Teflon to avoid contamination of the fuel by dissolution process of the piping materials. The O-rings were made of Viton and were replaced every six month. All gas lines were made of thick walled Teflon. The orifices used for flow control were watch jewels. The system pressure was monitored with pressure transducer (Omega 240 series).

3.1.2 The Burner System

The premixed gases from the mixing chamber were fed to a flat flame burner system (Figure 3.2) as designed by McKinnon [31]. The burner system consisted of a combustion chamber, a burner, a burner positioner, an igniter and a vacuum pump. Each of these systems is described below.

The combustion chamber was constructed of stainless steel. The chamber had many radially mounted ports for viewing and probing access. The upper flange of the chamber was water cooled and acted as the primary sink for the flame heat.

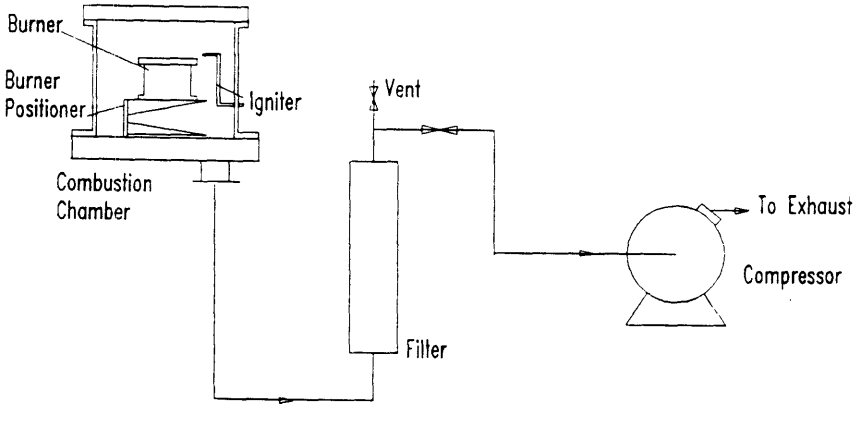

Figure 3.2 The flat flame burner system

The burner (Figure 3.3) was constructed out of copper and brass to enhance the heat transfer. The burner top was a 100 mm diameter by 12 mm thick drilled copper plate. The side walls of the burner were water cooled thus enabling a radially uniform low temperature during combustion.

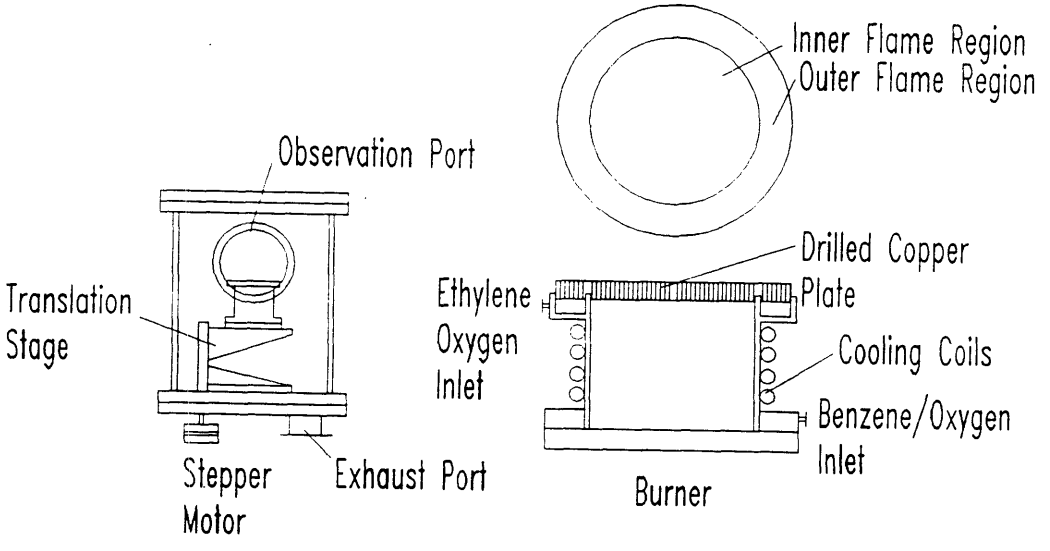

Figure 3.3 Schematic of the burner

The inner 70 mm of the burner surface was used for fullerene synthesis in flames and this flame was called the inner flame. The inner flame was stabilized with an annular 15 mm outer flame. The outer flame was a non-sooting ethylene flame that helped maintain radial temperature and concentration uniformity.

The inner cavity of the burner body was filled with stainless-steel wool that served two purposes. First, the wool quenched the flame in case of any flashback, thereby avoiding an explosion. Next, the wool provided a flow resistance greater than the drilled top plate that ensured a uniform flow distribution.

The burner positioner was a vertical translation stage coupled to a stepper motor. The translation stage allowed the precise setting of the distance between the burner plate and the sampling probe position vertically above the burner plate. Such a control of the sampling height above burner was essential to determine where in the flame is the thermally metastable fullerene formed. McKinnon [31] has discussed the design of the burner positioner extensively.

The igniter for flame startup was based on electric spark. The electric spark was generated using a tesla coil connected to a metal electrode inside the chamber. The electrode struck an arc to the side of the burner plate. The start up procedure involved first starting up a diffusion flame with the igniter, because a premixed vapor explodes on ignition. The diffusion flame was obtained by letting pure ethylene flow to outer part of the burner plate and letting pure oxygen flow to the inner part of the burner plate. Once the diffusion flame was on line, slowly the outer premixed flame was brought in line. Once the outer flame was stabilized, the desired premixed benzene/oxygen/inert feed was introduced to the inner part of the burner.

The vacuum pump provided the required low pressure in the combustion chamber. The pump was a large capacity (80 L/sec) vane type vacuum pump (Mannesmann-Demag Model WPSO 53). Critical flow was maintained across a valve in the vacuum line so as to ensure that oscillations in pump pressure would not propagate upstream to the chamber. The pressure in the chamber was controlled by a series of four manually controlled metering valves that bled air into the vacuum line. Each valve was attached to an orifice that allowed twice the air flow of the one just below it in the sequence. Such a combination gave a flexible control in the desired pressure range: 15 torr to 200 torr.

3.1.3 The Sampling System

The sampling system provided samples for determining where in the flame is the thermally metastable fullerene formed. The sampling system consisted of a probe, a

vacuum pump, and a gas flow metering system. Figure 3.4 shows the sampling system.

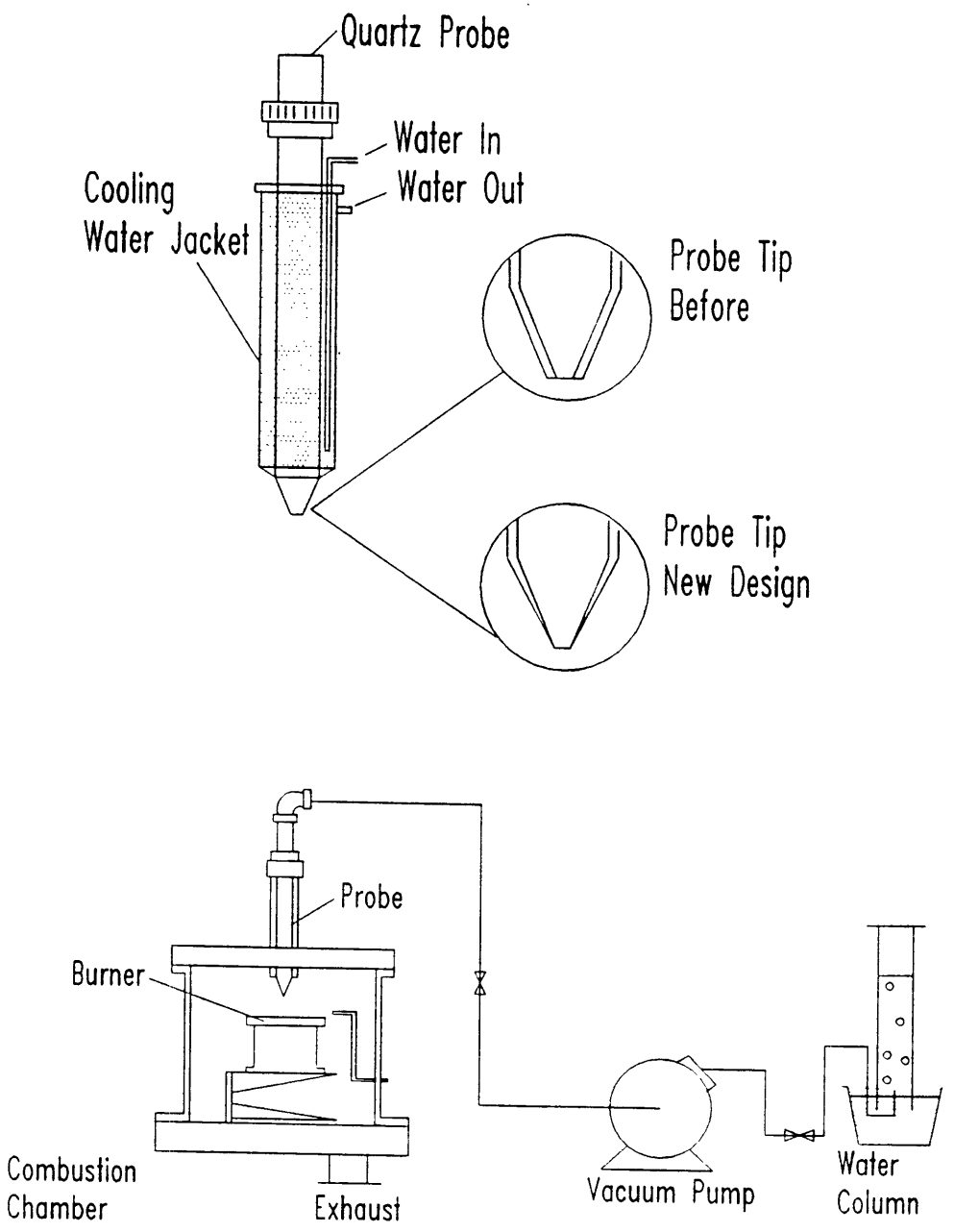

Figure 3.4 The sampling system

The probe's purpose was to convect a representative sample of the flame gases for analysis. In order to ensure that the sample was representative of the flame, it was essential to stop all reactions, i.e., quench the sample as soon as it enters the probe. Furthermore, it is essential that the presence of the probe be such that it has negligible effect on the flame chemistry (concentration, flow, temperature fields).

The probe assembly used for this thesis' work was of a modification of the design that had been successfully and repeatedly used in polycyclic aromatic hydrocarbon study by McKinnon [31]. Like the McKinnon's probe, the probe assembly consisted of a quartz probe surrounded by a copper cooling jacket as shown in Figure 3.4(a). The McKinnon probe which worked fine for mildly sooting flames, did not work well with highly sooting flames. Used without any modification, a rapid deposition of soot occured at the probe tip, which stopped all sampling in minutes. This thesis found that a minor modification to the McKinnon probe solved this problem. The modification was to eliminate any flow distorting flat surfaces at the probe tip. The probe used in this thesis was ground to an aerodynamic angle as shown in Figure 3.4(b).

The probe was surrounded with a water cooled copper jacket whose tip was about 15 mm above the tip of the probe. The orifice size of the probe used, ranged from 0.9 mm to 1.3 mm depending on the height from where the sample was collected. The larger orifice was used to avoid adverse effect on sampling flame region with higher soot loads. The probe wall thickness was as small as possible so as to minimize the distortion of the flame temperature profile. Such a distortion results from the heat sink at the probe tip because of conduction through the quartz wall. Another advantage of such a design is the ability to measure more accurately the flame temperature profile by pyrometric techniques such as the one described by McKinnon [31].

A vacuum pump (Sargent-Welch Model 1376) was used to withdraw flame samples from the flame. The exhaust of the pump went to an inverted water column that served as an integrating gas flow metering system. The vacuum pump was started up at least 1 hour in advance to drive off any condensed volatiles in the pump oil. The vacuum pump maintained a pressure of at least 2 torr in the probe, a pressure that was sufficient to ensure a pressure ratio of better than 20:1 across the probe tip. Such a pressure drop was needed to quench the flame gases as soon as they entered the

probe. The volumetric flow rate of the flame gases through the probe was determined using an inverted water column, whose readings were corrected for the pressure differential in the water column and for the saturation of the flame gases with water vapor because of the direct contact of the gases with water.

The samples were collected by trapping the soot entering the probe along with the flame gases. The trap consisted of a pyrex wool slug inside an aluminum foil and was placed inside the probe about 1 cm above the probe tip.

3.1.4 The Post Run Activities

After the run was over, the shut down procedure consisted of first isolating the sampling system. Next, the inner (benzene) flame was extinguished. This was followed by the extinguishing of the outer (ethylene) flame. Once all flames had been extinguished, the vent valves upstream of the main vacuum pump were opened so as to break the combustion chamber vacuum. Finally the main vacuum pump was shut off, which brought the combustion chamber up to the ambient pressure.

Once the combustion chamber's pressure was same as the ambient pressure, the sample in the probe was carefully removed and extracted in benzene. It was observed that the sample was collected on two surfaces: the pyrex wool plug collected the major part of the sample, while the probe walls (particularly the entrance region between the probe tip and the wool plug) collected a minor portion of the sample. The extraction procedure was established as follows: the probe plug rich in soot was removed and placed in 50 ml of benzene. Next, the soot deposit on the inner walls of the probe was wiped and washed with benzene and added to the probe plug containing sample. This solution was, next, sonicated for 5 minutes. The solution was then filtered. The plug and the filter paper were recovered from the filtration step and placed again in 50 ml of benzene and the extraction procedure repeated. The analysis of the two solutions showed that more than 99% of the sample gets extracted during the first extraction. These extraction results were reproduced so as to eliminate any sources of systematic experimental error. The final extraction procedure for the wool plug that was used for

achieving the goals of this thesis, consisted of just the first extraction and sonication step. For analysis work, the sonicated extract was filtered and was concentrated under a stream of nitrogen from an original volume of about 75 ml to about 5 ml. The concentration step allowed the detection of many minor constituents in the sample that would otherwise be below detection limit for the analytic methods described below.

3.2 The Analysis

Two of the major objectives of this thesis were to establish the identity of one of the many thermally metastable fullerenes in premixed flames; and, to learn about the nature of the thermally metastable fullerene studied by this thesis. This thesis accomplished these objectives by the systematic use of following analytical methods and apparatus: High Performance Liquid Chromatography (HPLC), Preparative Column Chromatography, Ultraviolet-Visible (UV-Vis) Spectroscopy, Mass Spectrometry (MS), Fourier Transformed Infra Red (FTIR) Spectroscopy, Nuclear Magnetic Resonance (NMR) Spectrometry and Chemical Tests. Each of these methods is discussed below.

3.2.1 High Performance Liquid Chromatography

A high performance liquid chromatograph (HPLC) uses adsorption to resolve a feed mixture into constituent components. An HPLC is made up of four parts:

- The sample injection system that injects the feed mixture and pumps solvent to elute the sample through the column
- The column that provides the necessary adsorption media for separation of components in the feed mixture
- The detector that detects the components in the effluent of the column
- The data acquisition system that translates the detector output into useful information.

This thesis used HPLCs for two purposes -- for analysis and for preparative separation of fullerenes in the flame soot samples. For the analytical purposes of this thesis, toluene extracts of soot samples were studied using a Hewlett-Packard 1090 HPLC equipped with a ternary pumping system and diode array detector. The instrument was controlled with a model 7994 Analytical Workstation. The HPLC column was 25-cm long x 4.6-mm I.D. packed with 5-μm particles of Nucleosil (Macherey-Nagel, Duren, FRG) octadecylsilyl bonded C-18 silica having 30-nm pores. A binary non-aqueous mobile phase of acetonitrile and dichloromethane was used in a gradient elution mode. The mobile phase program consisted of a linear increase in dichloromethane concentration from 10 minutes at 100% in 40 minutes with a holding time of 10 minutes at 100%. The flow rate was 1.0 ml/min.

The HPLC column was calibrated with pure C_{60} and pure C_{70}. The calibration was reproduced twice so as ensure the validity. Standard samples and blanks were run before and after a batch of runs to check for any possible malfunction.

The HPLC start up procedure consisted of equilibrating the column for at least two hours with 100% acetonitrile. After the equilibration, 150 μl of a sample was injected into the injection loop, out of which 50 μl of the sample entered the HPLC column (the excess flushed the injection looped). The chromatogram and the absorption spectra were collected with the Hewlett-Packard model 7994 Analytical Workstation software. The detection limit for any species with this equipment and method, in terms of ansorbance area, was 35 mAU.

3.2.2 Preparative Column Chromatography

The facts collected with HPLC were not sufficient to determine the identity of the thermally metastable fullerene. In order to obtain the additional required information (for instance from ^{13}C NMR analysis) it was essential to purify milligram quantities of the thermally metastable fullerene. This was accomplished by using preparative scale column chromatography.

The preparative column chromatography was performed in three steps. First a fresh batch of soot extract was separated into three fractions with a 22 mm inner diameter, 30 cm long poly(divinylbenzene) column (Jordi Gel 500, Jordi Associates, Bellingham, MA). The second fraction from the Jordi Gel column was re-separated into three fractions with a semi-preparative Nucleosil octadecylsilyl-bonded silica C-18 column 25-cm long, 1.0-cm inner diameter packed with 7-μm material having 6-nm pores. The second fraction from the C-18 column was re-polished, finally, on a preparative Hypersil ODS octadecylsilica (C-18) column as discussed by Anacleto et al. [32]. This three step purification was done in order to assure that the purity of the thermally metastable fullerene was as high as possible.

For the Jordi column based preparative separation, a ternary non-aqueous mobile phase of acetonitrile, dichloromethane and benzene was used in a gradient elution mode. The mobile phase program consisted of the following: the column was equilibrated in 40% acetonitrile, 60% dichloromethane mix, 4 ml/min flow rate. After injection, the eluent composition linearly increased in dichloromethane concentration in 2 minutes to 100%, the flow rate linearly increased to 8 ml/min, with a flow rate holding time of 4 minutes at 100%. Next, the composition of the eluent was linearly changed to 50% benzene, 50% dichloromethane in 2.5 minutes. After the composition change to 50% benzene, the flow rate was linearly reduced to 4 ml/min in 7.5 minutes; which was followed by a linear composition change to 100% benzene in 20 minutes. The 100% benzene elution was held for 5 minutes, after which the composition was linearly changed to 100% dichloromethane in 6 minutes. Finally, the composition was brought to the equilibration composition in 5 minutes. The total run time was 52 minutes, and the re-equilibration took less than 15 minutes.

For the C-18 column based preparative separation, a binary non-aqueous mobile phase of acetonitrile and dichloromethane was used in a gradient elution mode. The mobile phase program consisted of a linear increase in dichloromethane concentration to 78% in 5 minutes, then a further linear increase in dichloromethane concentration to 92% in 4 minutes; and then a final linear increase in dichloromethane concentration to 100% in an additional 20 minutes. The 100% dichloromethane elution was held for 3 minutes. This was followed by a linear change to the starting composition (100%

acetonitrile) in 3 minute. The flow rate was 4.0 ml/min during all stages of elution and the total run time was 34 minutes.

For the final Hypersil based preparative purification step, the mobile phase was initially acetonitrile/dichloromethane (50:50), programmed linearly to 100% dichloromethane over 15 minutes, held for 10 min and then programmed back to the initial composition over 5 minutes. The total run time was 30 minutes, and the equilibration took about 15 minutes. The eluent flow rate was constant at 4 ml/min.

The samples were injected manually using a syringe. The separated fractions were collected using an auto-sampler. The auto-sampler was programmed to collect all the fractions in separate vials at pre-determined time levels.

3.2.3 Ultraviolet-Visible Spectroscopy

The UV-Visible spectrum of a molecule is the result of electronic transitions in a molecule in presence of UV-Visible light. Since the origin of the UV-Vis spectrum lies in the molecular orbitals, the UV-Vis spectrum of a molecule depends on the molecule as a whole.

The UV-Visible spectroscopy is a useful method to study structural differences between molecules. That is, if two molecules have different UV-Vis spectra, then these molecules have different structures. However the reverse is not essential true, for two different molecules may have the spectra that are indistinguishable. There are many other applications of UV-Vis spectra such as those mentioned by McKinnon [31].

This thesis work obtained UV-Vis spectra for different samples in two ways. Whenever possible, the UV-Vis spectra were obtained with a diode array detector that was on line with the Hewlett Packard model 1090 HPLC. Alternatively, the UV-Vis spectra were obtained using a Hewlett-Packard model 8450A diode-array spectrophotometer with a 7225B plotter and 9121B disc drive. With the spectrophotometer, ultra-pure glass distilled decahydronaphthalene (decalin) was used

as the solvent in order to ensure adequate dissolution and to minimize any absorbency interference by the solvent in the UV region.

3.2.4 Mass Spectrometry

Mass spectrometers are tools of choice if one needs to determine the molecular weight of the species in a sample. Essentially, mass spectrometers are made up of four integrated units:

- The vaporizer that vaporizes the species in a sample
- The ionizer that ionizes the vaporized species
- The mass analyzer that magnetically resolves the ions by the charge/mass ratio
- The detector that senses the magnetically resolved ions
- The data acquisition system that translates the sensed ions into useful data

The facts obtained by using a mass spectrometer are suspect if either of above units have the potential of destroying the integrity of the sample. For instance, if the vaporizer can thermally degrade the sample or if the ionizer can fragment the vaporized species, the results obtained from the mass spectrometer require prudent interpretation.

Numerous design attempts have been made by mass spectrometer designers so as to take care of these problems at the conceptual stage. Thus, there are mass spectrometer designs that use thermal vaporization methods versus other designs that use laser vaporization techniques; and there are mass spectrometer designs that use charge impact methods of generating ions versus other designs that use charge transfer techniques. In the charge transfer methods, such as the ionspray, the ionization is very soft in the sense that the fragmentation problem is, in all known cases, eliminated.

This thesis used facts collected on three different mass spectrometers. The first source of facts was from a specialized mass spectrometry set up described in the work of Anacleto et al. [32, 37-38]. Briefly, the data was obtained from a charge transfer ionspray based mass spectrometer in tandem with a high performance liquid chromatography (HPLC/MS); and a HPLC/MS in tandem with another mass

spectrometer (HPLC/MS/MS). More details about this mass spectrometry can be found in Anacleto et al. [32]. The second source of facts was from an electron impact based mass spectrometer (EI-MS). The last source of facts was a time-resolved mass spectrometry at Naval Research Laboratories, Washington DC, USA.

The interpretation of all the facts collected during this thesis work with the use of mass spectrometers, were hampered by the observed thermal metastability of the fullerene being studied. Nevertheless, the mass spectrometers provided useful observations that any proposed structure must explain. This thesis used the observations in mass spectrometers to eliminate any inconsistent hypotheses about the identity and the nature of the thermally metastable fullerene studied.

3.2.5 Fourier Transformed Infra Red Spectroscopy

The infrared spectrum is one of the more characteristic properties of any given compound. An infrared spectrum is observed when a sample is irradiated by infrared light (wavelength, 2.5 to 50 μm). The physical principle behind the infrared spectrum emanates from the following facts [88]:

- all molecules are made up of atoms linked by chemical bonds
- all atoms in a molecule vibrate
- all the vibrational energies are quantized
- the quantized nature implies that a frequency corresponding exactly to that required to raise the energy level of a bond will be absorbed by the molecule
- for bond energies, such frequencies lie in the infrared range; therefore, a sample when exposed to infrared beam, absorbs certain frequencies and the transmitted beam shows the absence of these specific frequencies -- i.e., the infrared spectrum.

The exact infrared spectrum is affected by the whole molecular environment. However, a useful and unique feature of the infrared spectrum is that the spectrum is primarily dependent on the particular bond and its immediate neighbors. Thus, infrared absorption frequencies for C-C, C-O and C-N vibrations always appear between 600 cm^{-1} and 1200 cm^{-1}; the absorption frequencies for C=C, C=O, C=N vibrations always

appear between 1200 cm^{-1} and 1900 cm^{-1}; the absorption frequencies for alkyne bond stretching frequencies appear between 2000 cm^{-1} and 2400 cm^{-1}; and the absorption frequencies for C-H, N-H, O-H stretching frequencies appear between 2800 cm^{-1} and 3600 cm^{-1}.

The unique relation of the infrared spectrum to particular bonds in the molecule makes the infrared spectrum useful for two purposes. First, it can be used to establish the absence of bond types (functional groups) if no peaks appear in the region where the peaks would otherwise be expected. Secondly, the spectrum can be used to generate systematic hypotheses of alternative bond types that the molecule may be made up of. However, while generating alternate hypotheses one needs to remember, that, the infrared spectrum represents the entire sample and not just the unknown molecule in the sample. That is, the infrared spectrum contains peaks from any impurities that may be present in the sample along with the molecule of interest. Thus, the presence of an infrared peak in the infrared spectrum is not, all by itself, a proof of existence of a bond in the unknown molecule.

This thesis used the infrared spectrum for both purposes - to establish the absence and to hypothesize the presence of functional group types in the thermally metastable fullerene being studied. The infrared spectrum was obtained from a Perkin Elmer series 1600 FTIR spectrophotometer. The scan range was 400 cm^{-1} to 4000 cm^{-1} with a resolution of 2.0 cm^{-1}. Sixty-four scans were taken for each sample and sixteen scans were taken for the background. The samples were prepared on a KBr disc by evaporating saturated solution of the sample in benzene under a stream of nitrogen. The sample was analyzed before and after the FTIR in the HPLC discussed above. This step ensured that the FTIR experiments did not change the identity of the thermally metastable fullerene during the course of the experiments.

3.2.6 Nuclear Magnetic Resonance Spectroscopy

Nuclear magnetic resonance (NMR) spectrum is a characteristic property of molecules with one or more nuclei that have non-zero nuclear spin. The NMR spectrum is the spectrum that is observed when a sample is placed in a strong magnetic

field and is subjected to a radio-frequency field. NMR spectroscopy differs from Infrared and UV-Vis spectroscopy in that NMR studies nuclei and not vibrating molecules or π-electron transitions.

The physical principle behind NMR spectroscopy emanates from the following facts [89]:

- The nuclei of certain isotopes possess an intrinsic angular momentum (non-zero nuclear spin)
- The atomic nuclei are also associated with an electric charge (protons)
- A charge with non-zero angular momentum behaves like a minute bar magnet the axis of which coincides with the axis of the spin
- Quantum mechanics suggests that the tiny proton magnet is restricted to just two spin states of quantum number +1/2 and -1/2 and that these spin states correspond to two different energy states
- A strong magnetic field can separate nuclei into two nearly equal populations representing the two different energy states
- Energetic transitions can be induced between two different energy states in an atom if the atom is placed in an electromagnetic field of suitable wavelength (for NMR, this is radio frequency)
- Systematic electronic transitions can be sensed as an absorption spectrum

The exact NMR spectrum depends not only on the physics of each individual nucleus, the exact spectrum also depends on environmental effects such as

- The modification of magnetic field because of the induced diamagnetic electronic currents (the chemical shifts)
- The effect of spin-spin coupling between nuclei
- The effect of any rapid inter-molecular or intra-molecular exchange of protons (the exchange effects)

Many different types of NMR spectroscopy exist. To name a few examples: the proton (^{1}H) NMR, the carbon-13 (^{13}C) NMR, the fluorine (^{19}F) NMR. The proton NMR can be used to identify the existence of protons in a molecule and to determine the relative

nature (hybridization for instance) of the protons in the molecule. The carbon-13 NMR is extremely useful for determining the structure of molecules containing carbon. Naturally occurring carbon is mostly made up of carbon-12 and carbon-13 isotopes, the later occurring with a 1.1% abundance. As mentioned above, NMR spectra depend on the nuclei and the overall nuclear environment. This implies that nuclei with identical nuclear environment absorb precisely the same wavelength. Therefore, carbon-13 NMR in combination with structural symmetry rules is a powerful method of establishing a carbon based molecule's identity. For example, in case of buckminsterfullerene (C_{60}) all carbon nuclei have identical nuclear environment and therefore the carbon-13 NMR is expected to have just one NMR peak. This has been confirmed by experimental results [15].

The proton NMR spectrum, like infrared spectrum, requires careful interpretation if the observations are being used to generate alternative hypotheses about the final structure. One needs to remember that the NMR spectrum represents the entire sample and not just the unknown molecule in the sample. That is, the NMR spectrum contains peaks resulting from any impurities that may be present in the sample along with the molecule of interest. However, carbon-13 NMR has a feature that is particularly valuable in studying the structure of any molecule. The feature is this: the absorption peak height for a nucleus in a distinct nuclear environment is directly proportional to the concentration of the particular nucleus in the sample. Thus, if the concentrations of the impurity nuclei are orders of magnitude lower than the relative concentration of the nuclei being studied, the NMR spectrum effectively consists entirely of peaks from the molecule of interest.

This thesis used the proton NMR and the carbon-13 NMR in order to determine the identity of the thermally metastable fullerene. Both, the proton NMR and the carbon-13 NMR spectra, were obtained from a Bruker NMR machine. The samples were prepared from the purified fraction (more than 98% pure on absorbance area basis) obtained from the three step purification method using preparative chromatography described above. First the purified sample was dried under nitrogen and washed (re-dissolved and re-dried to remove any trace of benzene or toluene) thrice in dichloromethane. The washed and dried sample was finally dissolved in deuterated 1,1,2,2 tetrachloroethane and chromium acac was added as relaxant.

3.2.7 Chemical Tests

Chemical tests are based on chemical properties of the sample. Chemical tests are useful methods that can be used to eliminate incorrect hypotheses and to discover the nature of an unknown molecule. Furthermore, often, the spectroscopic techniques are expensive and time consuming. Chemical tests are comparatively more economical and much faster. However, the chemical tests (particularly for organic molecules) have poor selectivity and the results from chemical tests with unknown molecules are suspect because the unknown molecule could behave differently. Therefore, results from chemical tests have to be interpreted with prudence.

This thesis used to one chemical test during its investigations. The test was based on the results of Creegan et al. [90] who reported a simple and fast method of converting the epoxide of C_{60} to C_{60}. Creegan et al. [90] reported that the epoxide of C_{60} converts to C_{60} with conversion yields of greater than 90% in a single pass through a neutral alumina chromatographic column. For this thesis work, 10 ml of a sample containing the thermally metastable fullerene (98% pure by absorbance area basis) was split into two 5 ml units. One of these was used as standard and the other was mixed with neutral alumina. The sample was kept in contact for 1 hour at room temperature. A part of this treated sample was analyzed using the analytical HPLC method. The rest of the treated sample was warmed with neutral alumina (40 °C) for 20 minutes and then analyzed using the HPLC. These analyses were compared with the analysis of the standard sample to determine the effect of neutral alumina on the thermally metastable fullerene.

3.3 The Computational Chemistry Software

Computational chemistry is rapidly becoming a tool to model complex molecules. The modeling provides good estimates for the molecular structure, thermodynamic properties, vibrational spectra, transition state location, reaction path coordinates and

many other data of engineering interest. This thesis used computational chemistry at many junctions as described later.

Computational chemistry can be crudely classified into three modeling groups:

- The Molecular Mechanics Models
- The Semi-empirical Quantum Models
- The Ab-initio Models

For all these methods the starting point is the famous Schrödinger equation of quantum mechanics. The ab-initio models (not used by this thesis) attempt to solve the Schrödinger equation as such, while the other two models begin with the commonly used Born-Oppenheimer approximation of quantum mechanics. The Born-Oppenheimer approximation states that the Schrödinger equation for the molecule can be separated into a part describing the motions of the electrons and a part describing the motions of the nuclei, and that these two sets of motions can be studied independently.

Ab initio methods often make fixed nuclei, independent particle approximations and many times the Born-Oppenheimer approximation. However unlike other models, the main advantage of the ab initio methods is that they do not rest on any of approximation that can not be reversed if need arise; no empirical parameters are built into ab initio methods, no integrals simplified and no equations modified on the basis of subjective guesses [91]. On the other hand, molecular mechanics models and the semi-empirical quantum models, the simplifying approximations are built into the model. The main difference between the molecular mechanics models and the semi-empirical quantum models is this: in molecular mechanics the motions of nuclei are studied and the motions of the electrons are not explicitly examined at all; in semi-empirical quantum models the motions of the electrons are also examined, however with many integrals simplified and equations modified so as to make the calculations manageable.

The weakest point of ab initio methods is the need to use a set of known functions to describe the potential energy surfaces (the basis set). Ventura [87] discusses this problem and the numerous attempts to solve this problem in detail. Furthermore, for

macromolecules like fullerenes, the computational needs for ab initio calculations were prohibitive. This thesis, therefore, did not use the ab initio methods. Molecular mechanics models and the semi-empirical quantum models are simpler and are computationally manageable. The molecular mechanics and the semi-empirical quantum models are briefly described below.

3.3.1 The Molecular Mechanics Models

Molecular mechanics models build on a force field that is derived based on classical mechanics model of nuclear interactions. For instance, motions such as stretching, bending and torsion are modeled with quadratic potentials; van der Waals type environmental interactions are studied by including expressions in several of the equations [87]. Such a classical mechanics model provides many advantages such as simplicity, speed and feasibility of computer graphics. However, the reliability of the molecular mechanics models to a novel class of molecules such as fullerenes is questionable. The reliability of molecular mechanics models to any molecule is dependent on the list of atoms and types of interaction that was used to derive the force field. Since no known molecular modeling software is based on the closed cage three dimensional interactions present, results obtained from molecular modeling software require prudent usage. The reliability limitation inherent in molecular modeling software is, however, being overcome by the recent developments in the form of MM3 by Burkert and Allinger [91]. The MM3 model is no longer purely empirical but explicitly uses ab initio experimental results along with experimental data so as to determine the parameters for non-bonded interactions. At the time of publication of this thesis, developments such as those being pioneered by Allinger were still in progress.

This thesis extensively used MM3 developed by Allinger group [91]. This usage was encouraged by the fact that MM3 software predicts the heat of formation for C_{60} within 10% error range. However, the predictions for the vibrational spectra of C_{60} were inconsistent with experimental observations. Similarly, the thermochemical properties (entropy, specific heat) predicted by MM3 did not agree with the experimental observations. The results are discussed in a separate chapter.

3.3.2 The Semi-empirical Quantum Models

Semi-empirical models simplify the complexity of ab initio methods by neglecting equations, introducing empirical parameters instead and then fitting these empirical parameters with experimental data. On the basis of the approximations and the simplifications made, many different semi-empirical quantum modeling software have been proposed. The most commonly used amongst these, particularly for the study of chemical reactions, are MNDO/AM1 (Modified Neglected Differential Overlap/ Austin Model 1) and MNDO/PM3 (Modified Neglected Differential Overlap/ Perturbation Molecular Orbital 3). Both of these software are available within MOPAC from QCPE, Indiana University.

MNDO/AM1 has been developed by Dewar et al. [92] and uses experimental heats of formation at room temperature to adjust the empirical parameters. However, despite many applications [93-97], AM1 has been shown to give results in hydrogen bonding systems that experimental observations do not support.

MNDO/PM3 has been developed by Stewart [98] and its development involved an extensive re-parameterization of AM1. The heats of reactions predicted by PM3 have been shown to be better than those predicted by AM1 or MNDO [87]. PM3 also corrects many of the AM1's flaws in chemical reactivity. However, PM3 too has some problems such as predicting a non-planar structure for glyoxal. [87]. Therefore, PM3 results too have to be used with prudence.

In summary, no semi-empirical quantum modeling software is reliable in all situations. For fullerenes, neither AM1 nor PM3 have been parameterized specifically and therefore the results predicted by both for fullerenes are more questionable.

3.3.3 Thermochemistry

The development of chemical kinetic models require the knowledge of the thermochemical properties of the species involved in the model; in particular, the following thermochemical properties: the enthalpy of formation, the entropy and the

specific heat as functions of temperature. If the chemical kinetics model uses transition states, then a knowledge of the transition state geometry is equally important. The thermochemical properties and the transition state can be calculated using computational chemistry. The thermochemical properties can be obtained from the force field calculations and the quantum mechanics based models. The following thermodynamic equations (for a detailed discussion, see Boudart [99] and Benson [100]) combined with the modeling results provide sufficient infrastructure to predict the equilibrium constant of the following bimolecular reaction:

$$C_{60} + X \leftrightarrow C_{60}X$$

$$K_p = k_f / k_b = \exp(-\Delta G(T)/RT)$$

$$\Delta G(T) = \Delta H(T) - T\Delta S(T)$$

$$\Delta H(T) = \Delta H(T_o) + \int \Delta C_p(T)\, dT$$

$$\Delta S(T) = \Delta S(T_o) + \int (\Delta C_p(T)/T)\, dT$$

$$K_c = K_p * R'Te$$

where,

K_p: equilibrium constant in pressure units, atm^{-1}

K_c: equilibrium constant in concentration units, ltr/mol

k_f: forward rate constant, $atm^{-1}\ sec^{-1}$

k_b: reverse rate constant, sec^{-1}

T: temperature, K

$\Delta G(T)$: Gibbs free energy change during the reaction as a function of temperature, cal/mol

$\Delta H(T)$: Enthalpy change during the reaction as a function of temperature, cal/mol

$\Delta S(T_o)$: Entropy change during the reaction as a function of temperature, cal/mol/K

$\Delta C_p(T)$: Heat capacity change during the reaction as a function of temperature, cal/mol/K

R: Gas constant, (=1.987 cal/mol/K)

R': Gas constant, (=0.082 atm ltr/mol/K)

e: natural logarithm base, (=2.718)

The rate constants can be predicted using the transition state theory [99]. For the C_{60} adduct formation, for instance, the following reaction may be conceptualized:

$$C_{60} + X \leftrightarrow [C_{60}X]^{\ddagger} \rightarrow C_{60}X$$

According to the transition theory, the rate of reaction can be given by

$$d[C_{60}X]/dt = (\kappa k_B T/h)[C_{60}X]^{\ddagger}$$

where,

[Z]: Concentration of species Z, atm

$[Z]^{\ddagger}$: Concentration of the activated (transition state) species Z, atm

d[Z]/dt: Formation rate of Z, atm/sec

κ: Transmission coefficient, usually taken to be 1.

k_B: Boltzmann's constant, cal/K

T: Reaction temperature, K

h: Planck's constant, cal sec

Since the transition state is considered to be in equilibrium with its component molecules in the transition state theory, we have

$$K_p^{\ddagger} = [C_{60}X]^{\ddagger} / [C_{60}][X]$$

Combining this expression, the rate expression and

$$K_p^{\ddagger} = \exp(-\Delta G^{\ddagger}(T)/RT)$$

$$\Delta G^{\ddagger}(T) = \Delta H^{\ddagger}(T) - T\Delta S^{\ddagger}(T)$$

gives the following equation

$$d[C_{60}X]/dt = (\kappa k_B T/h)\exp(-\Delta S^{\ddagger}/R)\ \exp(-\Delta H^{\ddagger}/RT)\ [C_{60}][X]$$

Thus, the activation energy and the pre-exponential factor in the Arrhenius equation can be given by:

$$A = (\kappa k_B T/h)\exp(-\Delta S^{\ddagger}/R)$$

$$E_a = \Delta H^{\ddagger}$$

where,
A: Pre-exponential factor, $atm^{-1}\ sec^{-1}$
E_a: Activation energy, cal/mol

The above equations imply that the rate constants can be predicted using transition state theory, if one could predict the thermochemical properties of the transition state. The thermochemical properties of the transition state can be predicted with the molecular modeling software discussed above, if the geometry of the transition state can be determined. With recent advances in computational chemistry, the geometry of the transition state can be determined. Specifically, modeling options in semi-empirical quantum packages (MOPAC) permit the determination and optimization of the saddle point (transition state) and the calculation of thermochemical properties for the optimized transition state. There are many ways to determine the saddle point using the MOPAC package. One way is to let the program determine the saddle point all by itself. This method is extremely slow and often leads to an energy minima that is not a saddle point. Alternatively, a guess structure can be specified which is evaluated and further refined by the program; the guess structure can be based on results from ab-initio heuristics or the guess structure can be based on the structure of a transition state from a similar reaction. Regardless of the calculation strategy used, one can determine whether the saddle point found is a true transition state by studying the vibrational frequencies of the saddle point. The transition state has exactly one

imaginary frequency, while hill top saddle points have more than one imaginary vibrational frequencies.

This thesis used the PM3 package (MOPAC) to determine the transition state structure, the vibrational frequencies and the thermochemical properties of the transition state. However, the results of these efforts - contained in the later part of this thesis - are to be taken with prudence as the MOPAC packages are still in the development stages and have in no way been evaluated for accuracy as far as fullerene chemistry is considered. The results from modeling software, as always, need to be checked against experimental facts. If the results of this thesis are any indication, the performance of computational chemistry packages in modeling chemical kinetics is full of potential and promise.

3.4 The Experimental Strategy

As mentioned in sections 3.1 and 3.2, the unequivocal identification of the metastable fullerene required collecting milligram quantities of the metastable fullerene in as pure state as possible. This task was formidable at the beginning because the concentration of the metastable fullerene in the flame soot was small (less than 0.05% by soot weight on 330 nm absorbance area basis). Furthermore, the procedure for prep scale purification of the metastable fullerene was unknown. The best alternative available at the beginning was the simple scaling up of the HPLC analytical method to prep scale. Such a prep scale would allow injection of 1 ml of fullerene saturated solution per run. Since the solubility of fullerenes in toluene was low (3 mg/ml) [101], and the relative concentration of the metastable fullerene with respect to C_{60}+C_{70} was less than 1% by weight, this implied that the best production rate achievable for purified metastable fullerene was about 25 micrograms per run. Thus, in order to collect 25 milligrams of the sample, about 1000 separation runs had to be done. With a 2 hour run time, this implied a 2000 man hours investment.

Instead of investing the 2000 man hours required, this thesis followed an alternate experimental plan that accelerated the accomplishment of the research objectives.

First, a study was made that discovered the operating conditions for the flame that increased the relative concentration of the thermally metastable fullerene in the fullerene rich soot. Secondly, a purification method was developed so as to maximize the product yield and product purity per unit man hour invested. The strategy used for both of these studies is described below.

The modeling of metastable fullerene using computational chemistry software was performed in parallel with the experimental effort. The results obtained from the modeling effort were instrumental in interpreting the experimental data. Furthermore, modeling provided a basis to propose and evaluate a mechanism for the thermal metastability of the unknown molecule.

3.4.1 Optimizing the Flame

The objective of optimizing the flame during this thesis' work was to maximize the relative concentration of the thermally metastable fullerene in the fullerene mix. The required effort to accomplish this objective was simplified when an observation was made that the yield of the metastable fullerene is positively correlated to the yield of C_{60}+C_{70} in flame. Given this fact, the general optimization strategy used was to first identify the set of independent variables in the process and then to study the effect of varying them one at a time on the yield of C_{60}+C_{70} in flame. The independent variables that were varied in this study were:

1. C/O atomic ratio, defined as the value of carbon to oxygen atomic ratio in the mixture fed to the burner
2. Burner velocity, defined as the cold (298 K) standard gas velocity of the mixture on the burner surface
3. Burner pressure, defined as the combustion chamber pressure as measured during the process
4. Inert concentration, defined as the molar concentration of the inert in the mixture fed to the burner
5. Inert type, defined as the inert's identity in the feed mixture. That is, whether the inert was argon, helium or nitrogen.

The next chapter presents the observed correlation between C_{60}+C_{70} yield and the yield of the thermally metastable fullerene. The next chapter also presents the results from the above study with independent variables.

3.4.2 Optimizing the Purification Method

As mentioned earlier, chromatography was the method used to purify milligram quantities of the thermally metastable fullerene for the purposes of this thesis. To accelerate the accomplishment of the thesis objectives, a chromatographic process was developed that maximized the purification rate. This process development was based upon a set of heuristic rules. The heuristics used were (*ceteris paribus*):

1. Select process conditions that minimize the time interval between distant peaks.
2. Maintain a minimum resolution time interval of 30 seconds between two peaks (to avoid sample contamination).
3. Once the molecule of interest has been collected, accelerate the elution of all other peaks.
4. Equilibrate the chromatographic column for the minimal time interval essential.
5. Change flow parameters if necessary; however, avoid solvent shocks or flow shocks to the column.

Again, as in the case of the flame, first a set of independent variables were identified for the purification process. Next, these independent variables were varied in accordance with above heuristic rules and the process that maximized the purification rate was chosen. The independent variables that were utilized during this thesis were:

1. The elution rate.
2. The solvent gradient; that is the rate of change of the concentration of a particular solvent in the eluent fed to the column.
3. The volume of saturated solution loaded per run.
4. The type of adsorption column used (C-18 silica, gel permeation).

The results observed by varying these process parameters are presented in the next chapter. The purification process that maximized the purification rate is described in section 3.2.2 and the chromatograms observed are presented in the next chapter.

Chapter Four

Experimental Results and Discussion

4.0 Overview

The experimental results obtained during this thesis work are described in four sections:

4.1 The Flame
4.2 The Purification Method
4.3 The Characterization
4.4 The Species Profile in the Flame

The first section on flame presents the evidence that the yield of the thermally metastable fullerene is correlated to the yield of C_{60}+C_{70}. This section also presents the effect on the yield of C_{60}+C_{70} with changes in the independent variables in the flame process. The second section presents the experimental observations during the development of the purification method. The third section presents the results from the characterization effort that established the true identity of the thermally metastable fullerene studied by this thesis; and the final section presents the results from the study that sought to answer: where in the flame is the thermally metastable fullerene formed? Each of these sections is now described in sequence.

4.1 The Flame

4.1.1 Correlating C_{60}+C_{70} Yield with Yield of Thermally Metastable Fullerene

Figure 4.1 shows the relationship between C_{60}+C_{70} yield and the relative abundance of the thermally metastable fullerene in the soot collected on the burner walls (the

data used for plotting Figure 4.1 is presented in Appendix A). The relative abundance of the thermally metastable fullerene is computed from the 330 nm absorbance of the thermally metastable fullerene. If we assume the yield of the thermally metastable fullerene to be proportional to the 330 nm absorbance of the thermally metastable fullerene (exact determination of the yield was not possible because of the non-availability of the pure standard), then the figure suggests that the conditions that favor the formation of C_{60}+C_{70} in general also favor the formation of the thermally metastable fullerene. Therefore this thesis used the flame that had best yields for C_{60}+C_{70} in order to produce the sufficient quantities of the thermally metastable fullerene needed to accomplish the thesis objectives.

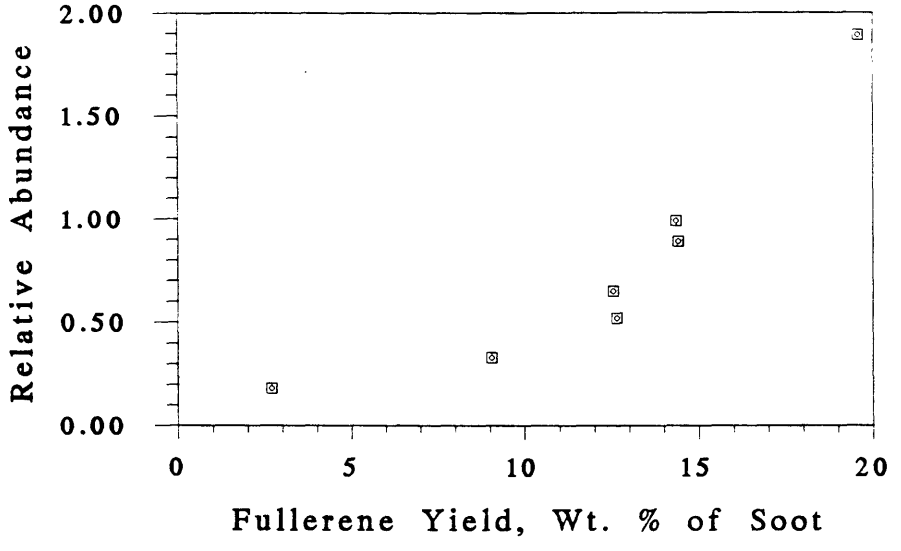

Figure 4.1 The relationship between fullerenes (C_{60} + C_{70}) yield and the relative abundance of the thermally metastable fullerene (data from Table A.1, Appendix A)

4.1.2 Developing the Flame Process for Increased C_{60}+C_{70} Yield

This subsection presents the experimental observations during the flame's process development study. Appendix A (Table A.1) presents the data collected and used in this section. This section begins by first presenting the effect of C/O ratio on the yield of C_{60}+C_{70}. This presentation is followed with the presentation of the effect of the

diluent concentration, the effect of diluent type, the effect of burner gas velocity and finally the effect of the combustion chamber pressure on the yield of C_{60}+C_{70}.

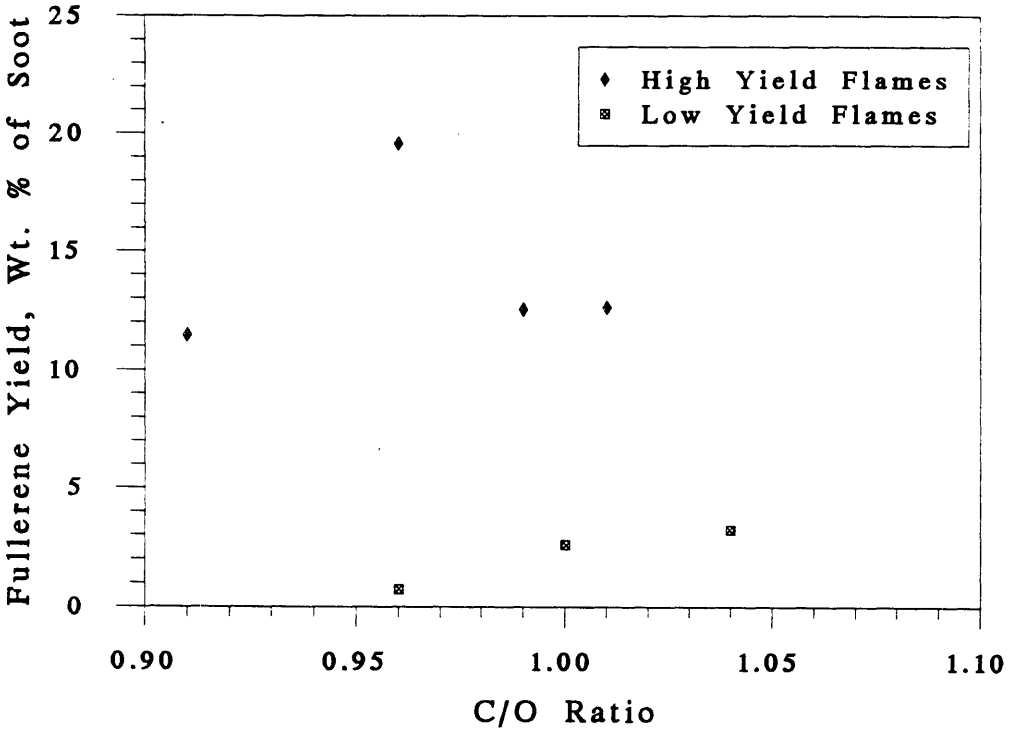

Figure 4.2 The effect of C/O ratio on the C_{60}+C_{70} yield

The effect of C/O ratio on the C_{60}+C_{70} yield, expressed as a fraction of the soot, is shown in Figure 4.2 for two sets of flame conditions. These sets of flame conditions represent two quite different extents of fullerene formation. Under the conditions giving the more prolific fullerene formation, the yields exhibit a maximum as the C/O ratio is increased. Under the conditions of lower extent of C_{60}+C_{70} formation, the yields increase with increasing C/O without attaining a maximum in the range of C/O values studied. The increase in C_{60}+C_{70} yield at the lower C/O values presumably reflects a species concentration effect; that is, the flame is richer in carbon thereby favoring the formation and growth of fullerene precursors. The decrease in C_{60}+C_{70} yield at the higher C/O values under one set of conditions may be the result of lower temperature and the associated slower kinetics, under the more heavily sooting conditions of the higher C/O ratio (the effect of C/O on the flame temperature has been presented by McKinnon [31]). In summary, C/O ratio variation experiments

suggest that increasing C/O ratio favors C_{60}+C_{70} yield from species concentration effects viewpoint; however, increases in the C/O ratio also lowers the flame temperature and thereby adversely affecting the C_{60}+C_{70} kinetics and therefore the yields.

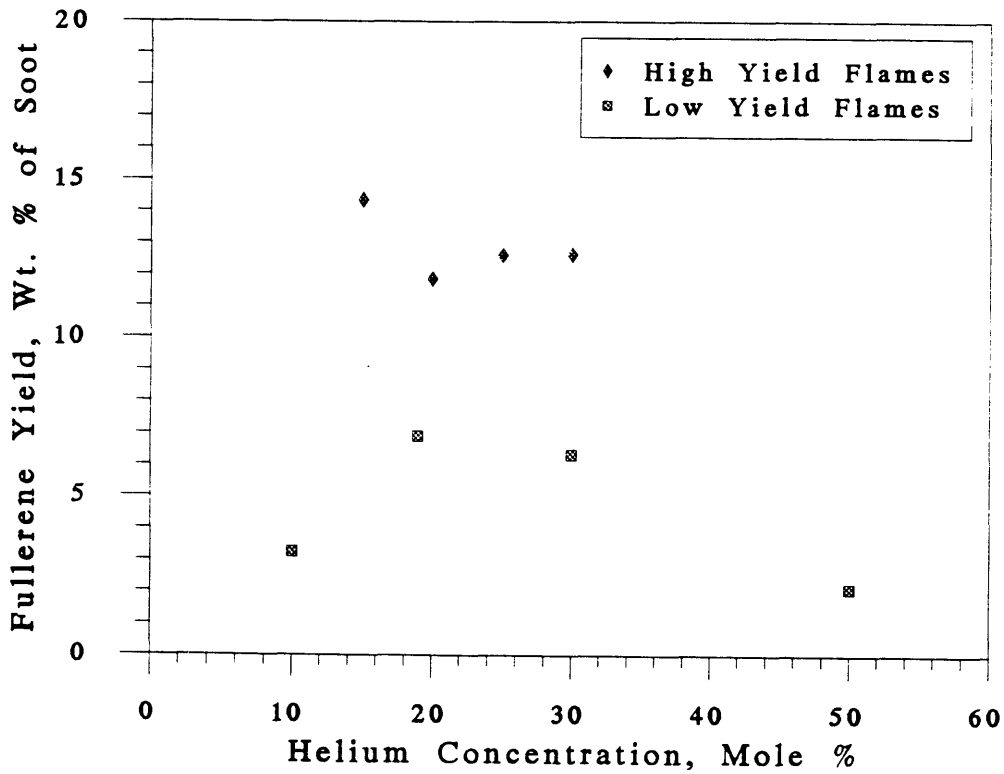

Figure 4.3 The effect of diluent concentration on the C_{60}+C_{70} yield

The effect of diluent concentration on the C_{60}+C_{70} yields is shown in Figure 4.3 for two flames, one with high yields (37.5 Torr, C/O=2.5, 40 cm/sec and helium diluent) and the other with low yields (20 Torr, C/O=2.6, 50 cm/sec and helium diluent). The effect is more pronounced for the low yield flame. The yield goes through a maxima as the helium concentration is varied from 10 to 50%. For the high-yield flame, the increased helium concentration marginally reduces the fullerene yield. The significant effect of helium concentration for the low yield flame may be conjectured to be because of some participation of helium in the fullerene formation reactions at the incipient stages of fullerene formation. However for flame conditions where C_{60}+C_{70} formation is favored, helium apparently reduces the species concentration thereby

reducing yields. In summary, low helium concentrations appear to favor higher yields of C_{60}+C_{70} under the explored window of conditions.

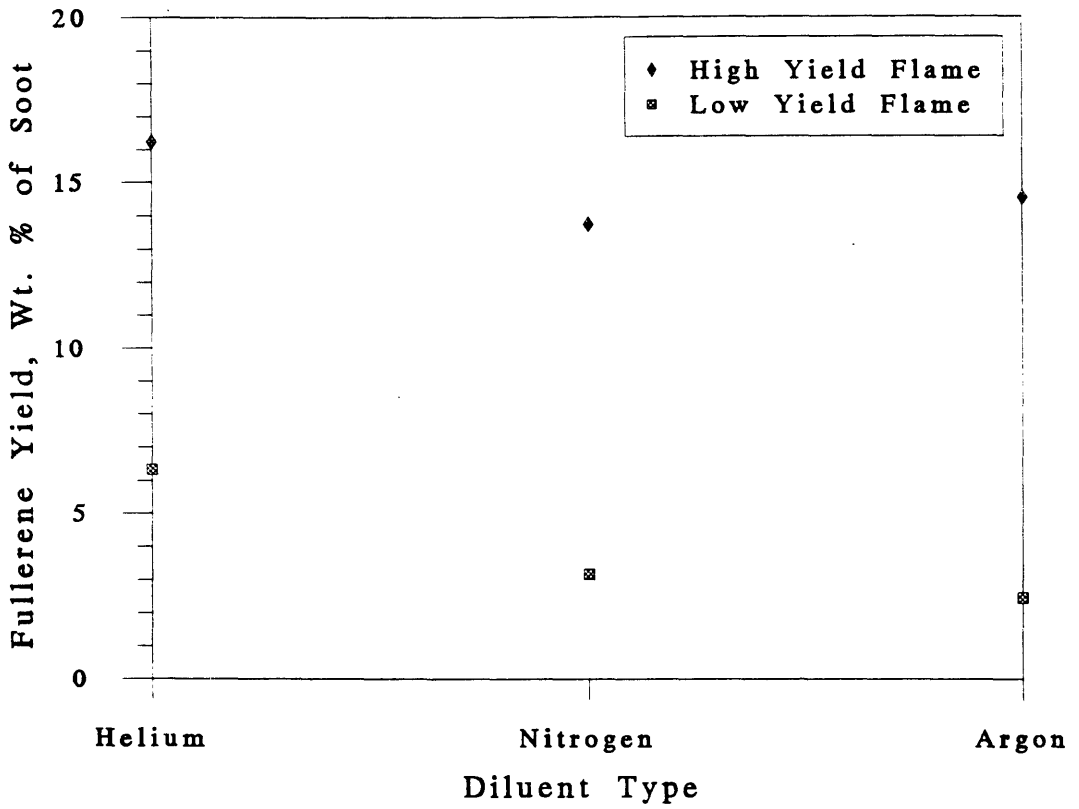

Figure 4.4 The effect of diluent types on the C_{60}+C_{70} yield

The effect of diluent types on the C_{60}+C_{70} yield is shown in Figure 4.4 for two flames; one with high yields (37.5 Torr, C/O = 0.96, 50 cm/sec and a diluent concentration of 25%) and one with low yields (20 Torr, C/O = 1.04, 50 cm/sec and a diluent concentration of 30%). Helium consistently gives higher yields than the other two. The effect of diluent type, as is clear from the figure, is prominent for low-yield flames. For instance, replacement of argon with helium in the low-yield flame more than doubles the yield of C_{60}+C_{70}. In high yield flames, the change in C_{60}+C_{70} yield when argon is replaced with helium is just 10%. These observations suggest that the presence of diluent may not be essential for C_{60}+C_{70} synthesis, particularly in flames that favor fullerene production. This suggestion was tested and the results (see Table

A.1, Appendix A) confirm that flames favoring fullerene production do produce double digit fullerene yields in absence of diluents. The relative effect of diluent presence and diluent type (He, Ar, N_2) on the C_{60}+C_{70} yields is in the order of their diffusivities. Whether the observed effect of the diluent on the C_{60}+C_{70} yield is because of the changes in thermal conductivity and the temperature profile, or the changes in molecular diffusivity and species concentration profiles, or both, remains to be established. In summary, the best condition for producing and collecting C_{60}+C_{70} is to include helium as diluent in the feed even when C_{60}+C_{70} yield is high.

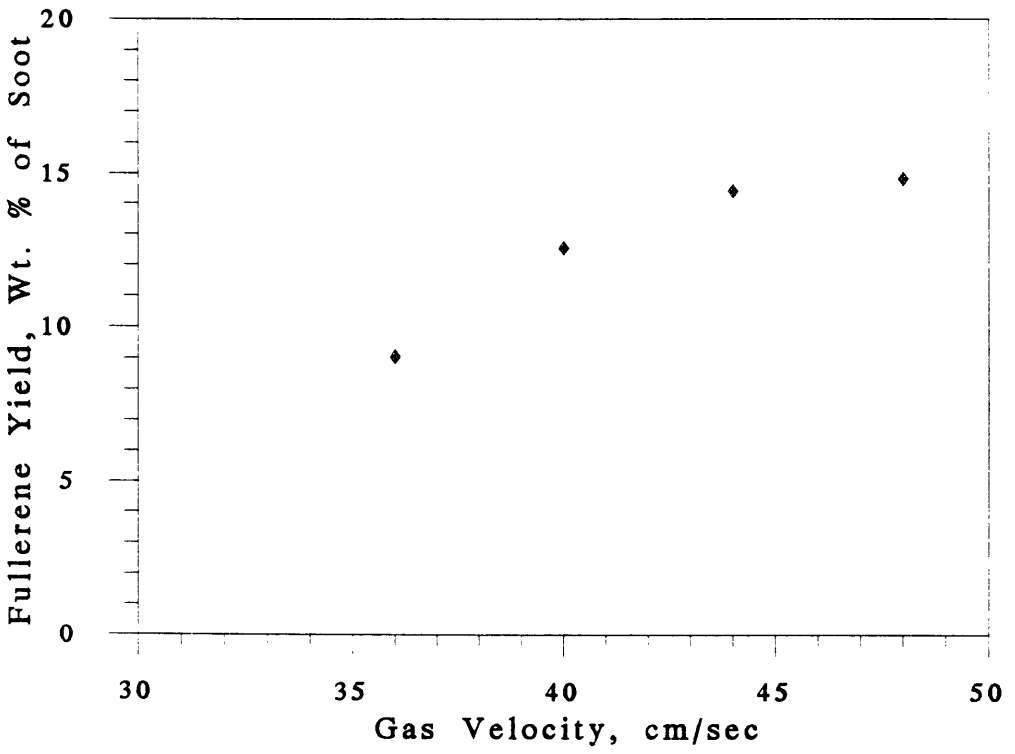

Figure 4.5 The effect of burner gas velocity on the C_{60}+C_{70} yield

The effect of burner gas velocity on the yield of C_{60}+C_{70} is shown in Figure 4.5 for a flame at 40 Torr with a C/O ratio of 0.99 and a helium concentration of 25%. The yield of C_{60}+C_{70} is observed to increase with increasing burner gas velocity. At higher velocities the flame front is stabilized farther from the burner and a smaller fraction of the heat released by combustion is lost by conduction into the water-cooled burner

plate, thus giving a hotter flame [31]. The increased temperature, presumably, favors the synthesis of C_{60}+C_{70}.

The positive effect of burner gas velocity on C_{60}+C_{70} yield is supported by other data sets in Table A.1, Appendix A.

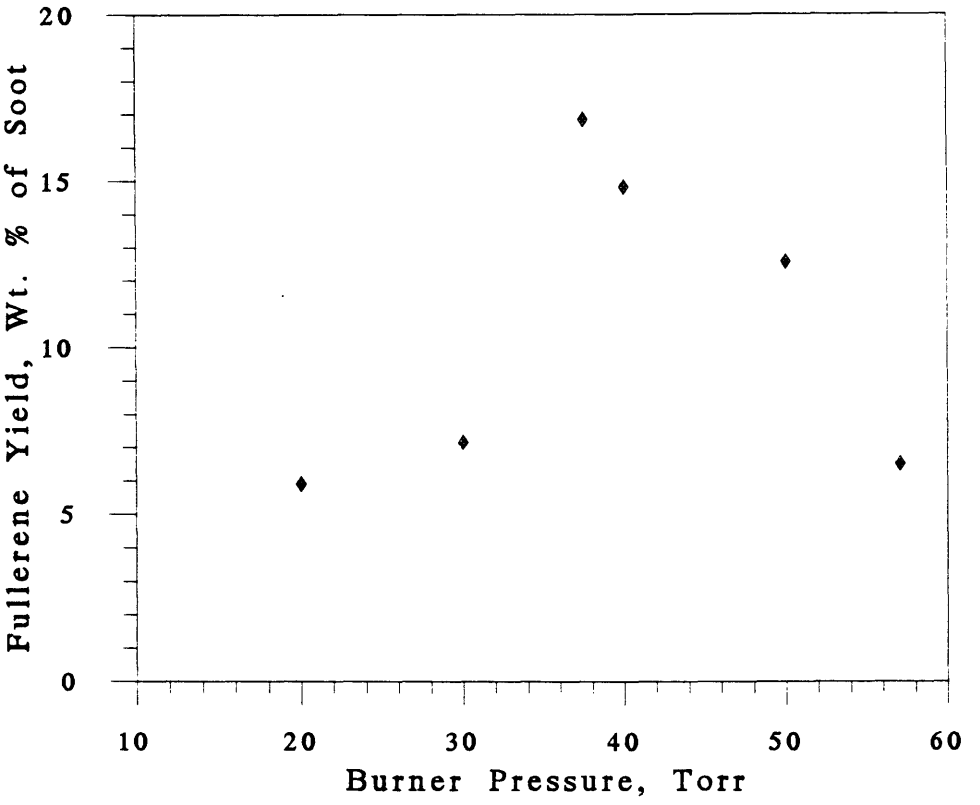

Figure 4.6 The effect of combustion chamber pressure on the C_{60}+C_{70} yield

The effect of combustion chamber pressure on the C_{60}+C_{70} yield is shown in Figure 4.6 for several flames operated under the same set of conditions (C/O = 1.0, 50 cm/sec, and helium concentration of 0 to 25%) except for pressure. The figure suggests that C_{60}+C_{70} yield peak around 40 torr.

In summary, the best flame (with a C_{60}+C_{70} yield of 20% on soot weight basis) was observed at a pressure of 37.5 Torr, a C/O ratio of 0.959, a velocity of 40 cm/sec, and 25% helium. However, it should be noted that these conditions by no means represent

experimental limits on C_{60}+C_{70} yield in flame because the equipment used by this thesis was not designed for C_{60}+C_{70} production and the equipment design features did not permit full exploration of independent variables. As suggested by Figure 4.1, this flame also produced the highest yields of the thermally metastable fullerene in the soot collected from the burner wall.

4.2 The Purification

As described in Chapter 3, the purification method consisted of three steps. The first step consisted of separating the soot extract into three fractions on a Jordi-Gel semi-preparative column. The second fraction from the Jordi-Gel column was next concentrated and then used as feed for the second step. This step consisted of liquid chromatography on a C-18 column. The second fraction from the C-18 column was again concentrated and as the final step purified on a Hypersil column.

The separation method on the Jordi-Gel column was developed using the heuristics mentioned in Chapter 3. Those heuristics led to the following observations:

- The increase in the elution rate reduced the run time but also slightly reduced the resolution.

- Any changes in the solvent gradient rate between dichloromethane and acetonitrile had no effect on the resolution of the three fullerene fractions. However, the solvent gradient rate between dichloromethane and benzene had a strong effect on the resolution.

- Changes in the volume of saturated solution injected had two effects. The resolution of the peaks varied as an inverse function of the volume of solution injected. The second effect was the occurence of a mechanical problem - i.e. with increased loading the fullerenes precipitated in the flow lines and choked the flow lines.

- If a C-18 column was used instead of the Jordi-Gel as the first column, it was found that the polyaromatic hydrocarbon content was unacceptably high in the fraction containing the thermally metastable fullerene.

Based on the above results, the purification strategy followed during this thesis work was a three step purification method as described in Chapter 3, section 3.2.2. Representative chromatograms are presented next.

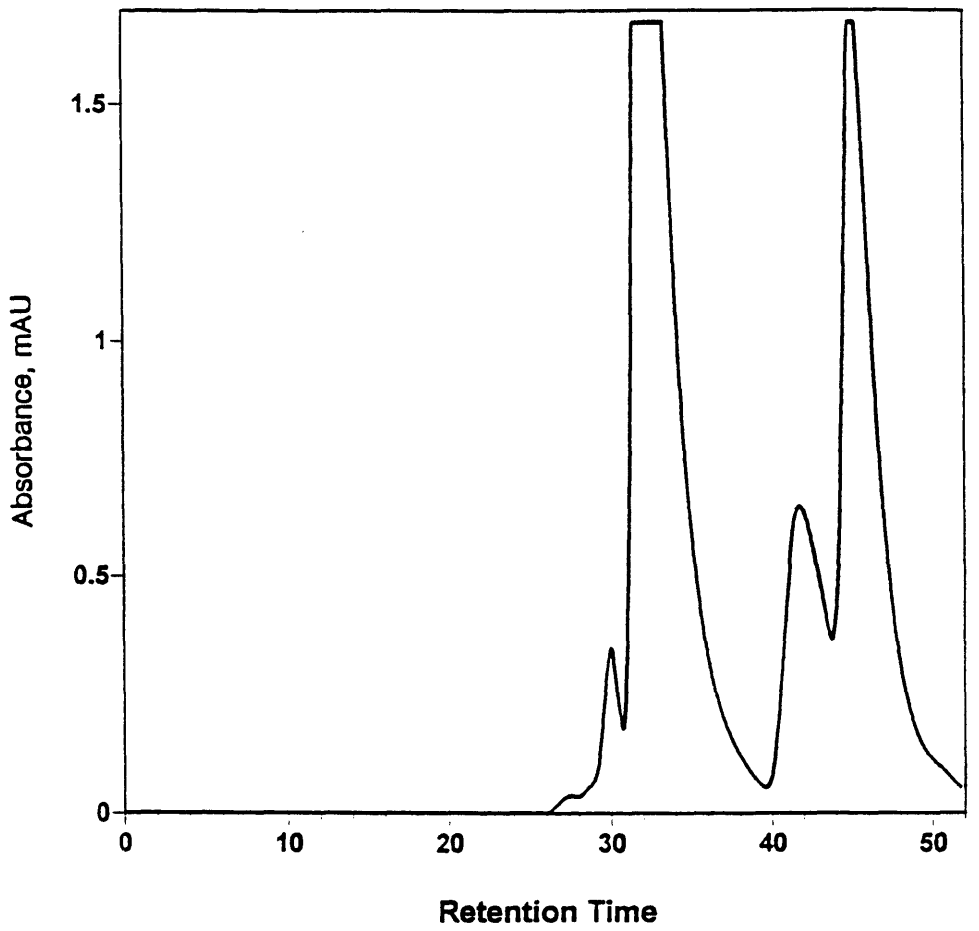

Figure 4.7 The chromatogram obtained on a Jordi-Gel preparative column

4.2.1 The Jordi-Gel Column

Figure 4.7 presents a chromatogram observed during the numerous runs made during the Jordi-Gel separation of concentrated fullerene extract. The elutant corresponding to the fraction between 26 minutes and 40 minutes was collected as the first fraction

and it was mainly composed of polycyclic aromatic hydrocarbons. The second fraction corresponded to the peaks between 40 minutes and 44 minutes and was mainly composed of some polycyclic aromatic hydrocarbons, $C_{60}O$, the thermally metstable fullerenes, C_{60} and some C_{70}. The last fraction corresponded to peaks after the 44 minutes and was composed of C_{60}, C_{70} and other higher fullerenes.

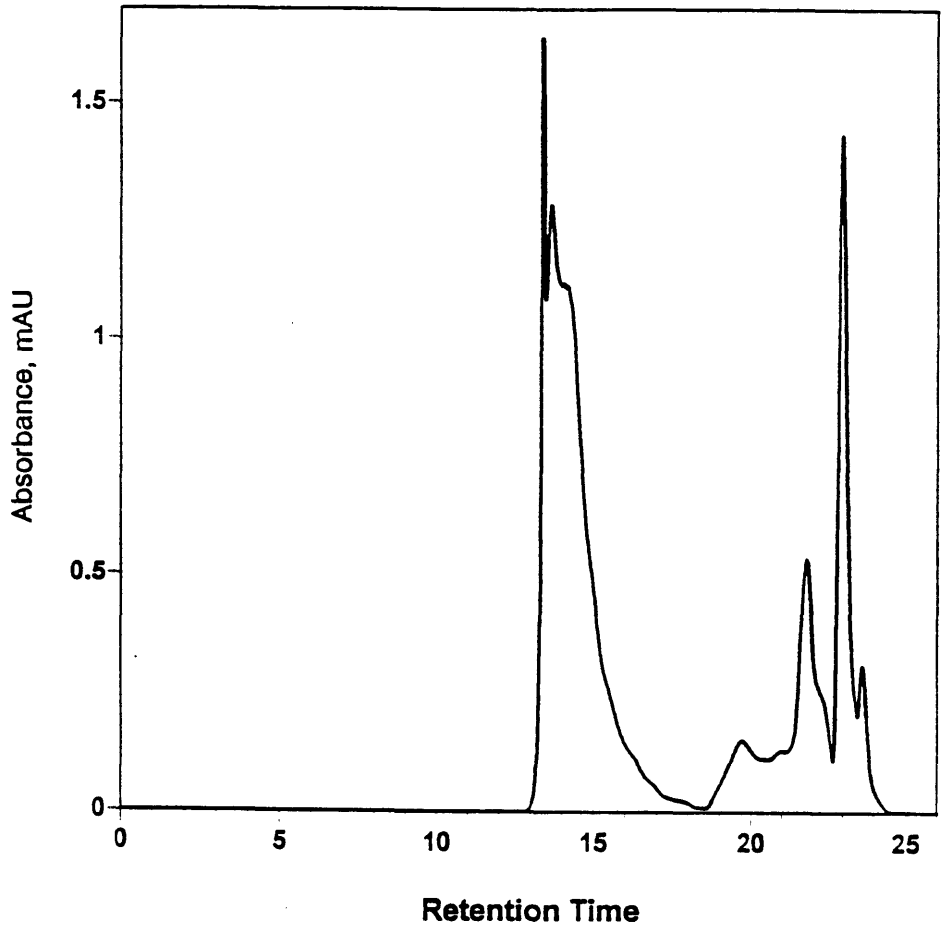

Figure 4.8 The chromatogram obtained on a C-18 preparative column

4.2.2 The C-18 Column

Figure 4.8 presents a representative chromatogram observed during the C-18 column separation of the concentrated second fraction from the Jordi-Gel column. The first fraction collected corresponded to the peaks between 13 minutes and 21.5 minutes and was mainly composed of polycyclic aromatic hydrocarbons and $C_{60}O$. The second fraction corresponded to the peaks between 21.5 minutes and 22.4 minutes and was

mainly composed of the thermally metastable fullerenes and some C_{60}. The last fraction corresponded to peaks after the 22.4 minutes and was mainly C_{60} and C_{70}.

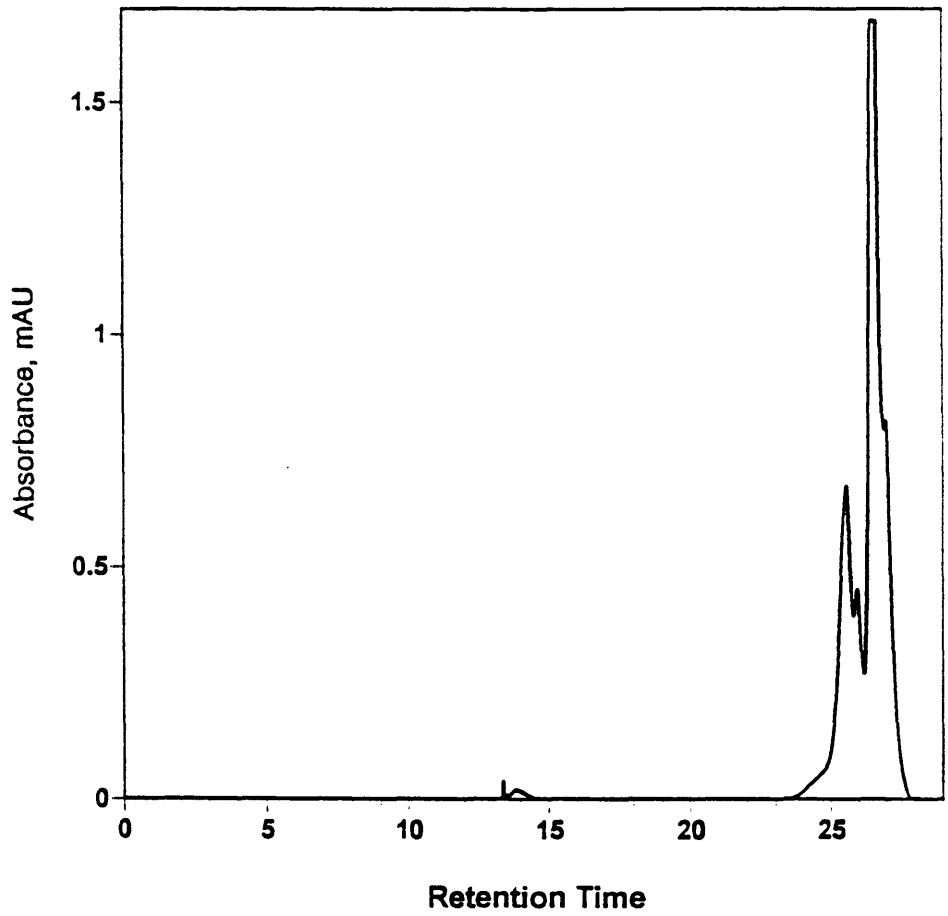

Figure 4.9 The chromatogram obtained on a Hypersil preparative column

4.2.3 The Hypersil Column

The Hypersil column based separation yielded a chromatogram as shown in Figure 4.9. The first fraction corresponded to peaks before 24 minutes. The thermally metastable fullerene that was studied in this thesis was collected in the fraction eluting between 24 minutes and 25.5 minutes. The third fraction consisted of peaks after 25.5 minutes. The third fraction consisted mainly of the larger peak which was C_{60} and a smaller peak eluting at 26th minute. The smaller peak corresponded to the originally discovered thermally metastable fullerene [36, 37] and has been studied and reported by Anacleto et al. [32].

4.3 Characterization

As discussed in chapter 2, the observed behavior of the thermally metastable fullerene could be explained by two competing hypotheses. Namely, the isomer hypothesis that assumed that the thermally metastable fullerene is a C_{60} isomer; and, the fragile adduct hypothesis that assumed that the thermally metastable fullerene is a fragile $C_{60}X$ molecule. Both these hypotheses explained all the observations of Anacleto et al. [36, 37]. The major challenge this thesis work faced was to establish which hypothesis was correct; that is, what is the true identity of the thermally metastable fullerene. This challenge was answered using the principle of proof by contradiction. Characterization experiments were performed to determine if one of the hypotheses contradicted fact(s) observed during the experiments. If so, then that hypothesis was discarded as an incorrect hypothesis. This procedure would leave the not disproved hypothesis as the only candidate that explained all the observed facts.

This thesis collected observations from numerous characterization experiments on the thermally metastable fullerene. These observations are presented in Figure 4.10 through Figure 4.18. Each of these observations is now discussed in sequence.

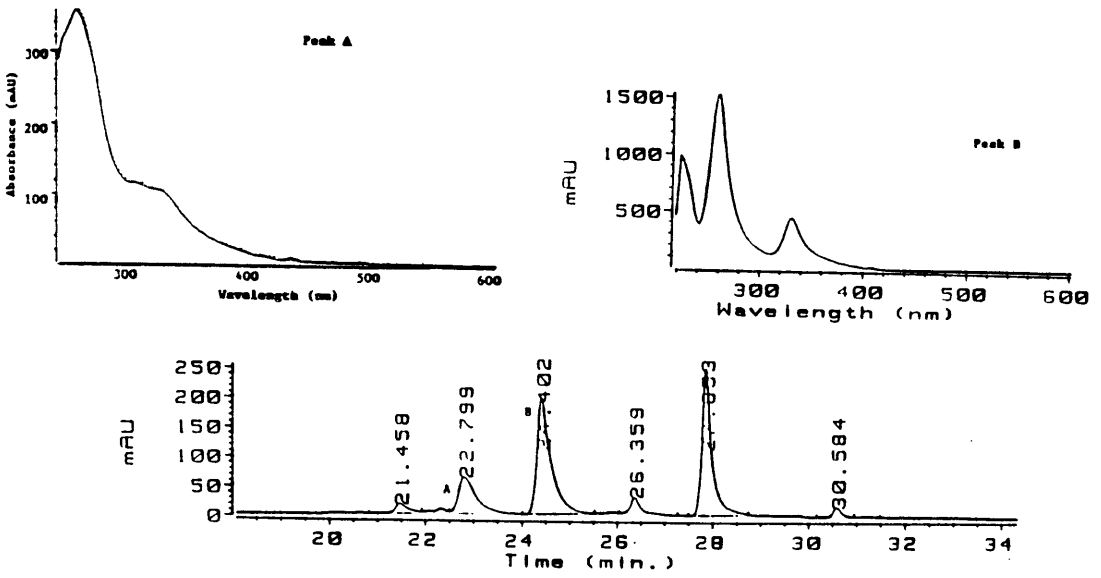

Figure 4.10 HPLC chromatogram of soot extract and the UV-Vis spectra of peaks marked A and B in chromatogram

Figure 4.10 presents the results obtained using an HPLC equipped with a diode array detector. Note the peak A and the peak B. The first observation one can make from the figure is that the species corresponding to these peaks have different retention times on the C-18 silica gel column. This implies that the species corresponding to peak A and peak B interact differently with the chromatographic column, every thing else being the same. Therefore, the difference in retention times supports the conjecture that the species corresponding to peak A and peak B have different identities. However, the difference in retention time does not prove that peak A and peak B have different identities, since the alternate possibility is that the chromatographic column is not functioning properly (due to fluid flow problems such as channeling). This alternate possibility of malfunctioning column was disproved in two ways.

First, the peak A was collected as a fraction from the HPLC runs. The fraction so collected was re-injected into the HPLC. If the column was malfunctioning, then peak A should once again reappear as two peaks with retention times matching those of peak A and peak B. However, it was observed that the re-injected fraction appeared as a single peak with retention time matching precisely that of peak A. Therefore, peak A and peak B were not a consequence of a malfunctioning equipment. The observation also establishes the fact that the chromatographic column does not chemically transform the species corresponding to the peak A.

Second, the UV-Vis spectra of peak A and peak B were obtained and are shown in Figure 4.10. The distinctly different UV-Vis spectra establish that the species corresponding to peak A and peak B are truly distinct. The UV-Vis spectrum for peak B matches those reported for C_{60} by Ajie et al. [15]. The match proves that peak B corresponds to C_{60}. Since the UV-Vis spectra corresponding to peak A is different from that for C_{60}, we can conclude that the species corresponding to peak A is different from C_{60}.

Figure 4.11 presents the results obtained using an HPLC/MS [38]. The figure shows that both, peak A and peak B, have an m/z ratio of 720. The m/z ratio of 720 implies that the molecular weight of the species corresponding to these peaks is 720 amu. On first glance, this observation would seem to eliminate the adduct hypothesis because

the molecular weight of $C_{60}X$ has to be greater than 720 (720 + molecular weight of X). However, this conclusion is suspect if we consider the possibility that the mass spectrometer may be fragmenting the fragile adduct. In other words, the very fact of observing the adduct may be changing the identity of the adduct. Since we could not figure out a method of determining if the HPLC/MS was fragmenting the thermally metastable fullerene, the objective conclusion was presume that neither of these hypotheses have been disproved. To confirm that the mass spectrometer in the HPLC/MS may be fragmenting the thermally metastable fullerene under study, we pursued electron impact mass spectrometry, one that did not have HPLC and MS in tandem arrangement.

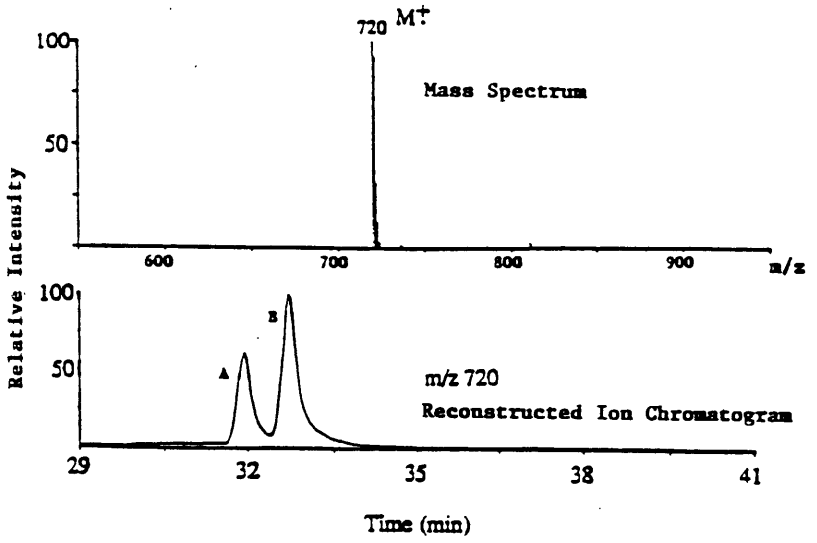

Figure 4.11 HPLC/MS spectrum

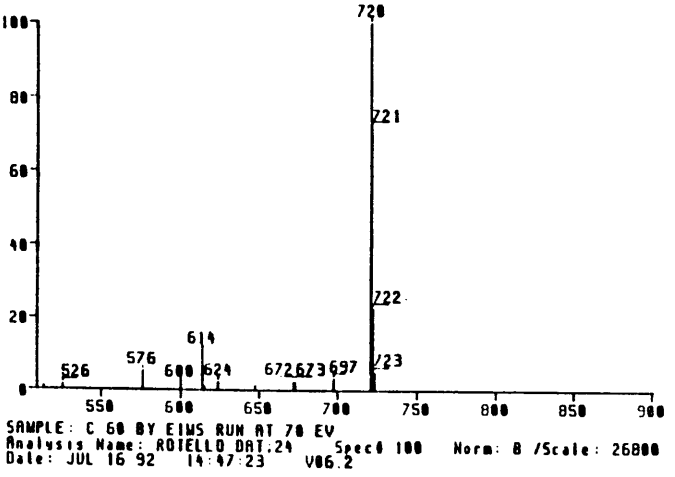

Figure 4.12 EI mass spectrum

[redacted]

[redacted]

[redacted]

[redacted]

nts, the number of possible functional groups that could make X use carbon and hydrogen by themselves can form infinite he fullerene's cage structure the possibilities further multiply group could be attached to the:

- fullerene cage, (exohedral: X-C_{60})
- e (-C-X-C-)
- (endohedral: X@C_{60})
- combinations of above three

ssibilities that X in C_{60}X may be endohedral or may be part of the e have noted in the results from mass spectrometer presented X had to be easily fragmentable so as to explain the observed 20 for C_{60}X in the mass spectrometer. If the functional group as part of the cage (for instance: an ether), fragmentation would ne or more bonds from the cage. The energy required to break ilerene cage far exceeds the energy available during mass ations. This has been experimentally established, since many s of fullerenes (such as He@C_{60}, La@C_{60}, Sc@C_{60} etc.) have using electron impact mass spectrometer [102-104]. Therefore, not be an endohedral functional group or part of the cage based . The elimination of these two possibilities leaves the exohedral remaining alternative.

ents that could possibly compose X in C_{60}X, helium was easiest easible candidate. First of, helium is a noble element and does any other element, leave alone the carbons in C_{60}. Second, the ts that replaced helium with argon and with nitrogen. In both erved to exist and the C_{60}X observed was indistinguishable from hen helium was used. Thus X in C_{60}X could not be helium on leaves only three possible candidate elements for X in C_{60}X: ydrogen.

Consider now the possible functional group combinations. There are seven possible functional group combinations as presented in Table 4.1. However, except for a pure carbon based functional group combination, all other combinations have either hydrogen or oxygen or both as part of the functional group. Thus, our task can be simplified to performing experiments that would eliminate the existence of hydrogen, of oxygen and of dimerization of C_{60} in our study of the $C_{60}X$ hypothesis. The results presented next consider these elements and their corresponding functional groups in order.

Functional Group Combination	Example: Functional group based on
Pure hydrogen based	hydrides
Pure oxygen based	epoxides
Pure carbon based	dimerization of C_{60}
Hydrogen-oxygen based	hydroxyls
Hydrogen-carbon based	aliphatic groups, arenes, cycloalkanes, cycloalkenes
Carbon-oxygen based	carbonyls
Carbon-oxygen-hydrogen based	alkanols, alkenols

Table 4.1

Figure 4.13 presents the fourier transformed infrared spectra of the thermally metastable fullerene under study. Note the lack of absorbance peaks between 4000-3200/cm and between 1870-1550/cm; also note the presence of absorbance peaks between 3100-2800/cm. The absence of absorbance peaks between 4000-3200/cm suggests that hydroxyl group is not present in the sample [105]. The lack of absorbance peaks between 1870-1550/cm suggests that the sample is devoid of

carbonyl group. Finally, the presence of absorbance peaks between 3100-2800/cm region suggests that the sample has hydride (proton) stretches [105].

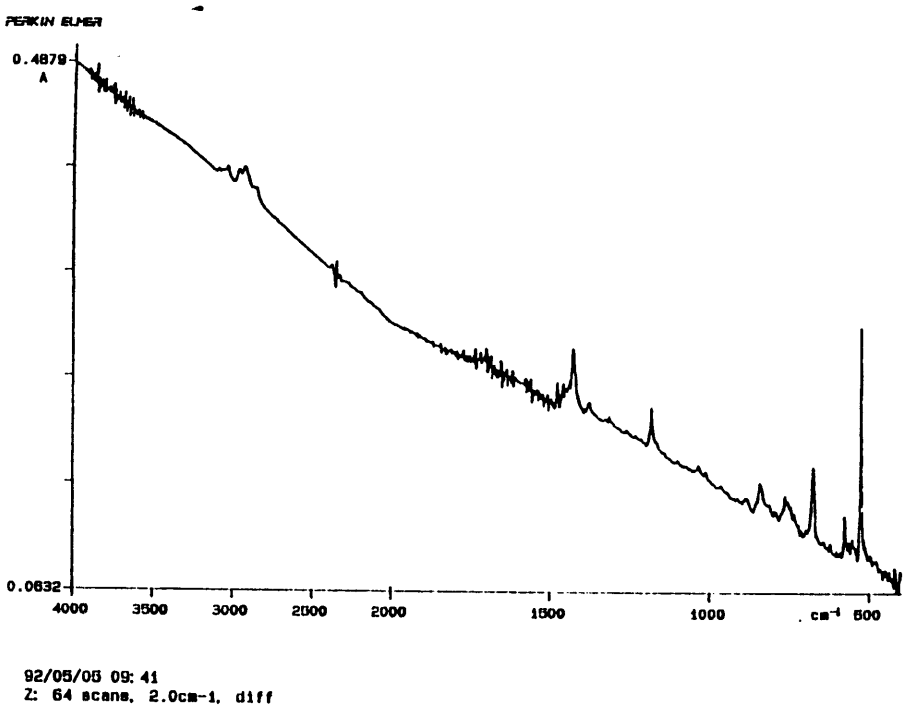

Figure 4.13 FTIR spectrum of the thermally metastable fullerene

The absence of hydroxyl groups and carbonyl groups in the sample implies that these groups are absent in the thermally metastable fullerene molecule too. However, the presence of proton stretches in the sample does not imply that the thermally metastable fullerene molecule, under study, has proton stretches. This is because the sample is not 100% pure thermally metastable fullerene. The sample has impurities, and these impurities could be responsible for the hydride (proton) stretches observed in Figure 4.13. Thus, we can not conclude whether or not proton stretches are present in the thermally metastable fullerene. On the other hand, we can conclude that the hydroxyl and the carbonyl groups are not present in the thermally metastable fullerene.

With the elimination of the hydroxyl group and the carbonyl group from the list of possible candidates for X in the $C_{60}X$ structure, we are left with the possibility of only one more exohedral oxygen based functional group - the epoxide group. This possibility was excluded by the Creegan test.

Creegan test [90] was performed by contacting a solution of the thermally metastable fullerene without C_{60}, with neutral alumina. Unlike Creegan et al. who observed 90% conversion of epoxides of C_{60} to C_{60} when a solution containing the epoxides of $C_{60}O$ was contacted with neutral alumina, the sample solution showed no change between the sample before and after the Creegan test. Thus, the sample did not have any $C_{60}O$ present - in other words, the thermally metastable fullerene is not an epoxide.

The elimination of the epoxide possibility, leaves only hydrogen based functional groups as the only other possible candidate for X in $C_{60}X$. This possibility was examined using the NMR techniques.

Figure 4.14 presents the proton NMR. The spectrum shows the following ppm downfield from TMS: δ 7.09 (2H, t, J=1.5Hz), 4.51 (2H, t, J=1.5Hz), 3.42 (1H, d, J=9.66 Hz, CH_AH_B), 2.52 (1H, d of t, J=9.6). The presence of proton peaks indicates that the sample has proton based functional groups. However, like the FTIR results, it was not clear whether the proton based peaks observed are due to the impurities in the sample or are due to the protons in the thermally metastable fullerene. Thus the results from proton NMR were inconclusive.

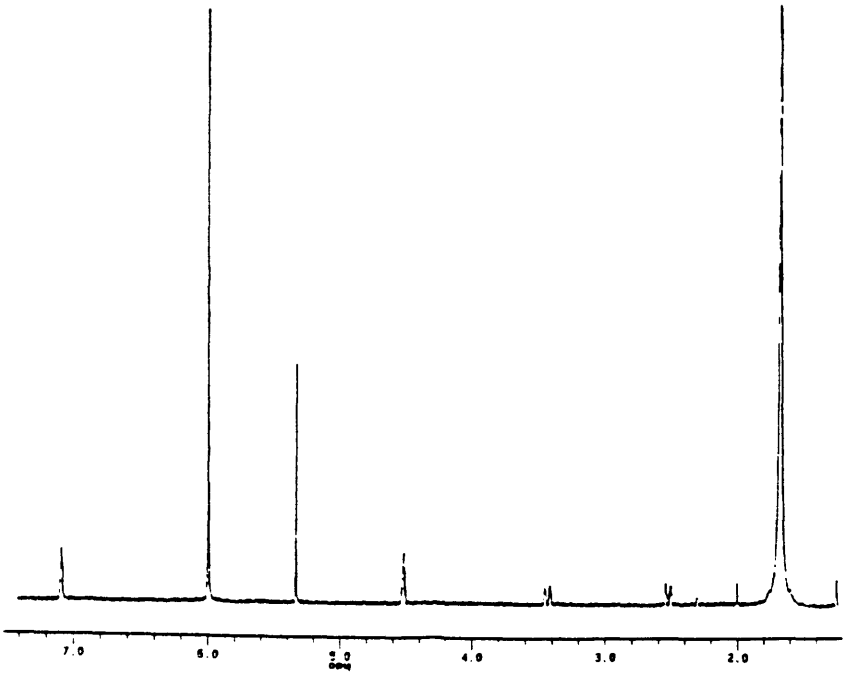

Figure 4.14 The proton NMR of the thermally metastable fullerene

With proton NMR results being inconclusive, one faces the question whether there is any method of analysis that can give conclusive results even in the presence of relatively small amount of impurities in the sample. Fortunately there is a method, though time consuming, that could accomplish such a feat - the ^{13}C NMR analysis. The ^{13}C NMR results are presented next.

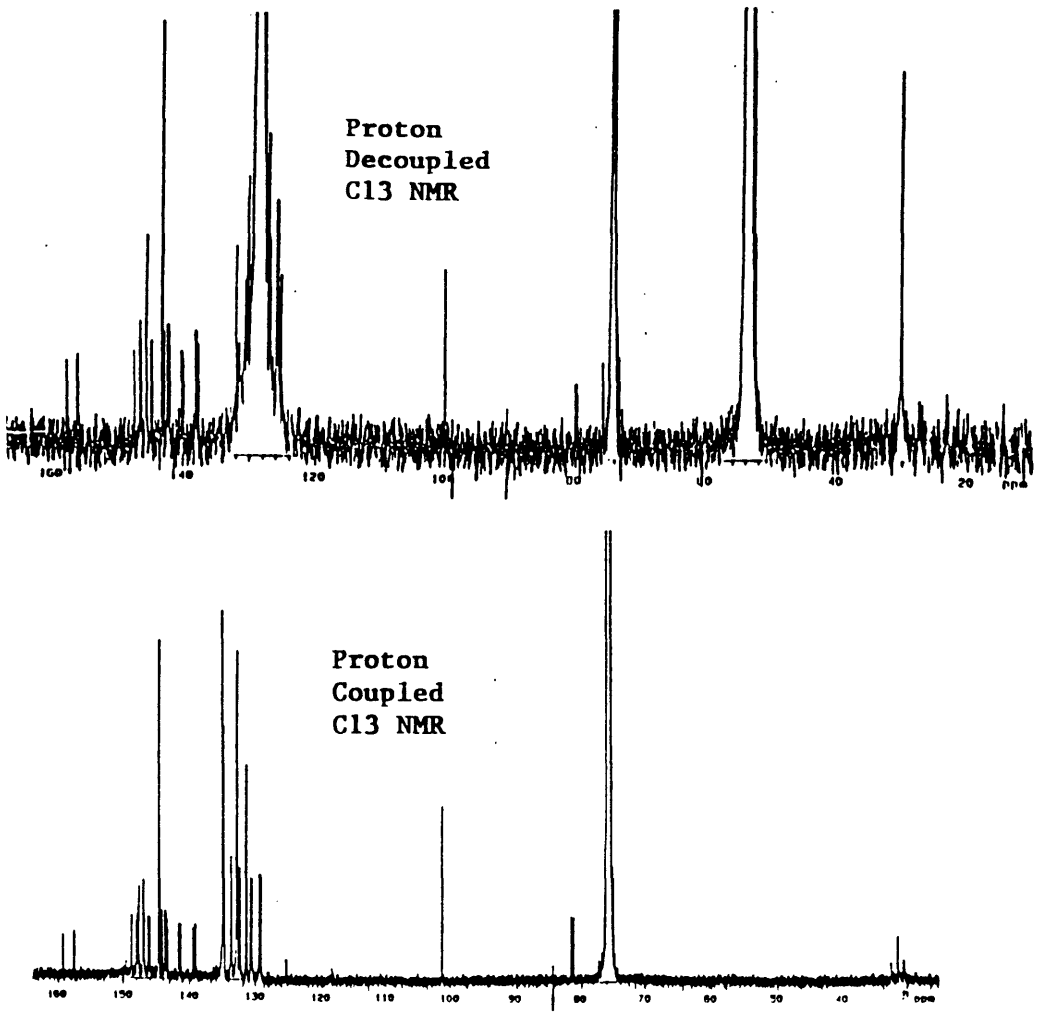

Figure 4.15 (a) ^{13}C NMR spectra of the thermally metastable fullerene with broad band decoupling (b) ^{13}C NMR spectra with broad band proton coupling

Figure 4.15(a) presents a part of the ^{13}C NMR spectra with broad band decoupling . The presence of peaks in the sp^3 region suggests that the thermally metastable fullerene, being studied, has at least one sp^3 carbon. Figure 4.15(b) presents a part of the ^{13}C NMR spectra in proton coupled mode.

The striking difference between Figure 4.15(a) and Figure 4.15(b) is the splitting of the 30.5 peak into three peaks. The split implies that the thermally metastable molecule has a $-CH_2$ group. Thus, the first unequivocal conclusion to be drawn from the ^{13}C NMR is that $C_{60}X$ is not an isomer of C_{60}. Second, the X in $C_{60}X$ is a hydride based functional group. Thirdly, we can conclude that the hydrogens in $C_{60}X$ are not bonded to the C_{60} cage directly. Instead the hydrogens in $C_{60}X$ are associated with the carbons in X.

The above ^{13}C NMR result now requires that all facts observed with different characterization experiments be explained in a non-contradictory way.

Consider first the observed molecular weight of 720 for the thermally metastable fullerene in the electron impact mass spectrometer. This can be explained by focusing on the operation of the mass spectrometer. EI mass spectrometry required the heating of the sample to 220°C - a temperature far in excess of the 100°C that is required to dissociate X from $C_{60}X$ [36]. If this explanation is true, then non-thermal techniques should be able to detect the true molecular weight of the thermally metastable fullerene. This explanation was confirmed using a charge transfer, ion spray based specialized mass spectrometry described in chapter 3, section 3.2.4. Figure 4.16 shows the reconstructed ion chromatogram from a positive ion charge transfer ionspray HPLC/MS/MS analysis. The results identify the molecular weight of the precursor (the thermally metastable fullerene being studied) to be 786 and that it is this precursor which yields a molecular weight of 720 in the second mass spectrometer.

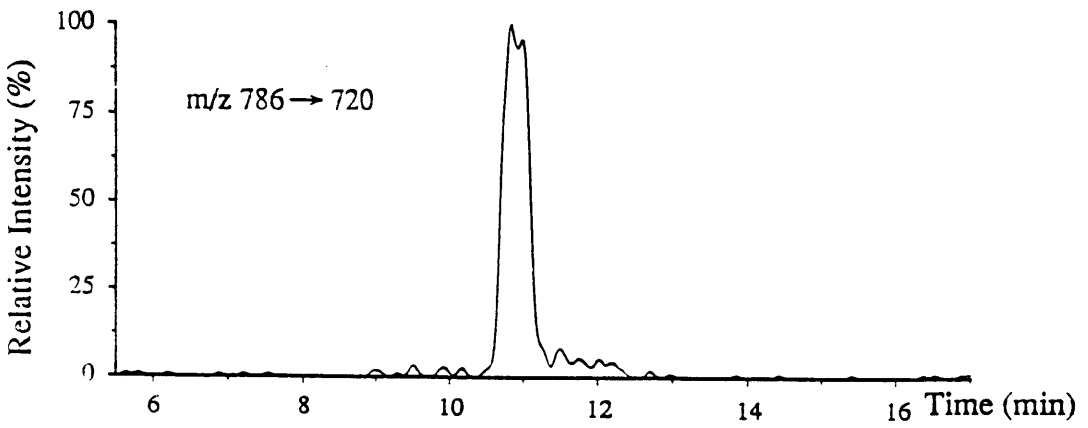

Figure 4.16 Reconstructed ion chromatogram from a charge transfer ionspray based HPLC/MS/MS analysis of a sample containing the thermally metastable fullerene

A molecular weight of 786 suggests that the molecular weight of X in $C_{60}X$ has to be 66. A hydrocarbon group of mass 66 must be C_5H_6. Thus, the X in $C_{60}X$ is C_5H_6 and the thermally metastable fullerene studied by this thesis is $C_{60}C_5H_6$.

The next task before the thesis was to consistently explain all the remaining facts observed during characterization. This task required identifying the structure of C_5H_6?

The structure of C_5H_6 was identified by considering the following facts:

1. The ^{13}C NMR spectra suggests that there is a $-CH_2$ group in C_5H_6.

2. The structure of C_5H_6 should allow C_5H_6 to form a biradical. This is necessary because the closed cage structure of C_{60} requires bonding at two positions to remain stable at room temperature. If C_5H_6 were to form a mono-radical and react with C_{60} to yield $C_{60}C_5H_6$, then $C_{60}C_5H_6$ would also be a radical that would immediately react with some species in the surrounding media to achieve stability. The requirement that C_5H_6 form a biradical implies that C_5H_6 have a -C=C- or a -C≡C- group in C_5H_6.

3. The structure should be flexible enough to avoid prohibitive strains in the $C_{60}C_5H_6$ structure. This constraint suggests that the -C≡C- group is unlikely, since this would impart rigidity to the C_5H_6 group.

4. Alkyl bonding sites and hydride bonding sites are stable to heat treatment and mass spectrometry, as discussed before. This fact implied that the bonding sites in C_5H_6 are unlikely to be like alkyl or hydride bonding sites. In other words, C_5H_6 is unlikely to be aliphatic in nature. A cyclic structure is likely.

The only conjecture for C_5H_6 structure that satisfies all the above structural constraints is the structure of cyclopentadiene.

Once again, we face the challenge to establish that the C_5H_6 structure is truly cyclopentadiene. But before we attempt that, the more simpler test was to examine if

the cyclopentadiene conjecture explained all known facts. Such an examination was performed and the results are as below:

1. C_5H_6 can readily undergo a Diels-Alder reaction with molecules with double bonds to produce an adduct [115-119]. In case of C_{60}, there are 30 double bonds and therefore C_5H_6 can structurally yield many isomers. Two possible isomers of $C_{60}C_5H_6$ are shown in Figure 4.17.

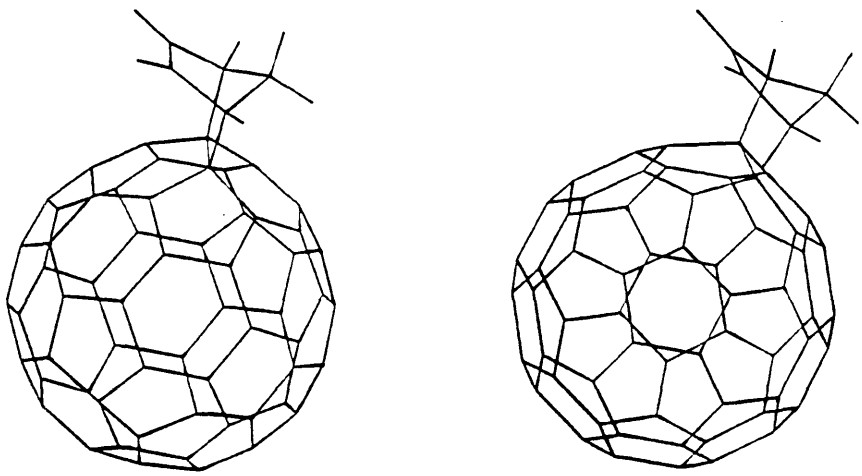

Figure 4.17 Two possible isomers of $C_{60}C_5H_6$

2. The thermal metastability can be explained by observing the fact that many Diels-Alder reactions are reversible and form products that are thermally metastable [115, 119]. Even cyclopentadiene all by itself dimerizes into dicyclopentadiene at room temperature by Diels-Alder reaction and the dicyclopentadiene so formed reverts back to cyclopentadiene upon heating by the retro-Diels-Alder reaction (about 450 K).

3. The observed proton stretches in the fourier transform infrared spectrum can be attributed to the protons in the C_5H_6.

4. The observed lower retention time during HPLC is consistent with reported lower retention time of other C_{60} compounds such as $C_{60}O$ [90].

5. The observed distinct UV-Vis spectrum would be expected for an adduct.

6. The features observed in the proton NMR spectrum are consistent with the proposed structure too. The peaks assignment can be done thusly: δ 7.09 (2H, vinyl CH), 4.51 (2H, bridgehead CH), 3.42 (1H, CH_AH_B), 2.52 (1H, CH_AH_B). This proton NMR spectrum is consistent with the proton NMR spectrum published by Tsuda et al. [106] for $C_{60}C_5H_6$.

7. The features observed in the ^{13}C NMR spectrum are also consistent with the proposed structure. Please note, however, that the spectrum is somewhat different from that published by Tsuda et al. [106] for $C_{60}C_5H_6$. This may have occurred because of unexplained solvent effects or by as yet unidentified thermal dissociation of $C_{60}C_5H_6$ during NMR experiments or both.

8. Flames that produce fullerene radicals also produce cyclopentadiene radicals as an intermediate product of combustion [12].

Thus all observed facts can be satisfactorily explained with the cyclopentadiene hypothesis. As final proof, two predictions were made and checked for consistency with the cyclopentadiene hypothesis. The first prediction was that it should be possible to synthesize the thermally metastable fullerene directly from C_{60} and C_5H_6 and the resulting adduct should be indistinguisable from the adduct formed in the flame. The second prediction was that one should, during EI mass spectrometry, be able to find a 66 fragment at moderate probe tip temperatures (373 K). Both these predictions were checked and the results are presented next.

In order to check the first prediction, the thermally metastable fullerene was prepared in the following way [107]. Freshly distilled cyclopentadiene (0.8 mg, 12 μmol) was added to a solution of C_{60} at 20°C. An immediate change in color from deep purple (C_{60}) to the characteristic golden brown color of the thermally metastable fullerene ($C_{60}C_5H_6$) was observed. The resulting solution when analyzed with HPLC, UV-Vis spectroscopy and proton NMR was indistinguishable from the thermally metastable fullerene synthesized in the flame and studied by this thesis.

The second prediction was checked so as to detect a fragment of the thermally metastable fullerene with molecular weight of 66. Figure 4.18 presents the result. The

prominent peak with 66 mass number confirms that the thermally metastable fullerene is $C_{60}C_5H_6$.

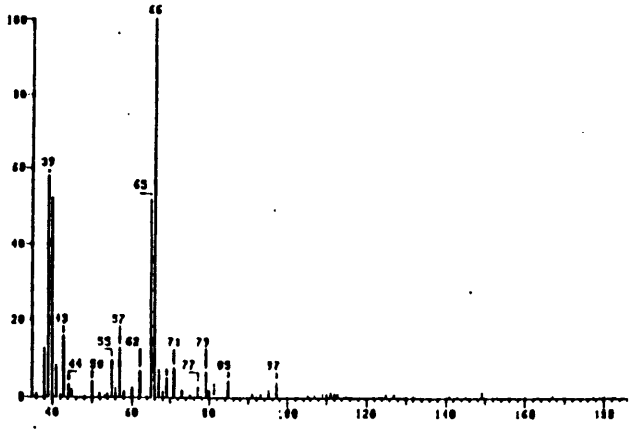

Figure 4.18 EI Mass Spectrum of thermal fragment

Above results establish that the thermally metastable fullerene truly is $C_{60}C_5H_6$.

4.4 The Species Profile in the Flame

Having established the true identity of the thermally metastable fullerene as $C_{60}C_5H_6$, the next question that this thesis addressed was: where in the flame is $C_{60}C_5H_6$ formed? To answer that question, the species concentration profile was obtained using the techniques described in chapter 3.

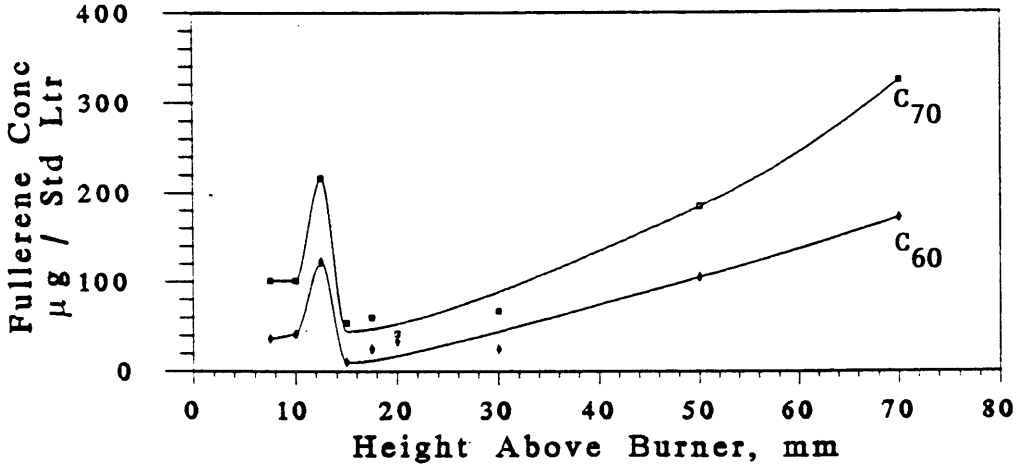

Figure 4.19 The concentration profile of fullerene species in the flame

Figure 4.19 presents the concentration profile of fullerene species in the flame (Appendix A, Table A.2 present the data used for Figure 4.19). Both C_{60} and C_{70} concentrations have an intermediate maxima, while the concentration of the thermally metastable fullerene in the flame gases along the flame length is lower than the detection limit (the detection limit in terms of absorbance area for $C_{60}C_5H_6$ in the chromatogram was 35 mAU). This observed below detection limit peak absorbance area is about 50 times lower than the expected peak absorbance area for the thermally metastable fullerene along the flame length (the expected absorbace area for $C_{60}C_5H_6$ in the chromatogram was 1809 mAU[1], if the concentration of $C_{60}C_5H_6$ relative to C_{60} were to be the same in the probe sample as in the burner wall sample). Although it is not surprising that the thermally metastable $C_{60}C_5H_6$ is not formed in the high temperature environment of the flame, it is surprising and remarkable that $C_{60}C_5H_6$ concentrations are below detection limit in the probe samples. It is surprising and remarkable because both the probe sample and the burner wall sample are quenched and are therefore subject to similar (although not identical) thermal profiles. One would, therefore, expect that at least in the probe samples that correspond to the higher heights above burner, there would be a trend of increasing concentration of $C_{60}C_5H_6$. The experimental facts suggest that up to 70 mm above the burner, the quenching of the flame gases does not yield detectable concentrations of $C_{60}C_5H_6$. This leaves us with the following hypotheses:

1. The species concentration of C_5H_6 (or some unknown precursor of C_5H_6 required for the synthesis of $C_{60}C_5H_6$) starts to increase only after 70 mm above the burner in flames that produce the thermally metastable fullerene.

2. The thermally metastable fullerene formation process is different for probe conditions and the wall conditions. The $C_{60}C_5H_6$ is formed as a consequence of post flame chemistry.

[1]Final volume of concentrated extract = 5 ml; Maximum C_{60} concentration in extract = 0.265 mg/ml (See Appendix A); Absorbance area for C_{60} corresponding to 0.265 mg/ml concentration = 9045 mAU; Relative Area of the thermally metastable peak to the C_{60} peak in the burner wall sample = 0.2; Expected area of the metastable fullerene peak = 0.2*9045 = 1809 mAU.

The results of Bittner and Howard [27], although not directly applicable to the thermally metastable fullerene producing flame, suggest that C_5H_6 concentration exhibits a strong peak well ahead of the post flame region. This strong presence of C_5H_6 in the flame well ahead of the post flame region, theoretically speaking, should provide the reactants (C_{60} and C_5H_6) required for the synthesis of $C_{60}C_5H_6$ in the quenched environment inside the probe. The experimental facts, on the other hand, establish that no detectable levels of $C_{60}C_5H_6$ is formed in the probe. This discrepancy between the theory and experiment seems to lead to the conclusion that the first hypothesis above may not be the likely explanation. However, this discrepancy between the theory and the experiment may be explained if we note that the pressure in the probe is much lower (about 20 fold lower) than the pressure in the burner. The lower pressure may be leaching out the C_5H_6 to the gas phase, thereby making the probe environment too starved of C_5H_6 for any $C_{60}C_5H_6$ to be formed and detected. If this rationalization is true, then we can predict that the C_5H_6 (or some unknown precursor of C_5H_6 required for the synthesis of $C_{60}C_5H_6$) concentration should increase beyond the 70 mm height above the burner so as to explain the observed concentration of $C_{60}C_5H_6$ in the soot samples from the burner walls. This prediction is further strengthened by the observation that the burner wall was more than 100 mm above the 70 mm position above the burner in all runs and that this is sufficient reaction length for the possible formation of C_5H_6 (or some unknown precursor of C_5H_6 required for the synthesis of $C_{60}C_5H_6$). This prediction could not be tested during the course of this thesis because of the burner and probe length design limitations.

The second hypothesis - $C_{60}C_5H_6$ is formed as a consequence of a unique post flame chemistry - is, like the first hypothesis, difficult to eliminate. The unique post flame chemistry may be because of the mixing of the combustion products from the outer flame and the combustion products from the flame at the interface of the inner and the outer flame. This explanation is somewhat unlikely because the outer flame was a non-sooting lean ethylene/oxygen/inert flame and such a lean flame is unlikely to yield the C_5H_6 concentrations needed for the observed concentrations of $C_{60}C_5H_6$ in the burner wall soot. Experimental evaluation of this explanation could not accomplished by this thesis because of equipment design limitations.

In summary, the synthesis of the thermally metastable fullerene in benzene/oxygen/ inert flames is either controlled strongly by pressure or is because of some as yet unknown post flame chemistry. Future work is recommended to explore, investigate and establish the origin of the thermally metastable fullerene in flames.

Chapter Five

Modeling Results and Discussion

5.0 Overview

This chapter presents and discusses the modeling results in light of all the experimental results presented in the previous chapter.

The modeling results are discussed under two sections:

5.1 Structural Studies
5.2 Thermochemical Kinetics Studies

The section on structural studies presents results that answer the question: which particular isomer of $C_{60}C_5H_6$ is the likely structure of the observed thermally metastable fullerene? The section on thermochemical kinetics studies presents results that answer the questions: Is the formation of $C_{60}C_5H_6$ mechanistically feasible? If so, then what is the predicted thermochemical rate? Each of these sections is discussed below.

5.1 Structural Studies

As mentioned in previous chapter, $C_{60}C_5H_6$ has many feasible isomers. Figure 5.1 presents two of these - the 1,2 $C_{60}C_5H_6$ (across the hexagon-hexagon edge) isomer and the 1,6 $C_{60}C_5H_6$ (across the hexagon-pentagon edge) isomer. Other structurally promising isomers are: 1,3 $C_{60}C_5H_6$, 1,9 $C_{60}C_5H_6$ (the numbers correspond to the positions shown in Figure 5.1).

These isomers were modeled using the force field MM3. The results are presented in Table 5.1. Out of the four isomers for $C_{60}C_5H_6$, the isomer with C_5H_6 placed across the hexagon-hexagon bridge of C_{60} has the lowest heat of formation. Thus, from the

heat of formation arguments, the 1,2 $C_{60}C_5H_6$ isomer structure is the most favored isomer structure amongst the four possible isomers. This structural result is consistent with all other reported structures for Diels-Alder products of C_{60} [106, 109-111].

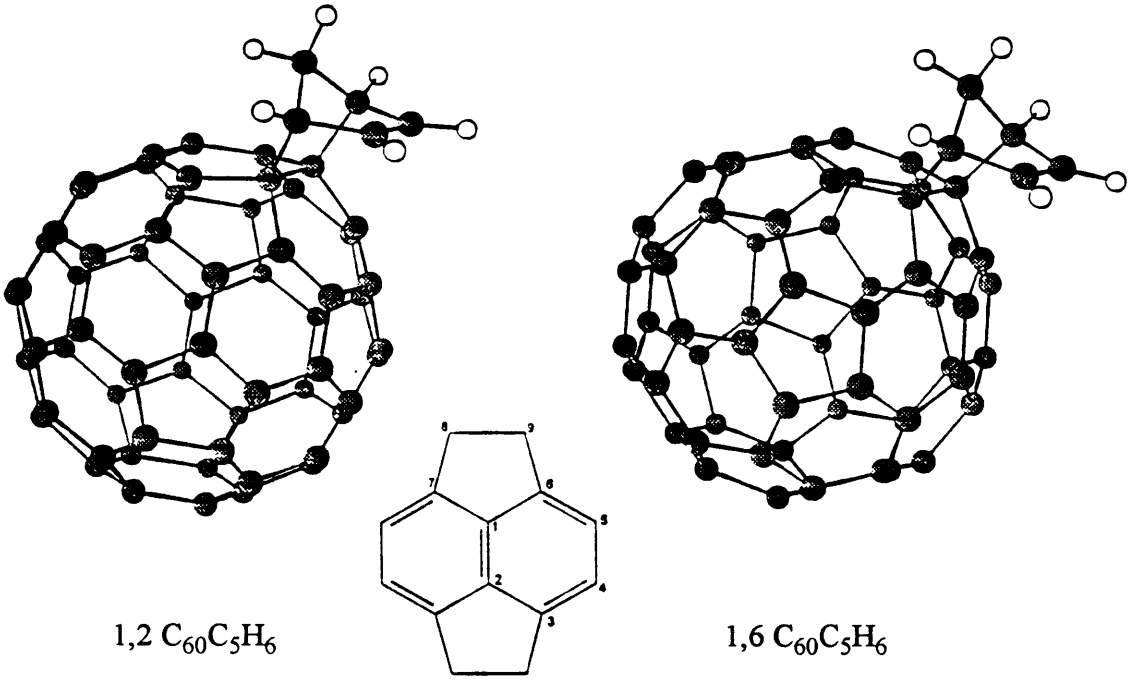

Figure 5.1 Illustrative $C_{60}C_5H_6$ isomers

Molecule	Standard Heat of Formation (ΔH_f^0)
	kcal/mol
1,2 $C_{60}C_5H_6$	612
1,6 $C_{60}C_5H_6$	629
1,3 $C_{60}C_5H_6$	655
1,9 $C_{60}C_5H_6$	671

Table 5.1 Enthalpy of formation for the isomers of $C_{60}C_5H_6$ at 298.15 K(calculated using MM3 1992).

Even though the difference between the heat of formation is large between the different isomers of $C_{60}C_5H_6$, Table 5.1 does not provide any indication whether the final product would be a single product (1,2 $C_{60}C_5H_6$) or a mixture of the isomers. This question can be addressed by considering the thermodynamic and the kinetic factors affecting the reaction. If a reaction is equilibrium controlled, then the final product is a mixture whose composition is determined energetically. However, if the reaction is kinetically controlled, then the final product is a mixture whose composition is determined by the activation energies required during the formation of the alternate products and by steric factors. As pointed out by Roberts and Caserio [127], for a Diels-Alder reaction to be kinetically controlled, it is necessary that the final products (isomers of $C_{60}C_5H_6$) can not in any way return to the reactants ($C_{60} + C_5H_6$) or that some of the reaction paths be sterically hindered. In other words, for kinetic arguments to apply, some of the reactions should be essentially irreversible or sterically hindered or both. Given the experimental facts presented and discussed in chapter 4 that prove that the thermally metastable $C_{60}C_5H_6$ undergoes a facile decomposition and formation, we conclude that the $C_{60}C_5H_6$ reaction is reversible. Furthermore, the unique three dimensional symmetry of C_{60} suggests that the steric hinderance will be identical for all reactions that yield $C_{60}C_5H_6$ isomers. Therefore, by the arguments of Roberts and Caserio [127], the reaction can not be kinetically controlled and, instead, must be equilibrium controlled. Given that the $C_{60}C_5H_6$ reaction is equilibrium controlled, we can determine the composition of the final product mixture by computing the equilibrium constant for the following reactions:

$$C_{60} + C_5H_6 \rightarrow 1{,}2\ C_{60}C_5H_6 \qquad (5.1)$$

$$C_{60} + C_5H_6 \rightarrow 1{,}6\ C_{60}C_5H_6 \qquad (5.2)$$

$$C_{60} + C_5H_6 \rightarrow 1{,}3\ C_{60}C_5H_6 \qquad (5.3)$$

$$C_{60} + C_5H_6 \rightarrow 1{,}9\ C_{60}C_5H_6 \qquad (5.4)$$

Once again, MM3 was used to compute the entropy and the specific heat of the reactants and the products. The results are presented in Table 5.2.

	Standard heat of formation (ΔH_f^0)	Standard Entropy (S^0)	Standard heat Capacity (C_p^0)
Molecule	kcal/mol	cal/(mol K)	cal/(mol K)
C_{60}	573.74	149.18	134.01
C_5H_6	32.78	66.00	18.33
1,2 $C_{60}C_5H_6$	612.32	173.29	152.50
1,6 $C_{60}C_5H_6$	629.08	173.90	153.11
1,3 $C_{60}C_5H_6$	654.88	173.77	152.37
1,9 $C_{60}C_5H_6$	671.08	173.77	153.09

Table 5.2 Thermodynamic properties of the reactants and the products at 298.15 K (calculated using MM3'92).

	Standard Heat of Reaction ΔH^0	Standard Entropy of Reaction ΔS^0	Standard Heat Cap. of Reaction ΔC_p^0	Standard Free Energy of Reaction ΔG^0	Standard Equil. Constant K_p^0
Reaction	kcal/mol	cal/(mol K)	cal/(mol K)	kcal/mol	atm^{-1}
$C_{60} + C_5H_6 \rightarrow 1,2\ C_{60}C_5H_6$	5.8	-41.9	0.15	18.29	$3.9*10^{-14}$
$C_{60} + C_5H_6 \rightarrow 1,6\ C_{60}C_5H_6$	22.56	-41.28	0.77	34.87	$2.7*10^{-26}$
$C_{60} + C_5H_6 \rightarrow 1,3\ C_{60}C_5H_6$	48.36	-41.42	0.03	60.71	$3.1*10^{-45}$
$C_{60} + C_5H_6 \rightarrow 1,9\ C_{60}C_5H_6$	64.56	-41.42	0.748	76.91	$4.2*10^{-57}$

Table 5.3 Equilibrium constants for the four reactions at 298.15 K (calculated using MM3'92).

The data presented in Table 5.2 were used to calculate the Gibbs free energy change and the equilibrium constant for reactions 5.1 through 5.4. The results are presented in Table 5.3.

The equilibrium constant data in Table 5.3 suggests that the relative concentration of 1,2 $C_{60}C_5H_6$ isomer at room temperature with respect to the concentration of next most stable product 1,6 $C_{60}C_5H_6$, is more than 11 orders of magnitude greater. Thus, the dominant product expected from purely thermodynamic arguments is 1,2 $C_{60}C_5H_6$. This result - the dominance of the hexagon-hexagon edge isomer - is consistent with other experimental results reported [83, 85-86, 107-114].

Other MM3 predicted structural properties (for example: heat of formation) for the 1,2 $C_{60}C_5H_6$ isomer are presented in Appendix B. Appendix B also presents the MM3 input file used during this thesis work.

While Table 5.3 predicts the equilibrium constant data for different isomers and suggests which isomer is *relatively* favored, the table falls short of explaining why the product is thermodynamically favored at room temperature in *absolute* terms. In other words, the data in Table 5.3 fails to explain why the thermally metastable fullerene, being studied, is formed at all at room temperature and why it decomposes at higher temperatures. Note from Table 5.3, that the $C_{60}C_5H_6$ formation reaction is endothermic. The endothermicity implies that higher temperatures will favor the formation of $C_{60}C_5H_6$. However, experimental facts (thermal metastability) presented in chapter 4 establish that higher temperatures do not favor the formation of $C_{60}C_5H_6$. Instead, higher temperatures favor formation of the reactants - which in turn implies that the reaction is exothermic. This failure of MM3 in predicting the exothermicity of the $C_{60}C_5H_6$ reaction, suggests that the MM3 is not a reliable means of modeling the thermochemical properties for the thermally metastable fullerene compound.

With MM3 failing to provide satisfactory results, it was first established whether semi-empirical quantum modeling with PM3 (MOPAC) might give more reliable results. This investigation on PM3's reliability was performed by studying the dimerization reaction of dicylopentadiene (see equation 5.5) with MM3'92 and with PM3 (MOPAC). The predicted thermochemical data by both methods were compared with the experimentally measured thermochemical data (discussed below) and, thereby, a measure of the modeling methods' relative reliability was obtained.

$$2\ C_5H_6 \leftrightarrow C_{10}H_{12} \qquad (5.5)$$

The dimerization of cyclopentadiene into *endo*-dicyclopentadiene[1] has been extensively studied and reviewed [115, 117, 128-139]. Table 5.4 presents the experimental kinetic data at 373 K along with the source from which the data has been obtained.

Reaction	Reaction Phase	Pre-exponential factor, A	Activation Energy, E_a	Reference
			kcal / mol	
$2\ C_5H_6 \rightarrow C_{10}H_{12}$	Paraffin	$10^{7.1}$ ltr/mol/sec	17.4	[136]
	Gas	$10^{6.1}$ ltr/mol/sec	16.7	[132, 138]
$C_{10}H_{12} \rightarrow 2\ C_5H_6$	Paraffin	$10^{13.0}$ /sec	34.2	[137]
	Gas	$10^{13.0}$ /sec	33.7	[134]

Table 5.4 Experimental Kinetic data for the dimerization of cyclopentadiene and the decomposition of *endo*-dicyclopentadiene

The data presented in Table 5.4 suggests that the experimental equilibrium constant for reaction 5.5 is given by $(10^{-5.9})$*exp(8454.96/T) ltr/mol in paraffin phase. In gas phase, the experimental equilibrium constant is given by $(10^{-6.9})$*exp(8555.61/T) ltr/mol (this calculation is in excellent agreement with the experimental equilibrium data for dimerization of cyclopentadiene in gas phase obtained by Khambata and Wassermann [136]). With the experimental equilibrium constant now available, we can compare the equilibrium constant as predicted by MM3 and MOPAC and thereby establish the relative reliability of the two methods in predicting the thermochemical data.

Table 5.5 presents the predicted thermochemical properties of cyclopentadiene and its dimer at 298.15 K. Using these predicted thermochemical properties and the equations discussed in chapter 3, we can calculate the thermochemical data for reaction 5.5. The results from these calculations is presented in Table 5.6. Table 5.6

[1]the endo isomer of dicyclopentadiene has been discussed by Khambata and Wassermann [133]

also compares the predicted thermochemical data with experimental data discussed above.

Species	Method	Standard heat of formation (ΔH_f^0)	Standard Entropy (S^0)	Standard Heat Capacity (C_p^0)
		kcal/mol	cal/(mol K)	cal/(mol K)
C_5H_6	MM3'92	32.8	66.0	18.3
	PM3	31.8	65.3	17.4
$C_{10}H_{12}$	MM3'92	48.8	86.4	35.5
	PM3	44.2	82.2	32.6

Table 5.5 Predicted thermochemical properties of cyclopentadiene and its dimer at 298.15 K

Prediction Method	Heat of Reaction ΔH_{rxn} (460 K)	Equilibrium Constant K_c (298.15 K)
	kcal/mol	ltr/mol
MM3'92	-16.9	$1.4*10^4$
PM3	-19.7	$2.7*10^5$
Experimental	-19.6[ζ]	$3.7*10^5$

[ζ]see Herndon and Lowry [117].

Table 5.6 Comparison of predicted and experimental thermochemical data for cyclopentadiene dimerization.

Table 5.6 shows that the PM3 predicted heat of reaction is much closer to the experimental heat of reaction than the MM3 predicted heat of reaction. Similarly, the

equilibrium constant as predicted by PM3 is closer to the experimental equilibrium constant than is the prediction by MM3. Table 5.6 therefore suggests that the PM3 (MOPAC) predictions are more reliable than MM3 and that atleast for the cyclopentadiene dimerization reaction at room temperature, the PM3 model performs remarkably well. Having now established that between molecular mechanics (MM3) and semi-empirical quantum model (PM3), the semi-empirical quantum model is more reliable in predicting the thermochemical data for cyclopentadiene dimerization reaction, an assumption was made that the semi-empirical quantum method will continue to perform better in predicting the thermochemical data for the reaction between cyclopentadiene and buckminsterfullerene. The rest of this chapter is based on the PM3 (MOPAC) model.

	Standard heat of formation (ΔH_f^0)	Standard Entropy (S^0)	Standard Heat Capacity (C_p^0)
Molecule	kcal/mol	cal/(mol K)	cal/(mol K)
C_{60}	811.7	122.7	104.6
C_5H_6	31.8	65.3	17.4
1,2 $C_{60}C_5H_6$	816.7	145.5	122.2

Table 5.7 Thermodynamic properties of the reactants and the products (calculated using PM3, MOPAC).

The results of the PM3 calculations on C_{60}, C_5H_6, 1,2 $C_{60}C_5H_6$ are presented in Table 5.7. The data presented in Table 5.7 was, once again, used to calculate the Gibbs free energy change and the equilibrium constant for reaction 5.1 (See Table 5.8). Noticing that the predicted values for ΔS^0 and ΔC_p^0 by MM3 (Table 5.3) and by PM3 (Table 5.8) for reaction 1 are close, it was assumed for modeling purposes, that for reaction 5.2, the ΔS^0 and ΔC_p^0 as predicted by MM3 are good approximate for PM3 values. The results so obtained, after making this approximation, are presented in Table 5.8.

	Standard Heat of Reaction ΔH^0	Standard Entropy of Reaction ΔS^0	Standard Heat Cap. of Reaction ΔC_p^0	Standard Free Energy of Reaction ΔG^0	Standard Equil. Constant K_p^0
Reaction	kcal/mol	cal/(mol K)	cal/(mol K)	kcal/mol	atm^{-1}
$C_{60} + C_5H_6 \rightarrow 1.2\ C_{60}C_5H_6$	-26.8	-42.5	0.2	-14.13	$2.5*10^{10}$
$C_{60} + C_5H_6 \rightarrow 1.6\ C_{60}C_5H_6$	-5.8	-41.3	0.8	6.5	$1.7*10^{-5}$

Table 5.8 Equilibrium constants at 298.15 K (calculated using PM3, MOPAC).

Table 5.8 predicts that, at room temperature, 1,2 $C_{60}C_5H_6$ would be the most favored product. It also predicts that the adduct synthesis reaction is exothermic and is associated with a large change in the Gibbs free energy. The large change in Gibbs free energy makes this reaction very sensitive to temperature changes (for every 10 K increase, the equilibrium for reaction 5.1 shifts backwards by an order of magnitude). These qualitatively correct predictions confirms that the semi-empirical quantum model (PM3) is more reliable in thermochemical equilibrium calculations over MM3. Since the transition state model for thermochemical kinetics involves implicit equilibrium calculations (see chapter 3), the above success suggests the assumption that PM3 would be more reliable for detailed thermochemical kinetic modeling of reaction 5.1. The thermochemical kinetic modeling calculations, based on this assumption, are presented next.

5.2 Thermochemical Kinetics Studies

The thermochemical studies were aimed to determine whether the formation of 1,2 $C_{60}C_5H_6$ is mechanistically feasible and if so whether the thermochemical kinetics can be predicted?

The formation of 1,2 $C_{60}C_5H_6$ from C_{60} and C_5H_6 is mechanistically feasible. The presence of thirty double bonds (with alkene character) on C_{60}, the high electronegativity of C_{60} [83] bestowing the double bonds of C_{60} with a dienophile character and the diene functional group in C_5H_6 makes C_{60} an ideal candidate for a reaction driven by the Diels-Alder mechanism [127]. Cyclopentadiene by itself has long been known to undergo dimerization to dicyclopentadiene, at room temperature, through the Diels-Alder mechanism and dicyclopentadiene has been known to dissociate to cyclopentadiene, upon heating, through the retro-Diels-Alder mechanism [115]. Cyclopentadiene is also known to react, through the Diels-Alder mechanism, with a host of alkene based molecules (See Table 5.9 for a few examples). It, therefore, isn't surprising that C_{60} and C_5H_6 react to form 1,2 $C_{60}C_5H_6$.

Reactants	Reference
$C_5H_6 + C_2H_4$	[116]
$C_5H_6 + C_2H_2$	[117]
$C_5H_6 + C_6H_4O_2$	[118]
$C_5H_6 + C_{10}H_6O_2$	[118]
$C_5H_6 + C_{11}H_{10}O_2$	[118]
$C_5H_6 + C_2(CN)_4$	[127]
$C_5H_6 + C_6H_5C_2H_2NO_2$	[127]

Table 5.9 Some illustrative Diels-Alder reactions

Given the mechanistic feasibility, the next issue is to predict the thermochemical kinetics of 1,2 $C_{60}C_5H_6$ formation. The general strategy was to use the transition state theory. That is, it was assumed that the reaction takes place through a transition state:

$$C_{60} + C_5H_6 \leftrightarrow [1,2\ C_{60}C_5H_6]^{\ddagger} \rightarrow 1,2\ C_{60}C_5H_6 \qquad (5.6)$$

Given this assumption and the theory presented in chapter 3, the chemical kinetics of the above reaction can be predicted. Such a prediction was made in three steps:

1. Determining the structure of the transition state

2. Modeling the thermochemical properties of the transition state
3. Predicting the activation energy and the pre-exponential factor

The results follow.

5.2.1 Determining the structure of the transition state

The transition state was determined using MOPAC. The internally provided transition state search option within MOPAC was used along the unrestricted Hartee-Fock specification. The starting geometry used for the MOPAC calculations was based on the results of Townshend et al. [119], Coxon et al. [120], Bach et al. [121] and Bernardi et al. [122]. Townshend et al. in their classic series on organic transition states, performed ab-initio calculations for Diels-Alder reactions using minimal STO-3G and extended 4-31G basis sets. Their results suggest that the bond length along the reaction coordinate on the Diels-Alder surface is 2.21 Å. More recent studies with more sophisticated theory - for instance, Coxon et al. [120] - confirm the results of Townshend et al. [119]. These results were used as the starting point for MOPAC calculations in this thesis. The detailed results of the MOPAC calculation are presented in Appendix C. The appendix also presents the full set of vibrational frequencies for the identified structure with an energy minima. The frequency set in Appendix C exhibits a single imaginary frequency that establishes that the identified structure is a transition structure. Figure 5.2 presents the salient structural features of the transition state (the dimensions are in Å). Note that the predicted reaction coordinate for $[C_{60}C_5H_6]^{\ddagger}$ is remarkably close to those predicted by Townshend et al. for Diels-Alder reaction [119].

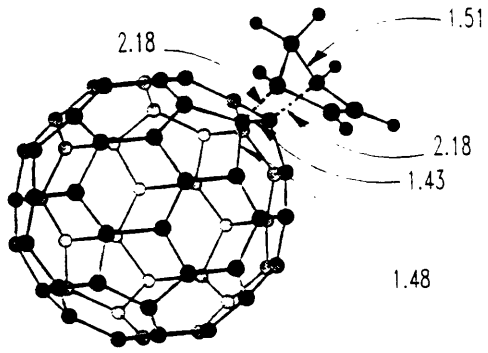

Figure 5.2 The structure of $[C_{60}C_5H_6]^{\ddagger}$ as identified using PM3 (MOPAC)

5.2.2 Modeling the thermochemical properties of the transition state

The thermochemical properties of C_{60}, C_5H_6, the transition state and the thermally metastable fullerene (1,2 $C_{60}C_5H_6$) were predicted by PM3. The PM3 results of the transition state are presented in Appendix C. The PM3 results of the thermally metastable fullerene is presented in Appendix D. For our immediate purposes, where we seek to predict the thermochemical kinetics for the formation of the thermally metastable fullerene, the standard state properties of the transition state and the thermally metastable fullerene are summarized in Table 5.10. The thermochemical properties of C_{60} and C_5H_6 were calculated in a manner identical to the method used for $C_{60}C_5H_6$ and these properties are also summarized in Table 5.10.

The properties listed in Table 5.10 are sufficient to predict the thermochemical kinetics for the formation of thermally metastable fullerene. The results of these calculations are presented in the next section.

Molecule	Standard heat of formation (ΔH_f^0)	Standard Entropy (S^0)	Standard Heat Capacity (C_p^0)
	kcal/mol	cal/(mol K)	cal/(mol K)
C_{60}	811.7	122.7	104.6
C_5H_6	31.8	65.3	17.4
[1,2 $C_{60}C_5H_6$]‡	867.5	151.4	124.6
1,2 $C_{60}C_5H_6$	816.7	145.5	122.2

Table 5.10 Thermodynamic properties of the reactants, the transition state and the product for the thermally metastable fullerene formation at 298.15 K (calculated using PM3).

5.2.3 Predicting the activation energy and the pre-exponential factor

The reaction of interest to us is the reaction 5.1, and for the sake of convenience it is the following reaction:

$$C_{60} + C_5H_6 \rightarrow 1{,}2\ C_{60}C_5H_6 \qquad (5.1)$$

With the available data in Table 5.10, the pre-exponential factor and the activation energy for this reaction can be predicted using the transition state theory. According to the transition state theory, the reaction path for reaction 5.1 is:

$$C_{60} + C_5H_6 \leftrightarrow [C_{60}C_5H_6]^{\ddagger} \rightarrow C_{60}C_5H_6$$

As discussed in chapter 3, under this model, a combination of the kinetic and thermodynamic arguments gives us an equation that we can now use to predict the reaction kinetics for reaction 5.1. For convenience, the equation is:

$$d[C_{60}C_5H_6]/dt = (\kappa k_B T/h)\exp(-\Delta S^{\ddagger}/R)\ \exp(-\Delta H^{\ddagger}/RT)\ [C_{60}][C_5H_6]$$

The activation energy and the pre-exponential factor in the Arrhenius equation can be given by:

$$A = (\kappa k_B T/h)\exp(-\Delta S^{\ddagger}/R)$$

$$E_a = \Delta H^{\ddagger}$$

In order to accomplish our mission, we need the heat of reaction and the entropy of reaction for the formation of transition state. From Table 5.10, we can obtain the heat of reaction and the entropy of reaction for the transition state as follows:

$$[\Delta H]^{\ddagger} = [\Delta H_f^0]^{\ddagger} - [\Delta H_f^0]_{C5H6} - [\Delta H_f^0]_{C60} = 24 \text{ kcal/mol}$$

$$[\Delta S]^{\ddagger} = [S^0]^{\ddagger} - [S^0]_{C5H6} - [S^0]_{C60} = -36.6 \text{ cal/(mol K)}$$

Substituting these numbers above, we get:

$$k_f = 6.26*10^4\ (T/300)\ \exp(-12078.51/T) \quad atm^{-1}\ sec^{-1}$$

Thus, at 298.15 K and for a gas phase reaction at constant pressure, we have:

$$\log_{10} A = 4.79\ atm^{-1}\ sec^{-1}$$

$$E_a = 24.0\ kcal/mol$$

We can now calculate the expected order of magnitude concentration of C_5H_6 that must exist in the flame so as to yield the observed concentrations of $C_{60}C_5H_6$ in the water cooled wall soot samples (T=298.15 K) from the flame. The PM3 predicted rate equation for the formation of the thermally metastable fullerene is:

$$d[C_{60}C_5H_6]/dt = 6.26*10^4\ (T/300)\ \exp(-12078.51/T)\ [C_{60}][C_5H_6] \quad atm/sec$$

In concentration units (see chapter 3), we have

$$d[C_{60}C_5H_6]/dt = 4.16*10^6\ (T/300)\ \exp(-12078.51/T)\ [C_{60}][C_5H_6]\ mol/(ltr\ sec)$$

For order of magnitude estimates, we can simplify this to:

$$[C_{60}C_5H_6]/\tau = 4.16*10^6\ (T/300)\ \exp(-12078.51/T)\ [C_{60}][C_5H_6]\ mol/(ltr\ sec)$$

where,

[Z]: concentration of species Z, mol/ltr
τ: reaction time during which high concentrations of C_5H_6 is available
(= 5 msec, see Bittner and Howard [27])

For order of magnitude esimates and noting the fact that the amount of the thermally metastable fullerene formed is small, we can take the relative concentration of $C_{60}C_5H_6$ and C_{60} to be:

$$[C_{60}C_5H_6] / [C_{60}] = 0.01$$

Therefore, we have

$$[C_5H_6] = 1.97*10^{11} \text{ mol/ltr} = 1.97*10^{8} \text{ mol/cc}$$

The expected concentration of C_5H_6 in the flame gases that is required to explain the observed concentration of $C_{60}C_5H_6$ in soot, according to the PM3 model, is $1.97*10^8$ mol/cc and is clearly very large. This anomaly leads us to two conjectures. First, that the observed concentration of $C_{60}C_5H_6$ is not the consequence of a gas phase reaction, and is, instead, the consequence of a solution phase reaction (that is, a reaction which happens after the flame derived soot is dissolved in toluene). Second, that the PM3 is currently unable to model this reaction. If the first conjecture is true, then the kinetics of a solution phase reaction should explain all experimental facts.

Solution based kinetics can be predicted by a simplified model. Lets assume:

1. The frequency factor in liquid phase will be the same as in gas phase. Kaufmann and Wasserman [129] show that this is the case for cyclopentadiene dimerization reaction in a number of polar and non-polar solvents.

2. The activation energy for the reaction in liquid phase should change to account for the heats of solution of all the species involved in the reaction. As noted by Wynne-Jones and Eyring [140] and Evans and Polanyi [141], the activation energies between the solution phase and the gas phase are related by the equation

$$[E_a]_{liq} = [E_a]_{gas} + [\Delta H_{soln}]_{C5H6} + [\Delta H_{soln}]_{C60} - [\Delta H_{soln}]_{trans\ state}$$

Wassermann [142] and Kaufmann and Wassermann [129] have shown that, in case of the dimerization of cyclopentadiene, the heats of solution for two molecules of cyclopentadiene is similar to the heat of solution for the cyclopentadiene-

cyclopentadiene transition state. Let us assume that this is true for the present case too. That is:

$$[\Delta H_{soln}]_{C5H6} + [\Delta H_{soln}]_{C60} = [\Delta H_{soln}]_{trans\ state}$$

Thus,

$$[E_a]_{liq} = [E_a]_{gas}$$

The rate equation for the formation of $C_{60}C_5H_6$ in solution is, therefore, given by:

$$d[C_{60}C_5H_6]/dt = 4.16*10^6\ (T/300)\ \exp(-12078.51/T)\ [C_{60}][C_5H_6]\ \ mol/(ltr\ sec)$$

We can now recalculate the required concentration of C_5H_6 in solution that would explain the observed concentration of $C_{60}C_5H_6$. The calculation strategy is identical to the one used for the gas phase calculations above. The reaction time in solution phase is now of the order of an hour (the time required to sonicate the soot in toluene and then filter the solution). With this as the only change, the required concentration of C_5H_6 in solution is:

$$[C_5H_6] = 2.73*10^5\ mol/ltr$$

This predicted concentration is also very large, although much lower than that required for a gas phase reaction. This unrealistically high concentration suggests that either the formation of $C_{60}C_5H_6$ is not a simple bimolecular process (it could be a catalytic process) or the PM3 model performs unsatisfactorily in predicting reactions kinetics of reaction 5.1.

We can establish the reliability of PM3 model by comparing its prediction with the experimentally determined kinetics for reaction 5.1 by Pang and Wilson [125] and Giovane et al. [126]. This comparison now follows.

Pang and Wilson [125] have recently determined the kinetic data for:

$$C_{60} + C_5H_6 \rightarrow C_{60}C_5H_6 \qquad \text{(in solution)}$$

According to their experiments,

$$A = 6.31*10^4 \text{ ltr/(mol sec)} \qquad \text{and} \qquad E_a = 6.94 \text{ kcal/mol}$$

The pre-exponential predicted ($A = 4.16*10^6$ ltr/(mol sec)) using the semi-empirical model is off by two orders of a magnitude. The activation energy as predicted by the semi-empirical model is about 4 times higher than the experimental value. Since, the activation energy is an exponential factor, this prediction is not satisfactory.

Giovane et al. [126] has predicted the thermochemical data for the decomposition reaction:

$$C_{60}C_5H_6 \rightarrow C_{60} + C_5H_6 \qquad \text{(in solution)}$$

According to Giovane et al. [126], the kinetic data for this reaction is:

$$A = 7.94*10^{12} \text{ /sec} \qquad \text{and} \qquad E_a = 27.3 \text{ kcal/mol}$$

Combining the two results, the experimental equilibrium constant can now be calculated.

$$K_c = k_f / k_b = 7.94*10^{-9} * \exp(10282.8/T) \quad \text{ltr/mol}$$

Therefore, at 298.15 K, the experimental equilibrium constant in solution is

$$K_c = 7.68*10^6 \text{ ltr/mol}$$

The predicted gas phase equilibrium constant using PM3 ($K_c = 1.66*10^{12}$ ltr/mol) is about 5 orders of magnitude off, if one assumes the equilibrium constant of the reaction to be same in liquid phase and in the gas phase. Nevertheless, considering the fact that semi-empirical quantum models such as PM3 have not been empirically

adjusted for fullerenes, the model has faired remarkably well in predicting the qualitative trends such as the effect of higher temperature on the concentration of $C_{60}C_5H_6$, the magnitude of the pre-exponential factor and the identity of the $C_{60}C_5H_6$ isomer that is formed.

Chapter Six

Conclusions

The conclusions that can be drawn from this thesis relate to four areas:

- Flame optimization
- Characterization of the thermally metastable fullerene
- Mechanism of thermal instability
- Computational chemistry

FLAME OPTIMIZATION

The following conclusions can be drawn from this thesis' flame optimization results:

1. Sooting flames can yield large quantities of fullerenes.

2. The yield of fullerenes in sooting flames depends on many variables -- gas velocity, feed C/O ratio, combustion pressure, concentration of the diluent present and the type of the diluent present. Of these, the gas velocity, the feed C/O ratio and the combustion pressure are the variables which have major impact on the fullerenes yield.

3. Given the high yields of fullerenes in the sooting flames studied here, it seems likely that fullerenes formation and soot formation involve some common reactants under the conditions studied.

4. The concentration of the thermally metastable fullerene along the flame length is at least two orders of magnitude less than what it would be if its concentration relative to C_{60} were the same in the probe sample as in the burner wall sample.

This suggests that the formation of the thermally metastable fullerene, studied by this thesis, is not because of a flame process.

CHARACTERIZATION OF THE THERMALLY METASTABLE FULLERENE

The characterization work done during the course of this thesis leads to the following conclusions:

1. The thermally metastable fullerene characterized by this thesis is not an isomer of C_{60}. However this does not mean that isomers of C_{60} do not exist. There is no experimental evidence known at the time of the publication of thesis that would eliminate the possibility that C_{60} isomers may exist in nature.

2. The thermally metastable fullerene characterized and studied during this thesis is $C_{60}C_5H_6$. This isomer is different from $C_{60}C_7H_{10}$, the thermally metastable fullerene isomer originally identified and studied by Anacleto et al. [32, 36, 37].

3. The thermally metastable fullerene identified ($C_{60}C_5H_6$) is consistent with the observed FTIR spectrum, proton NMR spectrum, ^{13}C NMR spectrum, EI mass spectrum, Ion Spray mass spectrum, Creegan $C_{60}O$ test, distinct UV-Vis spectrum and the lower retention time during HPLC on C^{18} column.

MECHANISM OF THERMAL INSTABILITY

The thermal instability observed can be summarized by the equation:

$$C_{60} + C_5H_6 \leftrightarrow C_{60}C_5H_6$$

Following conclusions can be made:

1. Diels-Alder and retro-Diels-Alder reaction mechanisms adequately explain the observed reversibility in the above reaction. The observed reversibility is consistent with the observed reversibility in other Diels-Alder reactions [129-139].

2. The $C_{60}C_5H_6$ formation reaction is not kinetically controlled. The unique three dimensional ball shape of C_{60} bestows all alternative Diels-Alder products from C_{60} and C_5H_6 with the same steric hinderance and therefore any kinetic control emanating from steric factors is not possible in the reaction studied. This fact, combined with the experimentally observed facile reversibility suggests that the $C_{60}C_5H_6$ formation reaction is not kinetically controlled.

3. The thermal instability can be best explained by thermodynamic arguments. The large Gibbs free energy change (predicted to be -14.13 kcal/mol at 298.15 K) for the $C_{60}C_5H_6$ reaction makes the equilibrium constant very sensitive to temperature changes. Every 10 degree increase in temperature, leads to about a ten fold decrease in the equilibrium constant and therefore leads to a large change in the thermodynamically expected relative concentration of C_{60}, C_5H_6, and $C_{60}C_5H_6$.

4. The observed ease and spontaneity with which $C_{60}C_5H_6$ forms suggests that Diels-Alder reactions can be used to develop novel compounds and materials from fullerenes as has also been observed recently by Rubin et al. [109], by Belik et al. [110], by Schlueter et al. [111] and Tsuda et al. [106].

COMPUTATIONAL CHEMISTRY

Computational chemistry tools have come a long way and are now in a shape that they can be used by chemical engineers to routinely study chemical reaction mechanisms. For engineering purposes, these tools are quite reliable and it can be expected that in future these tools will become more accurate since these tools are in the process of being improved. Even for a novel application such as fullerenes, these computational chemistry tools have qualitatively explained the formation of the thermally metastable fullerene in the following way:

1. The $C_{60}C_5H_6$ formation reaction is predicted to be exothermic.

2. The $C_{60}C_5H_6$ formation reaction is predicted to have large Gibbs free energy change. This suggests that the reaction will be sensitive to temperature changes (i.e. thermally metastable). This prediction is qualitatively correct vis-a-vis the observed facts.

3. During Diels-Alder reactions, bonding across the hexagon-hexagon edge in fullerene cage is thermodynamically favored over hexagon-pentagon edge. This conclusion is consistent with all other reported adducts of C_{60} [108-114].

4. The predicted bond length along the reaction coordinate for the Diels-Alder transition state, formed during [$C_{60}C_5H_6$] synthesis, is 2.18 Å. This value is remarkably close to the 2.21 Å value predicted by Townshend et al. [119] for other Diels-Alder reactions using ab-initio methods.

RECOMMENDATIONS:

1. The results and conclusions in this thesis should be true in analogous terms for the thermally metastable fullerene observed with C_{70}. A test of this prediction can provide an independent test for the methodology and arguments provided in this thesis.

2. Experimental evidence for the proposed 1,2 $C_{60}C_5H_6$ structure can be obtained with ^{13}C NMR of other Diels-Alder products - for instance with an adduct synthesized with cyclohexadiene or with cyclobutadiene. This would test out the thermodynamic prediction obtained during this thesis' computational chemistry modeling work.

3. The mechanism of formation of fullerenes in flames is an open question. The computational tools used in this thesis coupled with the experimental methods used in this thesis would go a long way in modeling the synthesis of fullerenes in flames.

Appendix A

A.0 Overview

This appendix presents and discusses the experimental data collected during this thesis' study of benzene/oxygen/inert flames. The data is, for the sake of clarity, presented and discussed in two sections:

A.1 The Flame Optimization Study
A.2 The Flame Profile Study

The section on the flame optimization study supplements section 4.1 of chapter 4. This section presents the yield of C_{60}+C_{70} as a function of the process variables. This section also presents the relative abundance of the metastable fullerene for these flames and explains the basis used to determine the relative abundance of the thermally metastable fullerene. The section on the flame profile study supplements section 4.4 of chapter 4. The section presents and discusses on the data used to plot Figure 4.19.

A.1 The Flame Optimization Study

Table A.1 presents the experimental data collected during the process development effort for the flame. The burner pressure represents the pressure in the combustion chamber during the formation of the fullerenes rich soot. The fuel C/O ratio represents the molar ratio of the carbon and the oxygen atoms in the premixed feed. The gas velocity is defined as the cold (298 K) standard gas velocity of the premixed feed on the burner surface. The diluent concentration is the molar concentration of the diluent in the premixed feed. The yield of C_{60}+C_{70} is listed on a % weight of soot basis. The yield is computed using the following equation:

Yield of C_{60}+C_{70} = (Concentration of C_{60}+C_{70} in the sample, mg/ml * Volume of the sample, ml) / (Weight of Soot used to prepare the sample, mg)

where,

Concentration of C_n in the sample= Slope of the C_n calibration curve * Absorbance area of C_n peak + Intercept of the C_n calibration curve

C_n : C_{60}, C_{70}

Sample	Burner Pressure (Torr)	Fuel C/O ratio (atomic)	Gas Velocity[a] (cm/sec)	% Diluent[b] (Diluent Type)	Yield of C_{60}+C_{70}, Wt. % of Soot	Metastable Fullerene, Rel. Abund.[c]
1	20	1.04	50	50 (He)	2.1	nm[d]
2	20	1.04	50	30 (Ar)	2.5	nm
3	20	1	50	10 (He)	2.6	nm
4	50	1.08	38	25 (He)	2.7	0.12
5	20	1.04	50	30 (N_2)	3.2	nm
6	20	1.04	50	10 (He)	3.2	nm
7	35	1	29	25 (He)	5.7	nm
8	20	1	50	20 (He)	5.9	nm
9	20	1.04	50	30 (He)	6.3	nm
10	57	0.99	46	25 (He)	6.5	nm
11	20	1.04	52	19 (He)	6.9	nm
12	30	1.01	50	25 (He)	7.2	nm
13	40	0.99	36	25 (He)	9.0	0.23
14	37.5	0.91	40	25 (He)	11.5	nm
15	37.5	1	40	20 (He)	11.9	nm
16	40	0.99	40	25 (He)	12.6	0.45
17	37.5	1.01	40	25 (He)	12.6	nm
18	37.5	1	40	30 (He)	12.7	0.36
19	37.5	0.94	50	*None*	12.7	nm
20	37.5	0.96	50	25 (N_2)	13.8	1.03
21	37.5	1	40	15 (He)	14.4	0.69
22	40	0.99	44	25 (He)	14.4	0.65
23	37.5	0.96	50	25 (Ar)	14.5	1.10
24	40	0.99	48	25 (He)	14.8	nm
25	37.5	0.96	50	25 (He)	16.2	0.95
26	37.5	0.96	40	25 (He)	19.6	1.30

[a] at inlet; [b] molar basis; [c] Relative Abundance; [d] not measured

Table 4.1 Representative data collected during the process development of fullerenes producing flame.

The following assumptions have been made so as to estimate the relative abundance of the thermally metastable fullerene:

- The slope of the actual calibration curve of the thermally metastable fullerene is same as that for C_{60}.
- The intercept of the actual calibration curve of the thermally metastable fullerene may be ignored in calculating the relative abundance.

The following equation has been used to estimate the relative abundance:

Relative Abundance = (Absorbance area for the thermally metastable fullerene * Calibration Slope for C_{60}, mg/ml * Volume of the Extract, ml / Weight of the Soot Extracted, mg) * 100

A.2 The Flame Profile Study

Table A.2 presents the data collected from the flame profile study during this thesis.

The burner pressure, in Table A.2, represents the pressure in the combustion chamber during the formation of the fullerenes rich soot. The fuel C/O ratio represents the molar ratio of the carbon and the oxygen atoms in the premixed feed. The gas velocity is defined as the cold (298 K) standard gas velocity of the premixed feed on the burner surface. The diluent concentration is the molar concentration of the diluent in the premixed feed. The height above the burner is the actual (not corrected in any way) height between the probe tip and the burner surface. The probe diameter is the inner diameter of the probe tip. The flame temperature is the temperature of the flame at the probe tip as measured by the pyrometer (not corrected in any way). The details about the pyrometer used, have been described by McKinnon [31]. The gas volume sampled through probe is the standard volume (300 K) of the flame gas that was sampled during the particular experiment. The gas volume sampled through probe is found by correcting the volume of gases collected in the inverted water column (described in chapter 3) collected during the time when the water column was on line. The correction was obtained by scaling the gas volume by the ratio of the actual probe run time to the time when the water column was on line. Total C_{60} and C_{70} collected in the probe are the total mass of the C_{60} and C_{70} collected in the soot sampled in the probe during the particular experiment (the soot collection and extraction procedure is described in chapter 3). Finally, the C_{60} and C_{70} concentrations in the flame are obtained by dividing the total C_{60} and C_{70} collected in the probe by the total gas volume sampled through the probe (no corrections for diffusivity or any other factors are made).

Sample	1	2	3	4	5	6	7
Burner Pressure, (Torr)	37.5	37.5	37.5	37.5	37.5	37.5	37.5
Fuel C/O Ratio, atomic	0.95	0.95	0.95	0.95	0.95	0.95	0.95
Gas Velocity[a] ,(cm/sec)	39.9	39.9	39.9	39.9	39.9	39.9	39.9
Helium Concn, (%)[b]	25	25	25	25	25	25	25
Height Above Burner, (mm)	**3**	**4**	**5**	**6**	**6.5**	**7.5**	**10**
Probe Diameter, (mm)	1.1	1.1	1.1	0.9	1.1	1.3	0.9
Flame Temperature[c], (°C)	1185	1168	1173	1143	1120	1138	1118
Gas Volume Sampled through Probe, (ltr)[d]	5.17	5.43	5.07	4.09	5.21	5.21	3.31
Total C_{60} collected in probe, (μg)	0.0	0.0	0.0	0.0	0.0	189.67	140.74
Total C_{70} collected in probe, (μg)	0.0	0.0	0.0	0.0	0.0	525.41	335.46
Concentration of C_{60} in the flame, (μg/ltr)[e]	0.0	0.0	0.0	0.0	0.0	36.42	42.48
Concentration of C_{70} in the flame, (μg/ltr)[e]	0.0	0.0	0.0	0.0	0.0	100.87	101.25

Sample	8	9	10	11	12	13	14
Burner Pressure, (Torr)	37.5	37.5	37.5	37.5	37.5	37.5	37.5
Fuel C/O Ratio, atomic	0.95	0.95	0.95	0.95	0.95	0.95	0.95
Gas Velocity[a] ,(cm/sec)	39.9	39.9	39.9	39.9	39.9	39.9	39.9
Helium Concn, (%)[b]	25	25	25	25	25	25	25
Height Above Burner, (mm)	**12.5**	**15**	**17.5**	**20**	**30**	**50**	**70**
Probe Diameter, (mm)	0.9	1.1	0.9	1.1	1.1	0.9	0.9
Flame Temperature[c], (°C)	1105	1112.5	1085	1052.5	1037.5	962.5	932.5
Gas Volume Sampled through Probe, (ltr)[d]	3.77	5.27	4.88	5.81	5.40	3.99	4.60
Total C_{60} collected in probe, (μg)	462.07	52.61	121.76	194.17	135.09	419.27	789.63
Total C_{70} collected in probe, (μg)	816.83	283.19	292.8	245.51	361.99	736.06	1489.39
Concentration of C_{60} in the flame, (μg/ltr)[e]	122.37	9.98	24.98	33.39	25.03	104.98	171.71
Concentration of C_{70} in the flame, (μg/ltr)[e]	216.33	53.73	60.08	42.22	67.06	184.29	323.88

[a]At Inlet, 300K; [b]Helium Concentration, molar basis; [c]Uncorrected, as measured by Pyrometer, see McKinnon [31]; [d]Standard Liters collected in water column, corrected for run time through probe as explained in Chapter 3; [e]Standard Liters

Table A.2 Data Collected during Flame Profile Study

Appendix B

An extract from the output file from MM3'92 that was obtained from simulating 1,2 $C_{60}C_5H_6$ (see chapter 5 for a schematic of the molecule).

```
*****************************************************************************
 C60C5H6 across C6-C6 bond                                          1 71 0 0 0 0 10.0
 TTTTTTTTT TTTTTTTTTTTTTTTTTTTTTTTTTTTTTTTTTTTTTTTTTTTTTTTTTTTTTTTTTTTTTTT01 2 0 0 0
0 0 000 0
0 34    0.0000400      6  0      0  0  0  0  1      1  0
   1  11  21  34  54
   1   3  13  23  36  56
   1   9  19  29  32
   2  12  22  35
   2  10  20  30  33  53
   2   4   6   8  10
   3   5   7   9
   4  14  24  37  57
   5  15  25  38  58
   6  16  26  39  59
   7  17  32  52
   8  18  28  31
  11  36
  12  37
  13  38
  14  39
  15  40  60
  16  31  51
  17  27  47  51  46
  18  33
  19  34
  20  35  55
  21  41  55  50  54  49
  22  42  56  41
  23  43  57  42
  24  44  58  43
  25  45  59  44
  26  46  60  45
  27  40
  28  48  52  47
  29  49  53  48
  30  50
   1  61  63  62  11
  62  64  65  61
  61  66  62  67  63  68  63  69  64  70  65  71
  3.28286  0.79340  0.19813 C  1(  1)
 -2.74949 -2.59709 -0.85807 C  2(  2)
  2.63841  1.45445 -1.02099 C  2(  3)
 -3.44703 -1.41918 -1.34369 C  2(  4)
```

1.84234	2.58139	-0.59701	C	2(	5)
-3.95900	-0.69447	-0.19306	C	2(	6)
1.76067	2.57114	0.85069	C	2(	7)
-3.57535	-1.42379	1.00385	C	2(	8)
2.49975	1.43501	1.34851	C	2(	9)
-2.82892	-2.59993	0.59276	C	2(	10)
3.28281	-0.79409	0.19516	C	1(	11)
-1.58881	-3.02766	-1.49148	C	2(	12)
2.23497	0.74411	-2.12965	C	2(	13)
-2.95316	-0.72193	-2.44054	C	2(	14)
0.75802	3.02412	-1.34832	C	2(	15)
-3.95900	0.69544	-0.19038	C	2(	16)
0.60277	3.01484	1.48315	C	2(	17)
-3.20421	-0.73088	2.15073	C	2(	18)
1.98366	0.73282	2.41312	C	2(	19)
-1.74406	-3.03313	1.34740	C	2(	20)
2.49999	-1.44022	1.34326	C	2(	21)
-0.45571	-3.47579	-0.70204	C	2(	22)
2.23479	-0.73580	-2.13237	C	2(	23)
-1.73886	-1.17011	-3.09912	C	2(	24)
0.37889	2.31134	-2.54415	C	2(	25)
-3.44702	1.42456	-1.33823	C	2(	26)
-0.53128	3.47526	0.69794	C	2(	27)
-3.20418	0.72270	2.15356	C	2(	28)
0.77107	1.16839	3.07189	C	2(	29)
-1.35652	-2.30956	2.54576	C	2(	30)
-3.57535	1.42013	1.00932	C	2(	31)
0.09586	2.30053	2.62827	C	2(	32)
-2.06927	-1.18199	2.93628	C	2(	33)
1.98398	-0.74235	2.41044	C	2(	34)
-0.53132	-3.47794	0.68444	C	2(	35)
2.63814	-1.45039	-1.02640	C	2(	36)
-1.07274	-2.29955	-2.63770	C	2(	37)
1.09840	1.18024	-2.91379	C	2(	38)
-2.95314	0.73150	-2.43775	C	2(	39)
-0.45557	3.47845	-0.68855	C	2(	40)
1.76053	-2.57462	0.84071	C	2(	41)
0.75783	-3.01896	-1.36004	C	2(	42)
1.09830	-1.16891	-2.91825	C	2(	43)
-0.98480	0.00671	-3.49885	C	2(	44)
-1.07268	2.30968	-2.62881	C	2(	45)
-2.74943	2.60049	-0.84808	C	2(	46)
-1.74403	3.02794	1.35914	C	2(	47)
-2.06927	1.17064	2.94075	C	2(	48)
0.02414	-0.00688	3.48287	C	2(	49)
0.09579	-2.31069	2.61943	C	2(	50)
-2.82893	2.59773	0.60281	C	2(	51)
-1.35650	2.29969	2.55460	C	2(	52)
-1.36351	-0.00669	3.42105	C	2(	53)
0.77097	-1.18057	3.06751	C	2(	54)
0.60283	-3.02083	1.47138	C	2(	55)

1.84212	-2.57901	-0.60687	C	2(56)
0.37872	-2.30155	-2.55298	C	2(57)
0.40151	0.00653	-3.40722	C	2(58)
-1.73885	1.18212	-3.09456	C	2(59)
-1.58867	3.03335	-1.47975	C	2(60)
4.79683	1.13569	0.33304	C	1(61)
4.79679	-1.13694	0.32860	C	1(62)
5.28411	-0.00243	1.25608	C	1(63)
5.46481	-0.66835	-0.96862	C	2(64)
5.46487	0.67214	-0.96600	C	2(65)
5.05485	2.16488	0.65544	H	5(66)
5.05481	-2.16738	0.64700	H	5(67)
4.79464	-0.00436	2.25345	H	5(68)
6.38904	-0.00272	1.39381	H	5(69)
5.83617	-1.33437	-1.75921	H	5(70)
5.83627	1.34122	-1.75397	H	5(71)

==========
FULL-MATRIX OPTIMIZER
==========

* * * ENERGY IS MINIMIZED WITHIN RMS OF FORCES 0.00009 Kcal/A * * *

HEAT OF FORMATION AND STRAIN ENERGY CALCULATIONS

(UNIT = KCAL/MOLE)
(# = TRIPLE BOND)

BE = 9521.17 SBE = 9526.53

PFC = 2.40

STERIC ENERGY (E)	381.13
SIGMA-STRETCHING (ECPI)	7.67
CORRECTED STERIC ENERGY (EC) = E-ECPI	373.46
ENERGY FROM PLANAR VESCF CALCULATION (ESCF)	-9284.71

HEAT OF FORMATION = EC + BE + PFC + ESCF	612.32
STRAINLESS HEAT OF FORMATION FOR SIGMA SYSTEM (HFS) HFS = SBE + T/R + ESCF - ESCF	236.55
INHERENT SIGMA STRAIN (SI) = E + BE - SBE	375.76
SIGMA STRAIN ENERGY (S) = POP + TOR + SI	375.76

(RESONANCE ENERGY NOT CALCULATED.)

END OF C60C5H6 across C6-C6 bond

TOTAL CPU TIME IS 508.23 SECONDS

Appendix C

An extract of the output file from PM3 (MOPAC) that was obtained from modeling the transition state [1,2 $C_{60}C_5H_6$]‡.

```
*****************************************************************************
** FRANK J. SEILER RES. LAB., U.S. AIR FORCE ACADEMY, COLO. SPGS., CO. 80840 **
*****************************************************************************

                    PM3 CALCULATION RESULTS

*****************************************************************************
*       MOPAC:  VERSION  6.00          CALC'D. 05-Mar-93
*****************************************************************************
MOPAC SIMULATION OF  C60C5H6 TRANSITION STATE

  (I)          NA:I       NB:NA:I     NC:NB:NA:I    NA   NB   NC

   1    C
   2    C     1.38382 *                    1
   3    C     1.45757 *   120.00362 *          2    1
   4    C     1.38420 *   119.97010 *   0.13294 *  3    2    1
   5    C     1.45736 *   119.99357 *  138.25581 *  2    1    3
   6    C     1.45732 *   120.03572 *  -0.00289 *  1    2    3
   7    C     1.45726 *   120.03031 * -138.31329 *  1    2    3
   8    C     1.38408 *   119.97394 *  -0.10738 *  6    1    2
   9    C     1.38408 *   119.98688 *   0.09535 *  7    1    2
  10    C     1.45727 *   107.99573 * -142.73478 *  6    1    2
  11    C     1.45726 *   107.99710 *  142.73921 *  7    1    2
  12    C     1.45709 *   119.99052 * -138.13704 *  8    6    1
  13    C     1.38412 *   119.99351 *  -0.02012 *  5    2    1
  14    C     1.45727 *   107.98480 * -142.63937 *  5    2    1
  15    C     1.45752 *   107.95872 *  142.62098 *  3    2    1
  16    C     1.45721 *   120.02375 *  138.08005 *  4    3    2
  17    C     1.38417 *   119.97845 *  142.60317 *  10   6    1
  18    C     1.38414 *   119.97234 * -142.60744 *  11   7    1
  19    C     1.45769 *   120.00276 *  -0.00694 *  18   11   7
  20    C     1.38388 *   120.01095 *  -0.07326 *  12   8    6
  21    C     1.38388 *   119.99861 *   0.01855 *  19   18   11
  22    C     1.45778 *   108.00058 * -142.56756 *  16   4    3
  23    C     1.45708 *   120.01141 * -138.16711 *  13   5    2
  24    C     1.38386 *   120.00867 *   0.01840 *  16   4    3
  25    C     1.38391 *   119.99890 *  -0.04143 *  23   13   5
  26    C     1.38424 *   119.99628 * -142.55945 *  15   3    2
  27    C     1.38420 *   119.96786 *  142.63134 *  14   5    2
  28    C     1.45736 *   119.95885 * -138.09363 *  27   14   5
  29    C     1.38328 *   120.01698 *  -0.09422 *  28   27   14
  30    C     1.45778 *   107.98642 *  142.53675 *  23   13   5
```

31	C	1.45734	*	119.95751	*	138.07305	*	18	11	7
32	C	1.38333	*	120.02711	*	0.09848	*	31	18	11
33	C	1.45807	*	107.92867	*	-142.41560	*	31	18	11
34	C	1.45753	*	119.97389	*	138.13259	*	20	12	8
35	C	1.38386	*	120.02110	*	142.48363	*	22	16	4
36	C	1.38504	*	120.06866	*	-0.21243	*	34	20	12
37	C	1.45352	*	108.04917	*	-142.35254	*	34	20	12
38	C	1.45343	*	108.07936	*	-0.22603	*	33	31	18
39	C	1.38378	*	119.99702	*	-142.43615	*	30	23	13
40	C	1.45808	*	107.93958	*	142.42580	*	28	27	14
41	C	1.45806	*	119.93805	*	138.05284	*	29	28	27
42	C	1.45340	*	108.07294	*	0.22119	*	40	28	27
43	C	1.45710	*	120.06395	*	-0.02113	*	35	22	16
44	C	1.38499	*	119.88468	*	0.25715	*	43	35	22
45	C	1.38497	*	119.60377	*	-142.54612	*	42	40	28
46	C	1.45467	*	120.15053	*	-138.24403	*	36	34	20
47	C	1.38510	*	119.83499	*	142.30984	*	37	34	20
48	C	1.38499	*	119.60255	*	142.55717	*	38	33	31
49	C	1.38517	*	120.03677	*	142.25163	*	33	31	18
50	C	1.38518	*	120.04193	*	-142.24956	*	40	28	27
51	C	1.38509	*	120.02477	*	-0.27838	*	41	29	28
52	C	1.45464	*	108.17982	*	-142.73660	*	43	35	22
53	C	1.45256	*	120.66697	*	138.67113	*	50	40	28
54	C	1.37914	*	120.38438	*	142.51781	*	52	43	35
55	C	1.37911	*	120.38611	*	0.36211	*	46	36	34
56	C	1.45472	*	120.17367	*	0.43891	*	48	38	33
57	C	1.37885	*	119.31038	*	-0.68752	*	53	50	40
58	C	1.37886	*	120.41523	*	-0.29375	*	56	48	38
59	C	1.47787	*	109.36283	*	-147.67914	*	53	50	40
60	C	1.47792	*	121.84040	*	-143.03519	*	58	56	48
61	**C**	**2.18487**	*	**109.17129**	*	**-103.31797**	*	**59**	**53**	**50**
62	**C**	**2.18487**	*	**109.18163**	*	**-110.68784**	*	**60**	**58**	**56**
63	**C**	**1.51004**	*	**90.11854**	*	**-164.04354**	*	**61**	**59**	**53**
64	C	1.39626	*	96.03446	*	56.33419	*	62	60	58
65	C	1.41591	*	108.83567	*	75.48018	*	64	62	60
66	H	1.09019	*	100.70613	*	72.23850	*	61	59	53
67	H	1.09018	*	100.71240	*	-72.25580	*	62	60	58
68	H	1.10609	*	114.53195	*	-51.61289	*	63	61	59
69	H	1.10760	*	110.63409	*	-171.72753	*	63	61	59
70	H	1.08943	*	125.98312	*	-99.53079	*	64	62	60
71	H	1.08946	*	124.96576	*	-175.06660	*	65	64	62

CARTESIAN COORDINATES

NO.	ATOM	X	Y	Z
1	C	0.0000	0.0000	0.0000
2	C	1.3838	0.0000	0.0000
3	C	2.1127	1.2622	0.0000
4	C	1.4200	2.4607	0.0028
5	C	2.1124	-0.9418	0.8404
6	C	-0.7294	1.2616	0.0001

7	C	-0.7293	-0.9422	0.8391
8	C	-0.0376	2.4604	0.0024
9	C	-0.0376	-1.8362	1.6379
10	C	-1.9097	1.0992	0.8393
11	C	-1.9096	-0.2630	1.3578
12	C	-0.4889	3.5602	0.8449
13	C	1.4200	-1.8357	1.6387
14	C	3.2914	-0.2616	1.3607
15	C	3.2915	1.1005	0.8417
16	C	1.8697	3.5607	0.8461
17	C	-2.3388	2.1443	1.6390
18	C	-2.3386	-0.5119	2.6500
19	C	-1.6100	-1.4532	3.4914
20	C	-1.6100	3.4068	1.6416
21	C	-0.4890	-2.0977	2.9983
22	C	0.6899	4.2390	1.3688
23	C	1.8698	-2.0970	2.9997
24	C	2.9897	3.4078	1.6443
25	C	2.9899	-1.4519	3.4942
26	C	3.7189	2.1457	1.6424
27	C	3.7189	-0.5103	2.6535
28	C	4.1672	0.5909	3.4964
29	C	4.1672	1.8835	3.0040
30	C	0.6899	-2.2561	3.8410
31	C	-2.7885	0.5891	3.4922
32	C	-2.7887	1.8819	3.0000
33	C	-2.3345	0.3279	4.8530
34	C	-1.6111	3.9235	3.0045
35	C	0.6890	4.7276	2.6636
36	C	-0.4896	4.5641	3.5047
37	C	-2.3344	2.9817	3.8426
38	C	-1.6112	-0.9328	4.8529
39	C	0.6890	-1.7595	5.1326
40	C	3.7118	0.3294	4.8567
41	C	3.7116	2.9830	3.8463
42	C	2.9892	-0.9316	4.8557
43	C	1.8665	4.5646	3.5061
44	C	2.9888	3.9244	3.0072
45	C	1.8665	-1.0774	5.6535
46	C	-0.0439	4.3020	4.8644
47	C	-1.8978	2.7312	5.1331
48	C	-0.4894	-1.0781	5.6521
49	C	-1.8978	1.3726	5.6508
50	C	3.2737	1.3739	5.6541
51	C	3.2736	2.7325	5.1362
52	C	1.4193	4.3023	4.8653
53	C	2.1037	1.2192	6.5008
54	C	2.1030	3.4104	5.6647
55	C	-0.7282	3.4099	5.6630
56	C	-0.0439	0.0217	6.4937
57	C	1.4194	0.0221	6.4945

58	C	-0.7288	1.2184	6.4991
59	C	1.4044	2.5164	6.6122
60	C	-0.0304	2.5160	6.6113
61	C	1.8443	3.4038	8.5596
62	C	-0.4732	3.4037	8.5580
63	C	0.6857	4.3572	8.3904
64	C	-0.0228	2.3225	9.3182
65	C	1.3931	2.3226	9.3191
66	H	2.8837	3.7004	8.4169
67	H	-1.5123	3.7001	8.4139
68	H	0.6862	4.9159	7.4358
69	H	0.6850	5.1176	9.1958
70	H	-0.6476	1.5508	9.7664
71	H	2.0172	1.5507	9.7682

H: (PM3): J. J. P. STEWART, J. COMP. CHEM. 10, 209 (1989).
C: (PM3): J. J. P. STEWART, J. COMP. CHEM. 10, 209 (1989).

GRADIENT NORM = 1.75060
TIME FOR SCF CALCULATION = 226.48
TIME FOR DERIVATIVES = 33.14
MOLECULAR WEIGHT = 786.76

PRINCIPAL MOMENTS OF INERTIA IN CM(-1)

A = 0.002743 B = 0.002049 C = 0.002048

PRINCIPAL MOMENTS OF INERTIA IN UNITS OF 10**(-40)*GRAM-CM**2

A =10206.953200 B =13664.245977 C =13669.191056

RESULTS

DESCRIPTION OF VIBRATIONS

-663.29,	79.02,	80.61,	109.31,	191.04,
191.53,	247.65,	263.46,	263.82	268.51,
271.07,	313.00,	351.22,	352.53,	354.73,
355.52,	358.42,	361.01,	396.60,	405.22,
407.48,	408.1,	412.59,	413.02 ,	438.76,
439.38,	439.56,	441.19 ,	451.62 ,	485.42,
487.39,	489.16 ,	490.6,	502.03,	535.33,
544.25,	544.68,	546.08 ,	548.0,	554.29,
557.36,	558.30,	585.56,	585.84,	588.87,
589.78,	593.57,	593.95,	594.47,	610.35,
611.89,	612.93,	613.66,	684.59,	698.10,
700.85,	701.31,	701.55,	705.01,	733.74,
735.07,	736.22,	743.27,	756.92,	758.12,
758.67,	761.25,	761.69,	764.09,	771.63,

780.45,	782.07,	782.16,	783.48,	802.79,
803.37,	810.83,	814.65,	816.20,	817.25,
817.33,	818.18,	819.03,	822.24,	837.47,
847.10,	847.82,	850.36,	857.65,	865.72,
866.36,	866.76,	888.07,	904.66,	906.36,
906.79,	908.26,	909.96,	910.28,	911.26,
912.21,	937.85,	941.74,	941.97,	944.57,
964.49,	971.95,	977.43,	1014.67,	1017.53,
1024.42,	1082.29,	1090.51,	1115.44,	1115.79,
1126.59,	1127.83,	1153.07,	1157.26,	1162.42
1220.63,	1240.69 ,	1243.96,	1245.01,	1246.79
1248.43,	1276.16,	1284.69,	1285.65,	1290.88,
1293.62,	1321.14,	1329.02,	1338.98,	1342.02,
1358.62,	1367.26,	1368.98,	1371.17,	1379.92,
1380.64,	1381.63,	1382.38,	1395.02,	1418.78,
1423.63,	1429.76,	1433.43,	1438.76,	1440.49,
1441.15,	1441.99,	1446.08,	1447.06,	1447.86,
1454.02,	1469.89,	1478.33,	1478.76,	1480.21,
1484.49,	1498.24,	1498.76,	1500.82,	1504.28,
1506.90,	1517.10,	1517.77,	1517.97,	1521.53,
1600.28,	1635.91,	1648.58,	1656.82,	1660.32,
1661.30,	1666.41,	1668.27,	1670.45,	1673.75,
1694.96,	1705.89,	1706.75,	1721.95,	1730.29,
1731.12,	1740.25,	1744.91,	1768.07,	1778.06,
1786.08,	1794.29,	1799.29,	1799.65,	1801.69,
1802.5,	1810.07,	1814.25,	1815.60,	1816.36,
1816.92,	2970.62,	3048.10,	3122.83,	3124.87,
3130.69,	3143.65			

SYSTEM IS A GROUND STATE
MOPAC SIMULATION OF C60C5H6 TRANSITION STATE

MOLECULE IS NOT LINEAR

THERE ARE 207 GENUINE VIBRATIONS IN THIS SYSTEM
THIS THERMODYNAMICS CALCULATION IS LIMITED TO
MOLECULES WHICH HAVE NO INTERNAL ROTATIONS

CALCULATED THERMODYNAMIC PROPERTIES

TEMP. (K)	H.O.F.(*) KCAL/MOL	HEAT CAPACITY CAL/K/MOL	ENTROPY CAL/K/MOL
298	867.468	124.6227	151.4202

348	874.371	151.2664	172.7807
398	882.567	176.2839	194.7501
448	891.966	199.3311	216.9687
498	902.465	220.2632	239.1658
548	913.957	239.0832	261.1417
598	926.340	255.8926	282.7545
648	939.516	270.8479	303.9067
698	953.397	284.1292	324.5355

* NOTE: HEATS OF FORMATION ARE RELATIVE TO THE
ELEMENTS IN THEIR STANDARD STATE AT 298K

TOTAL CPU TIME: 55271.68 SECONDS

== MOPAC DONE ==

Appendix D

An extract of the output file from PM3 (MOPAC) that was obtained from modeling 1,2 $C_{60}C_5H_6$.

```
*****************************************************************************
** FRANK J. SEILER RES. LAB., U.S. AIR FORCE ACADEMY, COLO. SPGS., CO. 80840 **
*****************************************************************************

                    PM3 CALCULATION RESULTS

*****************************************************************************
*       MOPAC:  VERSION  6.00          CALC'D. 22-Feb-93
*****************************************************************************
MOPAC SIMULATION OF  C60C5H6

  (I)          NA:I       NB:NA:I     NC:NB:NA:I    NA   NB   NC

   1    C
   2    C     1.38439 *                     1
   3    C     1.45773 *   120.07707 *            2    1
   4    C     1.38426 *   119.98993 *   0.16559 *  3    2    1
   5    C     1.45774 *   120.07544 *  138.25901 *  2    1    3
   6    C     1.45804 *   119.91846 *  -0.16550 *  1    2    3
   7    C     1.45784 *   119.94240 * -138.04493 *  1    2    3
   8    C     1.38460 *   120.02103 *   0.05167 *  6    1    2
   9    C     1.38459 *   120.00410 *  -0.06024 *  7    1    2
  10    C     1.45724 *   108.03250 * -142.55853 *  6    1    2
  11    C     1.45732 *   108.02731 *  142.54377 *  7    1    2
  12    C     1.45679 *   120.03848 * -138.19412 *  8    6    1
  13    C     1.38433 *   119.97185 *  -0.24132 *  5    2    1
  14    C     1.45735 *   108.04759 * -142.87346 *  5    2    1
  15    C     1.45709 *   108.06822 *  142.88873 *  3    2    1
  16    C     1.45681 *   119.99087 *  138.19650 *  4    3    2
  17    C     1.38476 *   120.00767 *  142.75882 * 10    6    1
  18    C     1.38469 *   120.00551 * -142.74382 * 11    7    1
  19    C     1.45770 *   119.99768 *   0.11076 * 18   11    7
  20    C     1.38379 *   120.03097 *  -0.15678 * 12    8    6
  21    C     1.38385 *   119.97027 *   0.03061 * 19   18   11
  22    C     1.45813 *   107.95818 * -142.36543 * 16    4    3
  23    C     1.45683 *   119.99061 * -138.13306 * 13    5    2
  24    C     1.38391 *   120.04038 *   0.20538 * 16    4    3
  25    C     1.38397 *   120.05463 *  -0.19387 * 23   13    5
  26    C     1.38468 *   119.99364 * -142.73248 * 15    3    2
  27    C     1.38464 *   120.01433 *  142.68549 * 14    5    2
  28    C     1.45745 *   119.93990 * -138.03182 * 27   14    5
  29    C     1.38259 *   120.05758 *  -0.16656 * 28   27   14
  30    C     1.45812 *   107.95360 *  142.37530 * 23   13    5
```

31	C	1.45738	*	119.95119	*	138.06039	*	18	11	7
32	C	1.38252	*	120.05162	*	0.14128	*	31	18	11
33	C	1.45850	*	107.92965	*	-142.21747	*	31	18	11
34	C	1.45803	*	119.92623	*	137.99724	*	20	12	8
35	C	1.38367	*	119.97810	*	142.15000	*	22	16	4
36	C	1.38592	*	120.16313	*	-0.50604	*	34	20	12
37	C	1.44920	*	108.16387	*	-142.19062	*	34	20	12
38	C	1.44916	*	108.08531	*	-0.30135	*	33	31	18
39	C	1.38362	*	119.96460	*	-142.12607	*	30	23	13
40	C	1.45847	*	107.91957	*	142.18513	*	28	27	14
41	C	1.45846	*	119.84425	*	137.88668	*	29	28	27
42	C	1.44920	*	108.08640	*	0.30171	*	40	28	27
43	C	1.45600	*	120.19818	*	0.08153	*	35	22	16
44	C	1.38587	*	119.76106	*	0.58640	*	43	35	22
45	C	1.38579	*	119.17814	*	-142.32806	*	42	40	28
46	C	1.45287	*	120.33253	*	-138.41167	*	36	34	20
47	C	1.38698	*	119.58873	*	142.37644	*	37	34	20
48	C	1.38583	*	119.17251	*	142.34222	*	38	33	31
49	C	1.38705	*	120.27764	*	142.07957	*	33	31	18
50	C	1.38706	*	120.27113	*	-142.07189	*	40	28	27
51	C	1.38693	*	120.23996	*	-0.36475	*	41	29	28
52	C	1.45284	*	108.50420	*	-142.99507	*	43	35	22
53	C	1.44577	*	121.29598	*	139.54584	*	50	40	28
54	C	1.36988	*	120.71616	*	143.49062	*	52	43	35
55	C	1.36985	*	120.71692	*	-0.15485	*	46	36	34
56	C	1.45289	*	120.36125	*	0.89681	*	48	38	33
57	C	1.37016	*	118.78390	*	-2.61181	*	53	50	40
58	C	1.37018	*	120.75036	*	0.33667	*	56	48	38
59	C	1.52280	*	110.19474	*	-155.45669	*	53	50	40
60	C	1.52290	*	124.44351	*	-150.74331	*	58	56	48
61	C	1.56155	*	114.26622	*	-102.66417	*	59	53	50
62	C	1.56146	*	114.27075	*	-106.33137	*	60	58	56
63	C	1.55339	*	100.68723	*	-160.78362	*	61	59	53
64	C	1.51909	*	106.76905	*	57.00671	*	62	60	58
65	C	1.34607	*	107.67112	*	70.80710	*	64	62	60
66	H	1.10324	*	114.24146	*	72.65110	*	61	59	53
67	H	1.10320	*	114.23598	*	-72.63535	*	62	60	58
68	H	1.10293	*	114.23081	*	-59.97172	*	63	61	59
69	H	1.10164	*	113.52943	*	176.49756	*	63	61	59
70	H	1.08706	*	123.25743	*	-108.49079	*	64	62	60
71	H	1.08710	*	129.06245	*	-179.24141	*	65	64	62

CARTESIAN COORDINATES

NO.	ATOM	X	Y	Z
1	C	0.0000	0.0000	0.0000
2	C	1.3844	0.0000	0.0000
3	C	2.1150	1.2614	0.0000
4	C	1.4242	2.4611	0.0035
5	C	2.1149	-0.9413	0.8398
6	C	-0.7272	1.2637	0.0037

7	C	-0.7276	-0.9394	0.8445
8	C	-0.0337	2.4621	0.0060
9	C	-0.0342	-1.8315	1.6448
10	C	-1.9058	1.1035	0.8456
11	C	-1.9060	-0.2583	1.3655
12	C	-0.4813	3.5621	0.8497
13	C	1.4238	-1.8329	1.6422
14	C	3.2972	-0.2629	1.3554
15	C	3.2974	1.0989	0.8358
16	C	1.8781	3.5602	0.8450
17	C	-2.3329	2.1501	1.6455
18	C	-2.3332	-0.5052	2.6593
19	C	-1.6028	-1.4448	3.5011
20	C	-1.6021	3.4114	1.6472
21	C	-0.4822	-2.0890	3.0069
22	C	0.7001	4.2376	1.3738
23	C	1.8774	-2.0913	3.0022
24	C	3.0020	3.4074	1.6379
25	C	3.0013	-1.4491	3.4918
26	C	3.7304	2.1447	1.6334
27	C	3.7300	-0.5109	2.6471
28	C	4.1823	0.5910	3.4869
29	C	4.1826	1.8827	2.9937
30	C	0.6992	-2.2434	3.8477
31	C	-2.7796	0.5975	3.5011
32	C	-2.7796	1.8890	3.0078
33	C	-2.3192	0.3393	4.8607
34	C	-1.5983	3.9251	3.0118
35	C	0.7034	4.7188	2.6711
36	C	-0.4712	4.5547	3.5157
37	C	-2.3185	2.9872	3.8496
38	C	-1.5992	-0.9183	4.8607
39	C	0.7025	-1.7367	5.1352
40	C	3.7272	0.3337	4.8484
41	C	3.7271	2.9818	3.8373
42	C	3.0047	-0.9226	4.8514
43	C	1.8811	4.5526	3.5109
44	C	3.0050	3.9209	3.0024
45	C	1.8802	-1.0534	5.6507
46	C	-0.0290	4.2908	4.8742
47	C	-1.8733	2.7395	5.1396
48	C	-0.4718	-1.0512	5.6556
49	C	-1.8744	1.3831	5.6585
50	C	3.2876	1.3784	5.6480
51	C	3.2868	2.7348	5.1290
52	C	1.4441	4.2894	4.8712
53	C	2.1368	1.2310	6.5107
54	C	2.1346	3.4183	5.6718
55	C	-0.7177	3.4210	5.6778
56	C	-0.0295	0.0507	6.4929
57	C	1.4436	0.0493	6.4898

58	C	-0.7205	1.2337	6.5167
59	C	1.5122	2.5913	6.7908
60	C	-0.0920	2.5928	6.7942
61	C	1.8479	3.1736	8.2003
62	C	-0.4202	3.1755	8.2052
63	C	0.7151	4.2252	8.3548
64	C	0.0423	2.1467	9.2227
65	C	1.3883	2.1457	9.2199
66	H	2.8863	3.5307	8.3073
67	H	-1.4575	3.5342	8.3170
68	H	0.7142	5.0072	7.5770
69	H	0.7177	4.7341	9.3319
70	H	-0.6421	1.5398	9.8100
71	H	2.0741	1.5376	9.8044

H: (PM3): J. J. P. STEWART, J. COMP. CHEM. 10, 209 (1989).
C: (PM3): J. J. P. STEWART, J. COMP. CHEM. 10, 209 (1989).

GRADIENT NORM = 1.05693
TIME FOR SCF CALCULATION = 197.32
TIME FOR DERIVATIVES = 34.06
MOLECULAR WEIGHT = 786.76

PRINCIPAL MOMENTS OF INERTIA IN CM(-1)

A = 0.002748 B = 0.002082 C = 0.002076

PRINCIPAL MOMENTS OF INERTIA IN UNITS OF 10**(-40)*GRAM-CM**2

A =10185.702701 B =13442.416248 C =13481.831200

RESULTS

DESCRIPTION OF VIBRATIONS

119.87,	143.55,	184.90,	227.21,	254.22,
254.55,	266.58,	267.79,	312.37,	341.89,
342.64,	347.11,	351.09,	353.10,	353.83,
365.87,	395.10,	397.96,	401.31,	409.17,
411.88,	431.76,	433.59,	438.50,	438.68,
445.90,	462.16,	462.60,	478.33,	488.43,
492.35,	501.88,	538.90,	539.43,	541.97,
543.42,	547.11,	552.50,	557.89,	558.39,
578.99,	585.04,	585.41,	593.22,	593.58,
598.04,	600.24,	602.90,	611.63,	616.12,
616.97,	682.93,	686.25,	694.58,	700.26,
702.78,	705.55,	715.62,	723.19,	734.44,
736.67,	754.74,	757.98,	759.72,	761.34,
762.14,	766.80,	772.79,	776.70,	779.07,

783.55,	785.53,	800.09,	805.60,	807.29,
808.87,	812.92,	817.00,	818.54,	820.06,
821.73,	831.81,	841.10,	845.60,	849.71,
851.29,	864.48,	868.14,	874.60,	878.45,
881.66,	907.63,	907.66,	908.41,	910.70,
910.90,	911.84,	933.24,	934.64,	939.53,
948.72,	954.54,	967.55,	975.88,	985.31,
990.83,	1013.11,	1041.68,	1055.25,	1069.22,
1089.00,	1096.45,	1099.34,	1126.58,	1128.89,
1138.33,	1147.02,	1152.63,	1165.37,	1183.99,
1204.02,	1205.38,	1233.30,	1237.93,	1246.87,
1249.95,	1251.92,	1257.91,	1267.48,	1283.09,
1291.49,	1292.09,	1293.62,	1310.27,	1316.95,
1321.53,	1325.25,	1337.67,	1340.30,	1364.07,
1366.63,	1379.15,	1380.23,	1383.68,	1385.24,
1393.02,	1402.63,	1407.13,	1420.31,	1427.86,
1439.57,	1439.84,	1442.90,	1443.12,	1446.38,
1449.65,	1451.04,	1456.82,	1459.66,	1466.58,
1476.87,	1484.90,	1494.71,	1498.86,	1499.25,
1508.93,	1510.68,	1516.59,	1519.95,	1521.71,
1531.64,	1637.28,	1658.16,	1660.47,	1661.92,
1662.77,	1666.37,	1668.80,	1677.80,	1691.71,
1703.47,	1705.96,	1726.47,	1731.51,	1734.90,
1741.27,	1750.82,	1773.22,	1781.37,	1781.64,
1798.35,	1799.45,	1803.74,	1804.04,	1804.18,
1810.12,	1813.11,	1826.45,	1827.67,	1828.60,
1828.96,	3027.14,	3030.76,	3034.42,	3090.66,
3144.49,	3162.48			

SYSTEM IS A GROUND STATE
MOPAC SIMULATION OF C60C5H6

MOLECULE IS NOT LINEAR

THERE ARE207 GENUINE VIBRATIONS IN THIS SYSTEM
THIS THERMODYNAMICS CALCULATION IS LIMITED TO
MOLECULES WHICH HAVE NO INTERNAL ROTATIONS

CALCULATED THERMODYNAMIC PROPERTIES

TEMP. (K)	H.O.F.(*) KCAL/MOL	HEAT CAPACITY CAL/K/MOL	ENTROPY CAL/K/MOL

298	816.704	122.2605	144.1117
398	831.592	174.4397	186.8265
498	851.331	218.9099	230.8840
598	875.090	254.8983	274.2589
698	902.060	283.3829	315.9061

* NOTE: HEATS OF FORMATION ARE RELATIVE TO THE
ELEMENTS IN THEIR STANDARD STATE AT 298K

TOTAL CPU TIME: 58792.78 SECONDS

== MOPAC DONE ==

References

1. Hoffmann R., *Sci. Am.*, February, 66 (1993).
2. Jones, D.E.H., *New Scientist*, **32**, 245 (1966).
3. Osawa E., *Kagaku (Kyoto)*, **25**, 854 (1970).
4. Yoshida Z. and E. Osawa, *Aromaticity (Kyoto)*, 174 (1971).
5. Bochvar D.A. and E.G. Gal'pern, *Proc. Acad. Sci. USSR*, **209**, 239 (1973).
6. Kroto H.W., J.R. Heath, S.C. O'Brien, R.F. Curl, and R.E. Smalley, *Nature*, **318**, 162 (1985).
7. Kroto H.W., A.W. Allaf and S.P. Balm, *Chem. Rev.*, **91**, 1213 (1991).
8. Kroto H.W., *Angew. Chem. Int. Ed. Engl.*, **31**, 111 (1992).
9. Curl R.F., and R.E. Smalley, *Sci. Am.*, October, 54 (1991).
10. Gerhardt Ph., S. Löffler, and K.H. Homann, *Chem. Phys. Lett.*, **137**, 306 (1987).
11. Gerhardt Ph., S. Löffler, and K.H. Homann, *Proc. of the 22nd Symp. (Int.) on Combustion*, The Combustion Institute: Pittsburgh, 395 (1989).
12. Löffler S., and K.H. Homann, *Proc. of the 23rd Symp. (Int.) on Combustion*, The Combustion Institute: Pittsburgh, 355 (1991).
13. Krätschmer W., L.D. Lamb, K. Fostiropoulos, D.R. Huffman, *Nature*, **347**, 354 (1990).
14. Krätschmer W., K. Fostiropoulos, D.R. Huffman, *Chem. Phys. Lett.*, **170**, 167 (1990).
15. Ajie H., M.M. Alvarez, S.J. Anz, R.D. Beck, F. Diederich, K. Fostiropoulos, D.R. Huffman, W. Krätschmer, Y. Rubin, K.E. Schriver, D. Sensharma, and R.L. Whetten, *J. Phys. Chem.*, **94**, 8630 (1990).
16. Howard J.B., J.T. McKinnon, Y. Makarovsky, A.L. Lafleur, M.E. Johnson, *Nature*, **352**, 139 (1991).
17. Howard J.B., J.T. McKinnon, M.E. Johnson, Y. Makarovsky, and A.L. Lafleur, *J. Phys. Chem.*, **96**, 6657 (1992).
18. Arizona Fullerene Consortium, *Fullerene Bibliography*, University of Arizona, December (1993).
19. Editors, *Fullerene Session Leaflet*, Session G, MRS Annual Meeting, Boston (1993).

20. Wilson M.A., L.S.K. Pang, G.D. Willett, K.J. Fisher, and I.G. Dance, *Carbon*, **30**, 4, 675 (1992).
21. Peters G., and M. Jansen, *Angw. Chem. Int. Ed. Eng.*, **31**, 2, 223 (1992).
22. Haufler R.E., J. Conceicao, L.P.F. Chibante, Y. Chai, N.E. Byrne, S. Flanagan, M.M. Haley, S.C. O'Brien, C. Pan, Z. Xiao, W.E. Billups, M.A. Ciufolini, R.H. Hauge, J.L. Margrave, L.J. Wilson, R.F. Curl, and R.E. Smalley, *J. Phys. Chem.*, **94**, 8634 (1990).
23. Yoshie K., S. Kasuya, K. Eguchi, and T. Yoshida, *Appl. Phys. Lett.*, **61**, 2782 (1992).
24. Frazee J.D., and R.C. Anderson, *Proc. Third Conf. on Carbon,* Buffalo, 405 (1957)
25. Davies R.A., and D.B. Scully, *Combustion and Flame*, **61**, 216 (1966)
26. Bittner J.D., *Ph.D. Thesis*; Department of Chemical Engineering, Massachusetts Institute of Technology (1981).
27. Bittner J.D., and J.B. Howard, *Eighteenth Symposium (International) on Combustion*, The Combustion Institute, 1105 (1981).
28. Bockhorn H., F. Fetting, and H. Wenz, *Ber. Bunsenges Phys. Chem.*, **87**, 1067 (1983).
29. Brei M., H. Jander, and H.Gg. Wagner, *Ber. Bunsenges. Phys. Chem.*, **91**, 30 (1987).
30. Howard J.B., A.L. Lafleur, Y. Makarovsky, S. Mitra, C. Pope, and T. Yadav, *Carbon,* **30**, 1183 (1992).
31. McKinnon J.T., *Ph.D. Thesis*, Department of Chemical Engineering, Massachusetts Institute of Technology (1989).
32. Anacleto J.F., M.A. Quilliam, R.K. Boyd, J.B. Howard, A.L. Lafleur, and T. Yadav, *Rapid Commun. in Mass Spectrom.*, **7**, 229 (1993).
33. Pope C.J., J.A. Marr and J.B. Howard, *J. Phys. Chem.*, **97**, 42, 11001 (1993).
34. Ebbesen T.W., J. Tabuchi and K. Tanigaki, *Chem. Phys. Lett.*, **191**, 336 (1992).
35. Lamb L.D. and D.R. Huffman, *J. Phys. Chem.* Solids, in press.
36. Anacleto J.F., H. Perreault, R.K. Boyd, S. Pleasance, M.A. Quilliam, P.G. Sim, J.B. Howard, Y. Makarovsky, and A.L. Lafleur, *Rapid Commun. Mass Spectrom.*, **6**, 214 (1992).

37. Anacleto J.F., H. Perreault, R.K. Boyd, S. Pleasance, M.A. Quilliam, P.G. Sim, J.B. Howard, Y. Makarovsky, and A.L. Lafleur, *Can. Jour. Chem.*, **70**, 2558 (1992).
38. Boyd B. and J. Anacleto, *personal communications.*
39. Stone A.J. and D.J. Wales, *Chem. Phys. Lett.*, **128**, 501 (1986).
40. Haymet A.D.J., *Chem. Phys. Lett.*, **122**, 421 (1985).
41. Haymet A.D.J., *J. Am. Chem. Soc.*, **108**, 319 (1986).
42. Fowler P.W. and J. Woolrich, *Chem. Phys. Lett.*, **127**, 78 (1986).
43. Fowler P.W., *Chem. Phys. Lett.*, **131**, 444 (1986).
44. Fowler P.W., *J. Chem. Soc. Faraday. Trans.*, **86**, 2073 (1990).
45. Haddon R.C., L.E. Brus, K. Raghavachari, *Chem. Phys. Lett.*, **125**, 459 (1986).
46. Haddon R.C., L.E. Brus, K. Raghavachari, *Chem. Phys. Lett.*, **131**, 165 (1986).
47. Ugarte D., *Nature*, **359**, 707 (1992).
48. Klein D.J., T.G. Schmalz, G.E. Hite, and W.A. Seitz, *J. Am. Chem. Soc.*, **108**, 1301 (1986).
49. Schmalz T.G., W.A. Seitz, D.J. Klein, and G.E. Hite, *J. Am. Chem. Soc.*, **110**, 1113 (1988).
50. Bakowies D. and W. Thiel, *J. Am. Chem. Soc.*, **113**, 3704 (1991).
51. Coulombeau C. and A. Rassat, *J. Chim. Phys.*, **84**, 875 (1987).
52. Schmalz T.G., W.A. Seitz, D.J. Klein, and G.E. Hite, *Chem. Phys. Lett.*, **130**, 203 (1986).
53. Newton M.D. and R.E. Stanton, *J. Am. Chem. Soc.*, **108**, 2469 (1986).
54. McKee M.L. and W.C. Herndon, *J. Mol. Struc.*, **153**, 75 (1987).
55. Shibuya T.I. and M. Yoshitani, *Chem. Phys. Lett.*, **13**, 137 (1987).
56. Lüthi H.P. and J. Almlöf, *Chem. Phys. Lett.*, **135**, 357 (1987).
57. Manolopoulos D.E., J.C. May and S.E. Down, *Chem. Phys. Lett.*, **181**, 105 (1991).
58. Manolopoulos D.E., *Chem. Phys. Lett.*, **192**, 330 (1992).
59. Liu X., T.G. Schmalz and D.J. Klein, *Chem. Phys. Lett.*, **188**, 550 (1992).
60. Liu X., T.G. Schmalz and D.J. Klein, *Chem. Phys. Lett.*, **192**, 331 (1992).
61. Scuseria G.E., *Chem. Phys. Lett.*, **176**, 423 (1991).
62. Guo T. and G.E. Scuseria, *Chem. Phys. Lett.*, **191**, 527 (1992).
63. Cioslowski J., *Chem. Phys. Lett.*, **181**, 68 (1991).

64. Dunlap B.I, D.W. Brenner, J.W. Mintmire, R.C. Mowrey and C.T. White, *J. Phys. Chem.*, **95**, 5763 (1991).
65. Matsuzawa N., D.A. Dixon and P.J. Krusic, *J. Phys. Chem.*, **96**, 8317 (1992).
66. Wu Z.C., D.A. Jelski and T.F. George, *Chem. Phys. Lett.*, **137**, 291 (1987).
67. Cyvin S.J., E. Brendsdal, B.N. Cyvin and J. Brunvoll, *Chem. Phys. Lett.*, **143**, 377 (1988).
68. Stanton R.E. and M.D. Newton, *J. Phys. Chem.*, **92**, 2141 (1988).
69. Weeks D.E. and W.G. Harter, *J. Chem. Phys.*, **90**, 4744 (1989).
70. Schulman J.M., R.L. Disch, M.A. Miller and R.C. Peck, *Chem. Phys. Lett.*, **141**, 45 (1987).
71. Schulman J.M., R.C. Peck and R.L. Disch, *J. Am. Chem. Soc.*, **111**, 5675 (1989).
72. Schulman J.M. and R.L. Disch, *J. Chem. Soc. Chem. Commun.*, 411 (1991).
73. Almlöf J. and H.P. Lüthi, *ACS Symp. Ser. 353*, Amer. Chem. Soc., Washington D.C. (1987).
74. McKinnon J.T., *J. Phys. Chem.*, **95**, 8941 (1991).
75. Rudzinski J.M., Z. Slanina, M. Togasl, E. Osawa and T. Iizuka, *Thermochim. Acta*, **125**, 155 (1988).
76. Jin Y., J. Cheng, M. Varma-Nair, G. Liang, Y. Fu, B. Wunderlich, X.D. Xiang, R. Mostovoy, and A.K. Zettl, *J. Phys. Chem.*, **96**, 5151 (1992).
77. Olson J.R., K.A. Topp, and R.O. Pohl, *Science*, **259**, 1145 (1993).
78. Beckhaus H.D., C. Ruchardt, M. Kao, F. Deiderich, C.S. Foote, *Ang. Chem. Int. Ed. Eng.*, **31**, 1, 63 (1992).
79. Steele W.V., R.D. Chirico, N.K. Smith, W.E. Billups, P.R. Elmore, and A.E. Wheeler, *J. Phys. Chem.*, **996**, 4731 (1992).
80. Atake T., T. Tanaka, H. Kawaji, K. Kikuchi, K. Saito, S. Suzuki, I. Ikemoto, and Y. Achiba, *Physica C*, 185, 427 (1991).
81. Ionov S.P., A.S. Alikhanyan, N.G. Spitsina, and V.G. Yarzhemsky, *Dokl. Akad. Nauk.*, **331**, 449 (1993).
82. Wudl F., A. Hirsch, K.C. khemani, T. Suzuki, P.M. Allemand, A. Koch, H. Eckert, G. Srdanov, H.M. Webb, *ACS Symposium Series 481*, 161 (1992).
83. Taylor, R. and D.R.M. Walton, D.R.M., *Nature*, **363**, 685 (1993).
84. Stanton, R.E., *J. Phys. Chem.*, **96**, 1, 111 (1992).

85. Henderson C.C., C.M. Rohlfing and P.A. Cahill, *Chem. Phys. Lett.*, **213**, 383 (1993).
86. Henderson, C.C. and P.A. Cahill, *Chem. Phys. Lett.*, **198**, 570 (1992)
87. Ventura O.N., in S. Fraga, Editor, *Computational Chemistry: Structure, Interactions and Reactivity*, vol 2., Elsevier Science Publishers, 600 (1992).
88. Nakanishi K. and P.H. Solomon, *Infrared Absorption Spectroscopy*, 2nd Ed, Holden-Day Inc. (1977).
89. Chapman D. and P.D. Magnus, *Introduction to Practical High Resolution Nuclear Magnetic Resonance Spectroscopy*, Academic Press (1966).
90. Creegan K.M., J.L. Robbins, W.K. Robbins, J.M. Millar, R.D. Sherwood, P.J. Tindall, and D.E. Cox, *J. Am. Chem. Soc.*, **114**, 3, 1103 (1992).
91. Burkert U. and N.L. Allinger, *Molecular Mechanics*, ACS Monograph 177, Amer. Chem. Soc. (1982).
92. Dewar M.J.S., E.G. Zoebisch, E.F. Healy and J.J.P. Stewart, *J. Am. Chem. Soc.*, **107**, 3902 (1985).
93. Quirante J.J., F. Enriquez and J.M. Hernando, *J. Mol. Struct. Theochem.*, **204**, 193 (1990).
94. Hernando J.M., J.J. Quirante, F. Enriquez and J.M. Hernando, *J. Mol. Struct. Theochem.*, **204**, 201 (1990).
95. Katagi T., *J. Comput. Chem.*, **11**, 524 (1990).
96. Dewar M.J.S. and Y.C. Yuan, *J. Am. Chem. Soc.*, **112**, 2088 (1990).
97. Dewar M.J.S. and Y.C. Yuan, *J. Am. Chem. Soc.*, **112**, 2095 (1990).
98. Stewart J.J.P., *J. Comput. Chem.*, **10**, 209 (1989).
99. Boudart M., *Kinetics of Chemical Processes*, Prentice-Hall, 35 (1968).
100. Benson S.W., *Thermochemical Kinetics*, 2nd Ed. (1976).
101. Ruoff R.S., D.S. Tse, R. Malhotra, D.C. Lorents, *J. Phys. Chem.*, **97**, 3379 (1993).
102. Chai Y., T. Guo, C. Jin, R.E. Haufler, L.P.F. Chibante, J. Fure, L. Wang, J.M. Alford, and R.E. Smalley, *J. Phys. Chem.*, **95**, 7564 (1991).
103. Ross. M.M., and J.H. Callahan, *J. Phys. Chem.*, **95**, 5720 (1991).
104. Wan Z., J.F. Christian, and S.L. Anderson, *Phys. Rev. Lett.*, **69**, 1352 (1992).
105. Socrates G., *Infrared Characteristic Group Frequencies*, John Wiley and Sons (1980).

106. Tsuda M., T. Ishida, T. Nogami, S. Kurono, and M. Ohashi, *J. Chem. Soc. Commun.*, 1296 (1993).
107. Rotello V.M., J.B. Howard, T. Yadav, M.M. Conn, E. Viani, L.M. Giovane, and A.L. Lafleur, *Tetrahedron Lett*, **34**, 1561 (1993).
108. Wudl F., A. Hirsch, K.C. Khemani, T. Suzuki, P.M. Allemand, A. Koch, H. Eckert, G. Srdanov and H.M. Webb, *ACS Symposium Series 481*, 161 (1992).
109. Rubin Y., S. Khan, D.I. Freedberg and C. Yeretzian, *J. Am. Chem. Soc.*, **115**, 344 (1993).
110. Belik P., A. Gugel, J. Spickermann and K. Müller, *Angew. Chem. Int. Ed. Engl.*, **32**, 78 (1993).
111. Schlueter J.A., J.M. Seaman, S. Taha, H. Cohen, K.R. Lykke, H.H. Wang, and J.M. Williams, *J. Chem. Soc. Chem. Commun.*, 972 (1993).
112. Hawkins J.M., A. Meyer, T.A. Lewis, and S. Lowen, *ACS Symp. Series 481*, 177 (1992).
113. Fagan P.J., J.C. Calabrese, and B. Malone, *J. Am. Chem. Soc.*, **113**, 9408 (1991).
114. Koefod R.S., M.F. Hudgens, J.R. Shapley, *J. Am. Chem. Soc.*, **113**, 8957 (1991).
115. Alder K. and G. Stein, *Liebigs Ann. Chem.*, **504**, 216 (1933).
116. Roquite B.C., *J. Phys. Chem.*, **69**, 1351 (1965).
117. Herndon W.C. and L.L. Lowry, *J. Am. Chem. Soc.*, **86**, 1922 (1964).
118. Wassermann A., *J. Chem. Soc. London*, 1028 (1936).
119. Townshend R.E., G. Ramunni, G. Segal, W.J. Hehre and L. Salem, *J. Am. Chem. Soc.*, **98**, 2190 (1976).
120. Coxon J.M., S.T. Grice, G.A.R. Maclagan and D.Q. McDonald, *J. Org. Chem.*, **55**, 3804 (1990).
121. Bach R.D., J.J.W. McDouall and H.B. Schlegel, *J. Org. Chem.*, **54**, 2931 (1989).
122. Bernardi F., A. Bottoni, M.J. Field, M.F. Guest, I.H. Hillier, M.A. Robb and A. Venturini, *J. Am. Chem. Soc.*, **110**, 3050 (1988).
123. Dolata D.P. and L.M. Harwood, *J. Am. Chem. Soc.*, **114**, 27, 10738 (1992).
124. Cole J.A., *M.S. Thesis*, Massachusetts Institute of Technology, Cambridge (1982).
125. Pang L.S.K. and M.A. Wilson, *J. Phys. Chem.*, **97**, 26, 6761 (1993).

126. Giovane L.M., J.W. Barco, T. Yadav, A.L. Lafleur, J.A. Marr, J.B. Howard, and V.M. Rotello, *J. Phys. Chem.*, **97**, 8560 (1993).
127. Roberts J.D. and M.C. Caserio, *Basic Principles of Organic Chemistry*, W.A. Benjamin Inc., Chapter 10, (1965).
128. Stobbe H. and F. Reuss, *Liebigs Ann. Chem.*, **391**, 151 (1912).
129. Kaufmann H. and A. Wassermann, *J. Chem. Soc. London*, 870 (1939).
130. Benford, G.A., H. Kaufmann, B.S. Khambata, and A. Wassermann, *J. Chem. Soc. London*, 381 (1939).
131. Wassermann A., *J. Chem. Soc. London*, 1028 (1936).
132. Kistiakowsky G.B. and W.H. Mears, *J. Am. Chem. Soc.*, **58**, 1060 (1936).
133. Barrett E.G.V. and L.J. Burrage, *J. Phys. Chem.*, **37**, 1029 (1933).
134. Harkness J.B., G.B. Kistiakowsky, and W.H. Mears, *J. Chem. Phys.*, **5**, 682 (1937).
135. Khambata B.S., and A. Wassermann, *Nature*, **138**, 368 (1936).
136. Khambata B.S., and A. Wassermann, *J. Chem. Soc. London*, 367 (1939).
137. Khambata B.S., and A. Wassermann, *J. Chem. Soc. London*, 375 (1939).
138. Benford G.A. and A. Wassermann, *J. Chem. Soc. London*, 362 (1939).
139. Wassermann A., *Monatsh. Chem.*, **83**, 543 (1952).
140. Wynne-Jones and Eyring, *J Chem Phys*, **3**, 492 (1935).
141. Evans and Polanyi, *Trans. Faraday Soc*, **31**, 890 (1935).
142. Wassermann A., *Trans. Faraday Soc.*, **34**, 128 (1938).